Transmission Line Protection in Systems with High Penetration of Inverter-Based Resources (IBR)

By

Kapuge Kariyawasam Mudalige Sachintha Kariyawasam

A Thesis submitted to
the Faculty of Graduate and Postdoctoral Studies of
The University of Manitoba
in partial fulfilment of the requirements for the degree of
Doctor of Philosophy

Department of Electrical and Computer Engineering
University of Manitoba
Winnipeg, Canada

October 2026

Copyright © 2026, Kapuge Kariyawasam Mudalige Sachintha Kariyawasam

Abstract

Ever increasing integration of renewable resources into contemporary power systems has imposed a unique set of challenges for system protection. In the wake of several real-world incidents, effectiveness of techniques based on conventional system protection theory in protecting power systems with higher penetration of inverter-based resources (IBRs) has been under scrutiny. Faulted phase identification and fault direction identification are commonly affected protection functions in the presence of IBRs. Effects of IBRs on power swing characteristics also remain a largely unexplored topic.

The work carried out in this Thesis firstly, investigates power system protection issues related to faulted phase identification and fault direction identification in systems with heavy IBR penetration and validates them using detailed simulations and testing of commercial protection relays. Secondly, this work attempts to overcome power system protection related challenges identified during initial investigations related to faulted phase identification and fault direction identification by developing new protection techniques. This work proposes a faulted phase identification method exploiting the relative strength of incremental voltages during faults, which is realized by specific processing of voltage measurements. In addition, this Thesis also presents a technique to correctly identify fault direction in transmission lines using negative-sequence admittance measurements. While both of the above-mentioned solutions are designed for systems with high IBR penetration, they have applicability in system with conventional power generation sources as well. Where applicable, the proposed protection methods have been grounded in and refined based on insights gained through theoretical analysis and, tested and validated using comprehensive Electromagnetic Transient (EMT) type simulation studies. Furthermore, this Thesis also investigates the effects of IBRs on the swing impedance trajectories during power swings by developing a theoretical model to incorporate

IBRs into classical power swing analysis designed for synchronous machines. The proposed method of analysis provides a convenient way to integrate IBRs into out-of-step protection and relaying, which in turn improves design and performance of power system protection.

The work carried out in this Thesis deepens the prevailing understanding of power system protection challenges caused by IBRs and proposes potential solutions for them, which have been validated by simulation studies to be reliable and robust.

Acknowledgments

During my quest to complete this Thesis over the past several years, I have had the luxury of finding the support of many, without whom the successful completion of this work would not have been possible. Therefore, it is only decent to mention a few of them at least.

First and foremost, I owe my sincerest gratitude to my advisor, Dr. Athula Rajapakse, who guided me and supported me in every possible aspect in completing this work. Further, I would like to convey my heartiest thanks to members of the examining committee, Dr. Aniruddha Gole, Dr. Vajira Pathirana, and Dr. Ramakrishna Gokaraju for accepting this Thesis for review and providing valuable feedback.

I would also like to acknowledge the support provided by Pauley Family Foundation, USA, and RTDS Technologies Inc., Canada. The ever-supportive staff and fellow graduate students of the Department of Electrical and Computer Engineering should also be mentioned. I am especially grateful to Shrimal Koruwage and Jagannath Wijekoon for their extended support. My loving wife Malsha, my brother, Anuradha and my caring friends, who are too many to enumerate, must not go without a mention, for they are the ones making my life enjoyable.

Finally, I would like to pay my tribute to each and everyone, who shared their thoughts of wisdom and knowledge under difficult circumstances to make this endeavor a success.

Sachintha Kariyawasam

Dedication

To my loving wife Malsha.

Contents

Front Matter

Contents vi

List of Tables xi

List of Figures xii

List of Copyrighted Material xix

List of Symbols xx

List of Abbreviations xxii

List of Appendices xxv

1 Introduction **1**

1.1 Introduction 1

1.1.1 Inverter Based Resources (IBRs) 2

1.1.1.1. Wind Power Generation 2

1.1.1.2. Solar PV and BESS based Generation 4

1.1.1.3. IBR Plant 5

1.1.1.4. Control and Protection Related to IBR Plants 7

1.1.1.5. Regulatory Bodies and Applicable Standards 10

1.1.2 Behaviour of IBRs during Faults on the AC Transmission System 11

1.2 Challenges to Traditional Protection Philosophy 16

1.2.1 Impact on Overcurrent Protection and Directional Elements 18

1.2.2 Negative-Sequence Quantities-based Protection Algorithms 18

1.2.2.1. Negative-Sequence Overcurrent Element (51-2) 19

1.2.2.2. Negative-Sequence Directional Element (67-2) 20

1.2.3 Impact on Distance Protection 21

1.2.3.1. Phase Current Supervision 21

1.2.3.2. Polarization Voltage 21
1.2.3.3. Faulted Phase Identification 22
1.2.4 Impact on Power Swing Protection Schemes 23
1.2.5 Objectives of the Thesis 25
1.2.6 Theis Overview 26

2 Challenges Posed by IBRs to Traditional Power System Protection 27
2.1 Introduction 27
2.2 Faulted Phase Identification 29
2.2.1 Conventional Methods 29
2.2.2 Transient-based Methods 32
2.2.2.1. Incremental (superimposed) Quantities based Methods 33
2.3 Identification of Fault Direction 38
2.3.1 Conventional Fault Direction Identification Methods 38
2.3.2 Recent Work on Fault Direction Identification with IBRs 40
2.4 Power Swing Protection 42
2.5 Overall System Protection of a System with IBRs 46
2.5.1 Line Current Differential Protection 46
2.5.2 Other Communication-assisted Protection Schemes 47
2.5.3 Back-up Protection 48
2.6 Known Real-world Incidents in Systems with IBRs 50
2.6.1 Evolving Ground Fault in BC Hydro System 50
2.6.2 Blue-cut Fire Event in Southern California 50
2.6.3 SSCI Event in Texas 51
2.7 Concluding Remarks 53

3 Investigation of Impacts of IBRs on Contemporary Faulted Phase Identification Methods and Techniques for Mitigation 54
3.1 Effect of IBR on Faulted Phase Identification Techniques 54
3.2 Testing and Analysis of Commercial Relays 59
3.2.1 Performance of Commercial Relays 59

3.2.2 Test Setup 59
3.2.3 Test Results and Discussion 62
3.2.4 Non-conventional Fault Classification Schemes 67
3.3 Improved Faulted Phase Identification in Systems with IBRs using Incremental Voltages 69
3.3.1 Theoretical Derivations 70
3.3.1.1. Line-to-Ground (LG) Fault 74
3.3.1.2. Line-to-Line-to-Ground (LLG) Fault 75
3.3.1.3. Line-to-Line (LL) Fault 77
3.3.2 Proof-of-Concept Simulations 78
3.3.3 Proposed Faulted Phase Identification Algorithm 80
3.3.3.1. Use of Integrals for Detecting LLG faults 80
3.3.3.2. Fault Indices 81
3.3.3.3. Implementation 84
3.3.4 Performance Evaluation 88
3.3.4.1. Impact of Fault Inception Angle 91
3.3.4.2. Impact of Fault Location 94
3.3.4.3. Impact of Fault Impedance 95
3.3.5 Further Testing 97
3.3.5.1. Performance on a Weak AC system 97
3.3.5.2. New Relay Location 98
3.3.5.3. MIL Implementation using Real IEC 61850 communication 99
3.3.5.4. Evolving Fault 102
3.3.5.5. Performance with Off-nominal Frequency Components 103
3.3.6 Discussion 104
3.4 Concluding Remarks 106

4 Investigation of Impacts of IBRs on Contemporary Fault Direction Identification and an Improved Algorithm 107

4.1 Introduction 107
4.2 Conventional Directional Identification with IBRs 109

4.3 Negative-Sequence Admittance-Based Directional Element 114
4.3.1 Principle of Operation 114
4.3.2 Application of the Proposed Technique 120
4.3.3 Calculation of Settings 121
4.4 Performance Evaluation 123
4.4.1 Impact of Fault Location 126
4.4.2 Impact of Fault Impedance 127
4.4.3 Type of Fault 128
4.4.4 Comparison with a Conventional Direction Element 130
4.4.5 Impact of Negative-Sequence Current Injection 132
4.4.6 Impact of Conventional Synchronous Generation at IBR Bus 133
4.4.7 Impact of a Weak Remote Grid 135
4.4.8 Impact of Series Compensation 137
4.5 Hardware Implementation 139
4.6 Discussion 141
4.7 Concluding Remarks 143

5 Theoretical Analysis of the Impact of IBRs on Impedance Trajectories during Power Swings 144

5.1 Introduction 144
5.2 Theoretical Analysis 146
5.2.1 Representing the IBR 150
5.3 Validation Using EMT Simulations 152
5.4 Results 157
5.4.1 Base Case 157
5.4.2 Impact of Short Circuit Ratio 158
5.4.3 Impact of IBR Active Power Output 160
5.4.4 Impact of Source Voltage Magnitudes 161
5.4.5 Impact of Current Injection during Voltage Ride-Through 162
5.4.6 Impact of IBR Type 163

5.4.7 Impact of System Impedances 164
5.5 Discussion 166
5.5.1 Interpretation of Results 166
5.5.2 Implications to Power System Protection 167
5.5.3 Benefits and Limitations of the Proposed Theoretical Model 169
5.6 Concluding Remarks 171

6 Conclusions and Contributions 172
6.1 Conclusions 172
6.2 Contributions 179
6.3 Future Work 181
Bibliography 183
Appendix A 187

List of Tables

Table 1.1: Electricity production comparison by source, 2010 & 2024 2

Table 1.2: Comparison of fault currents from conventional synchronous generators and IBRs 15

Table 2.1: Comparison of faulted phase identification methods 34

Table 3.1: Fault type identification of relays for low impedance faults 63

Table 3.2: Fault type identification of relays for high impedance faults 63

Table 3.3: Overall performance of relays for various fault types 64

Table 3.4: Fault type identification of relays with added synchronous generation 66

Table 3.5: Fault type identification of transient quantities-based faulted phase identification algorithm 67

Table 3.6: Overall performance of transient-based faulted phase identification algorithm 68

Table 3.7: Fault type identification using indices (unbalanced faults), shaded indices are the two largest for each fault type 83

Table 4.1: Fault direction identification using negative-sequence measurements for forward faults 110

Table 4.2: Fault direction identification using zero-sequence measurements for forward faults 112

Table 4.3: Fault direction identification for different faults 129

List of Figures

Figure 1.1 Type III wind turbine generation based IBR unit 3

Figure 1.2 Type IV wind turbine generation based IBR unit 4

Figure 1.3 Solar PV generation based IBR unit 5

Figure 1.4 BESS based IBR unit 5

Figure 1.5 An example IBR plant 6

Figure 1.6 Typical IBR interconnections to a transmission network 17

Figure 2.1 a) Angle difference between 'Phase A' negative and zero-sequence current phasors during bolted faults (i.e., α), (b) Angle difference between 'Phase A' negative and positive-sequence current phasors during bolted faults (i.e., β). 30

Figure 2.2 Conventional directional elements (a) 90-60directional element and (b) sequence impedance based directional element 39

Figure 2.3 Swing impedance trajectory of the most stable power swing, with and without IBRs 43

Figure 2.4 Weak Infeed trip scheme 48

Figure 3.1 Logic diagram of the implemented impedance-based phase identification technique 56

Figure 3.2 Single line diagram of the power system used for comparing a conventional source and an IBR 56

Figure 3.3 (a) Results for faulted phase selection for a BG fault at the mid-point of the line with the conventional source. Results for faulted phase selection of a BG fault at the mid-point of the line with the IBR, (b) Results for faulted phase selection of a BG fault at the mid-point of the line with the IBR. 58

Figure 3.4 Single line diagram of the power system model used for testing commercial relays 60

Figure 3.5 Schematic of the test setup 61

Figure 3.6 (a) General fault circuit for the system under investigation and (b) the circuit corresponding to incremental quantities.....71

Figure 3.7 Equivalent incremental fault circuit.....73

Figure 3.8 Single line diagram of the simplified power system used for theoretical simulations 78

Figure 3.9 Incremental voltages seen at the relaying location for (a) AG fault, (b) ABG fault and (c) AB fault 79

Figure 3.10 Incremental voltages seen at the relaying location for ABG faults with fault inception angle (a) 450, (b) 900 and (c) 1350 80

Figure 3.11 Digital signal processing and implementation of the proposed method 85

Figure 3.12 Variation of algorithm parameters with time for a ABG fault (a) incremental voltages, (b) integrated incremental voltages and (c) fault indices.....86

Figure 3.13 Variation fault indices with fault inception angle ϕ for different sample-and-hold times (Ts) (a) Ts=7 ms, (b) Ts=8.33 ms and (c) Ts=10 ms 86

Figure 3.14 Single line diagram of the test network simulated in the DRTS 88

Figure 3.15 Measurements/fault parameters for a mid-line ABG fault (a) Phase-to-ground voltage (b) incremental voltage, (c) integrated incremental voltages and (d) fault indices, (e) fault detection signal (f) ground fault indicator and (g) ABG fault detection.....90

Figure 3.16 Variation fault indices with fault inception angle ϕ for different fault types for mid-line faults (a) AG, (b) BG, (c) CG, (d) AB, (e) BC, (f) CA, (g) ABG, (h) BCG, and (i) CAG 92

Figure 3.17 Variation of fault indices with fault inception angle ϕ for different fault locations (a) AG, (b) BC, and (c) CAG fault....93
Figure 3.18 Variation of fault indices with fault inception angle ϕ for 3-phase faults on Line 12 at different locations (a) 5%, (b) 50%, and (c) 90%....94
Figure 3.19 Variation of fault indices with fault location (%) along Line 12 for (a) AG, (b) BC, and (c) CAG fault....94
Figure 3.20 Variation of fault indices with fault resistance for mid-line faults (Line 12) (a) AG, (b) BC, and (c) CAG fault....95
Figure 3.21 Variation of fault indices with fault inception angle ϕ for a mid-line fault (Line 12) with a fault resistance of 100 Ω for (a) AG, (b) BC, and (c) CAG fault....96
Figure 3.22 Variation of fault indices with fault inception angle ϕ for a mid-line fault (Line 12) with an inductive fault impedance of 7.54 Ω for (a) AG, (b) BC, and (c) CAG fault....96
Figure 3.23 Single line diagram of the modified test networks simulated in the DRTS for a weaker AC grid....97
Figure 3.24 Variation of fault indices with fault inception angle ϕ for a mid-line fault (Line 12) with a weak AC grid for (a) AG, (b) BC, and (c) CAG fault....98
Figure 3.25 Single line diagram of the modified test networks simulated in the DRTS for a different relay location....98
Figure 3.26 Variation of fault indices with fault inception angle ϕ for a mid-line (Line 34) CAG fault (a) with only the IBR connected and, (b) with only the SG connected....99
Figure 3.27 Schematic of the test system simulated in the DRTS for Model-in-the-loop simulations with real IEC 61850 communication....100
Figure 3.28 Measurements/fault parameters for a mid-line ABG fault (a) Phase-to-ground voltage (b) voltage from subscribed SV, (c) voltage resampled at 16 S/C, (d) incremental

voltages, (e) integrated incremental voltages, (f) fault indices, (g) ABG phase selection (h) ABG phase selection sent via GOOSE message 101

Figure 3.29 Measurements/fault parameters for a mid-line evolving fault, AG to ABG (a) Phase-to-ground voltage (b) incremental voltage, (c) integrated incremental voltages and (d) fault indices, (e) AG inception (f) evolving to an ABG fault and (g) ABG fault detection . 102

Figure 3.30 Variation of fault indices with fault inception angle ϕ for a mid-line fault (Line 12) with 15% 2nd harmonic component 103

Figure 4.1 Single line diagram of the test network simulated in the DRTS 109

Figure 4.2 (a) Simplified network with two sources connected by a transmission line, (b) Negative-sequence impedance circuit and (c) Negative-sequence voltage magnitude profile for a forward fault 114

Figure 4.3 (a) Simplified network with two sources connected by a transmission line, (b) Negative-sequence impedance circuit and (c) Negative-sequence voltage magnitude profile for a reverse fault 115

Figure 4.4 (a) Simplified system with an IBR, Sequence networks for (b) a single-line-to-ground fault and (c) a line-to-line fault 116

Figure 4.5 Y Plain, forward and reverse zones are indicated 118

Figure 4.6 Flow diagram of the proposed direction element algorithm 119

Figure 4.7 Single line diagram of the test network simulated in the DRTS 123

Figure 4.8 Trajectory of negative-sequence admittance on a G-B plain (a) forward short circuit AB fault at 50% of Line 12 (b) magnified view 124

Figure 4.9 Trajectory of negative-sequence admittance on a G-B plain (a) reverse bolted AB fault at Bus 1 (b) magnified view 125

Figure 4.10 Trajectory of negative-sequence admittance on a G-B plain for a forward BC fault at (a) 10%, (b) 50%, (c) 80% of Line 12, and (d) reverse fault at Bus 1 126
Figure 4.11 Trajectory of negative-sequence admittance on a G-B plain for (a) forward BC fault at 50% of Line 12, short circuit fault and with a fault resistance of 50 Ω and (b) reverse (Bus 1) short circuit fault and with a fault resistance of 50 Ω 127
Figure 4.12 Trajectory of negative-sequence admittance on a G-B plain for (a) forward bolted faults at 50% of Line 12, BC and AG and (b) reverse fault (Bus 1) BC and AG 128
Figure 4.13 Results for a forward bolted AB fault at 50% of Line 12 (a) Line Current, (b) Bus voltage, (c) Zone 1 AB impedance element, (d) Negative sequence impedance angle, (e) conventional directional element pickup and (f) proposed directional element pickup..... 130
Figure 4.14 Results for a forward bolted AB fault at 50% of Line 12 (a) Zone 1 AB impedance trajectory on R-X plain, (b) trajectory of negative-sequence admittance on a G-B plain 131
Figure 4.15 Results for a forward bolted AB fault at 50% of Line 12 with negative sequence current injection (a) K = 0, (b) K = 1 and (c) K = 2 132
Figure 4.16 Results for a forward AB fault at 50% of Line 12 with additional synchronous generation connected to Bus 1 (a) 10 MVA, (b) 20 MVA and (c) 50 MVA..... 133
Figure 4.17 Results for a reverse fault (a) with additional 50 MVA synchronous generation connected to Bus 1 (b) magnified view 133
Figure 4.18 Results for a forward bolted AB fault at 50% of the Line 12 with only synchronous generation connected to Bus 1 (a) 10 MVA, (b) 20 MVA and (c) 50 MVA..... 134
Figure 4.19 Results for a reverse bolted AB fault with only synchronous generation connected to Bus 1 (a) 10 MVA, (b) 20 MVA and (c) 50 MVA 135
Figure 4.20 Results for a weaker remote grid (a) reverse fault AB fault on Bus 1 and (b) forward AB fault at 50% of the Line 12 136

Figure 4.21 Application of the proposed method in a system with series compensation (a) with an IBR, (b) conventional sources 137
Figure 4.22 Schematic of the hardware-in-the-loop test setup 139
Figure 4.23 Trajectory of negative-sequence admittance on a G-B plain (a) forward AB fault at 50% of Line 12 (b) magnified view (c) reverse bolted AB fault at Bus 1 (d) magnified view 140
Figure 5.1 Simplified single line diagram of the power system during a power swing following a disturbance 146
Figure 5.2 Example positive-sequence current injection requirements during voltage ride-through 151
Figure 5.3 Comparison of theoretical and EMT results, (b) Magnified plot with impedances Zs, Zl and Zr 152
Figure 5.4 Comparison of theoretical and EMT results for different system SCR 155
Figure 5.5 Simplified single line diagram of the power system during a power swing following a disturbance 155
Figure 5.6 Comparison of theoretical and detailed EMT simulation results 156
Figure 5.7 (a) Swing impedance trajectories for no-IBR and base-case IBR scenarios, (b) magnified plot with impedances for Zs, Zl and Zr 157
Figure 5.8 (a) Swing impedance trajectories for different SCR values, (b) magnified plot with respective line impedance for Zs, Zl and Zr, (c) variation of δ 159
Figure 5.9 (a) Swing impedance trajectories plotted with δ for different SCR values; data points correspond to δ=1800 160
Figure 5.10 (a) Swing impedance trajectories for different active power injection, (b) magnified plot with respective line impedances for Zs, Zl and Zr 161

Figure 5.11 Swing impedance trajectories for different source voltage magnitudes (a) no IBR, (b) magnified plot of (a), (c) base-case IBR, and (d) magnified plot of (c) 162
Figure 5.12 (a) Swing impedance trajectories for different levels of reactive current injection during VRT, (b) magnified plot with respective line impedances for Zs, Zl and Zr 163
Figure 5.13 (a) Swing impedance trajectories for different IBR types, (b) magnified plot with respective line impedances for Zs, Zl and Zr 164
Figure 5.14 (a) Swing impedance trajectories for different source impedances, (b) magnified plot with respective line impedances for Zs, Zl and Zr 165
Figure 5.15 Swing impedance trajectories for SCR=2.5 plotted with respective line impedance for Zs, Zl, Zr, and inner and outer PSB and OST blinders 168

List of Copyrighted Material

Not Applicable.

List of Symbols

t : Time

f : Frequency

$\mathbf{R}_f$: Fault Resistance

ϕ : Phase angle

ω : Angular frequency

$\mathbf{L}_{sp1}$: Local source self impedance (rectance) - phase p

$\mathbf{M}_{spq1}$: Local source mutual impedance (rectance) - phase p to q

$\mathbf{L}_{l1p}$: Line self impedance from local end (relay) to fault - phase p

$\mathbf{M}_{l1ab}$: Line mutual impedance from local end (relay) to fault - phase p to q

$\mathbf{L}_{l2p}$: Line self impedance from fault to remote end - phase p

$\mathbf{M}_{l2pq}$: Line mutual impedance from fault to remote end - phase p to q

$\mathbf{L}_{sp2}$: Remote source self impedance - phase p

$\mathbf{M}_{spq2}$: Remote source mutual impedance (rectance) - phase p to q

$\mathbf{\Delta v}_{fp}$: Incremetal voltage at the fault location - phase p

$\mathbf{\Delta v}_{Rp}$: Incremetal voltage at the realying location - phase p

$\mathbf{\Delta i}_{p1}$: Incremetal current flowing into the local source end - phase p

$\mathbf{\Delta i}_{p2}$: Incremetal current flowing into the remote source end - phase p

$\mathbf{Z}_1$: Positive-sequence impedance

$\mathbf{Z}_2$: Negative-sequence impedance

$\mathbf{Z}_0$: Zero-sequence impedance

$\mathbf{G}_2$: Negative-sequence conductance

$\mathbf{B}_2$: Negative-sequence susceptance

$\mathbf{V_1}$: Positive-sequence voltage phasor

$\mathbf{V_2}$: Negative-sequence voltage phasor

$\mathbf{V_0}$: Zero-sequence voltage phasor

$\mathbf{I_1}$: Positive-sequence current phasor

$\mathbf{I_2}$: Negative-sequence current phasor

$\mathbf{I_0}$: Zero-sequence current phasor

$\mathbf{Z_S}$: Positive-sequence impedance of local source

$\mathbf{Z_r}$: Positive-sequence impedance of remote source

$\mathbf{Z_l}$: Positive-sequence impedance of transmission line

$\mathbf{X_d'}$: Transient reactance of the synchronous generator

List of Abbreviations

AC : **A**lternating **C**urrent

BESS : **B**attery **E**nergy **S**torage **S**ystems

CHIL : **C**ontrol **H**ardware-**I**n-the-**L**oop

CT : **C**urrent **T**ransformer

DC : **D**irect **C**urrent

DCB : **D**irectional **C**omparison **B**lock

DDSFR : **D**ecoupled **D**ouble **S**ynchronous **R**eference **F**rame

DER : **D**istributed **E**nergy **R**esource

DFIG : **D**oubly-**F**ed **I**nduction **G**enerator

DFT : **D**iscrete **F**ourier **T**ransform

DRTS : **D**igital **R**eal-**T**ime **S**imulator

DUTT : **D**irect **U**nderreaching **T**ransfer **T**rip

ECA : **E**lement **C**haracteristic **A**ngle

EMT : **E**lectro-**M**agnetic **T**ransient

ERO : **E**lectric **R**eliability **O**rganization

FIA : **F**ault **I**nception **A**ngle

GFL : **G**rid-**F**ollowing

GFM : **G**rid-**F**orming

GOOSE : **G**eneric **O**bject-**O**riented **S**ystem **E**vent

HIL : **H**ardware-**I**n-the-**L**oop

HV : **H**igh **V**oltage

HVDC : **H**igh **V**oltage **D**irect **C**urrent

IBR : **I**nverter **B**ased **R**esource

IEC : **I**nternational **E**lectrotechnical **C**ommission

IEEE : **I**nstitute of **E**lectrical and **E**lectronics **E**ngineers

IGBT : **I**nsulated-**G**ate **B**ipolar **T**ransistor

LADWP : **L**os **A**ngeles **D**epartment of **W**ater and **P**ower

LPF : **L**ow-**P**ass **F**ilter

LAN : **L**ocal **A**rea **N**etwork

LVRT : **L**ow-**V**oltage **R**ide-**T**hrough

LV : **L**ow-**V**oltage

MPT : **M**ain **P**ower **T**ransformer

MV : **M**edium **V**oltage

NERC : **N**orth **A**merican **E**lectric **R**eliability **C**orporation

NIC : **N**etwork **I**nterface **C**ards

OOST : **O**ut-**O**f-**S**tep **T**ripping

PLL : **P**hase **L**ocked **L**oop

POC : **P**oint-**O**f-**C**onnection

POI : **P**oint-**O**f-**I**nterconnection

POM : **P**oint-**O**f-**M**easurement

POTT : **P**ermissive **O**verreaching **T**ransfer **T**rip

PPC : **P**ower **P**lant **C**ontroller

PSB : **P**ower **S**wing **B**locking

PU : **P**er-**U**nit

PV : **P**hoto-**V**oltaic

RES : **R**enewable **E**nergy **S**ource

RFT : **F**ault **R**ide-**T**hrough

SCE : **S**outhern **C**alifornia **E**dison

SCL : **S**hort **C**ircuit **L**evel

SCR : **S**hort **C**ircuit **R**atio

SG : **S**ynchronous **G**enerator

SPC : **S**amples **P**er **C**ycle

SRF : **S**ynchronous **R**eference **F**rame

SSCI : **S**ub-**S**ynchronous **C**ontrol **I**nteractions

STATCOM : **S**tatic **S**ynchronous **C**ompensator

SV : **S**ampled **V**alues

TS : **T**ransmission **S**ystem

VSC : **V**oltage **S**ource **C**onverter

VT : **V**oltage **T**ransformer

WTG : **W**ind **T**urbine-**G**enerator

List of Appendices

Appendix A

Fault Detection in Systems with High IBR Penetration Using Instantaneous Power Measurements..... 187

Chapter 1

Introduction

1.1 Introduction

Electricity production using renewable energy sources (RES) such as hydro, wind and solar power has long been an appealing prospect due to their sustainability and lower environmental impacts. However, only hydroelectricity generation has significantly contributed to world electricity production until recent times. According to reports, 31.82% of electricity produced in the world was from RES, with hydroelectricity accounting for 14.3% of that figure at the end of 2024 [1]-[2]. Contribution of wind and solar power to global electricity production was at 8.1% and 6.64%, respectively [1]. The last decade has seen a drastic reduction of cost of wind and solar PV installations owing to bulk production and technological advances. As a result, wind and solar power integrations into power systems have grown exponentially, as evident from Table 1.1. These RES are integrated into the power grid as small-scale installations at distribution level as well as large-scale plants interfaced at transmission level.

Table 1.1: Electricity production comparison by source, 2010 & 2024

	Electricity production (TWh)			
	Solar	Wind	Coal	Hydropower
2010	32.21	345.93	8,458.00	3,428.15
2024	2,128.37	2,505.35	10,543.84	4,419.95
% change	**+6,508%**	**+624%**	**+25%**	**+29%**

1.1.1 Inverter Based Resources (IBRs)

Due to their off-nominal frequency outputs, a majority of renewable energy-based power sources and accompanying Battery Energy Storage Systems (BESS) require a power electronics inverter at the interface with the main power grid. Power sources interfaced with the grid via inverters are referred to as inverter-based resources (IBRs) [3], [4]. Type IV wind power plants, solar Photovoltaic (PV) generation and BESS facilities are the quintessential examples of IBRs in modern power systems. While IBRs offer a number of desirable features such as generation of relatively clean electricity, their presence introduces a unique set of challenges to the operation and protection of an electric power system [4]-[22].

1.1.1.1. Wind Power Generation

Last decade has seen an exponential growth in wind power generation around the world, both on and off-shore. Several stability and control issues in electrical power systems stem from the ever-increasing penetration of wind generation, which is inherently intermittent [4]. Power system stability issues associated with high levels of wind penetration are well-understood, while finding remedies to them still remains a popular area of research in electrical

power engineering [17]-[33][32] . There are five basic types of wind power plants, which are usually categorized based on the type of wind turbine generator [4], [23]. Type III and Type IV wind systems are of particular interest when system protection is concerned as both types require inverters to be interfaced to the main power system. Type III wind systems use Doubly-Fed Induction Generators (DFIG) to produce electricity, where the wound rotor of the generator is applied an AC excitation from an AC-DC-AC (AC: Alternative Current, DC: Direct Current) frequency converter connected to the stator. A Type IV wind system converts all its output power via a full-rated AC-DC-AC frequency converter before connecting to the main grid. Figure 1.1 and Figure 1.2 depict Type III and Type IV wind turbine-generator systems, respectively.

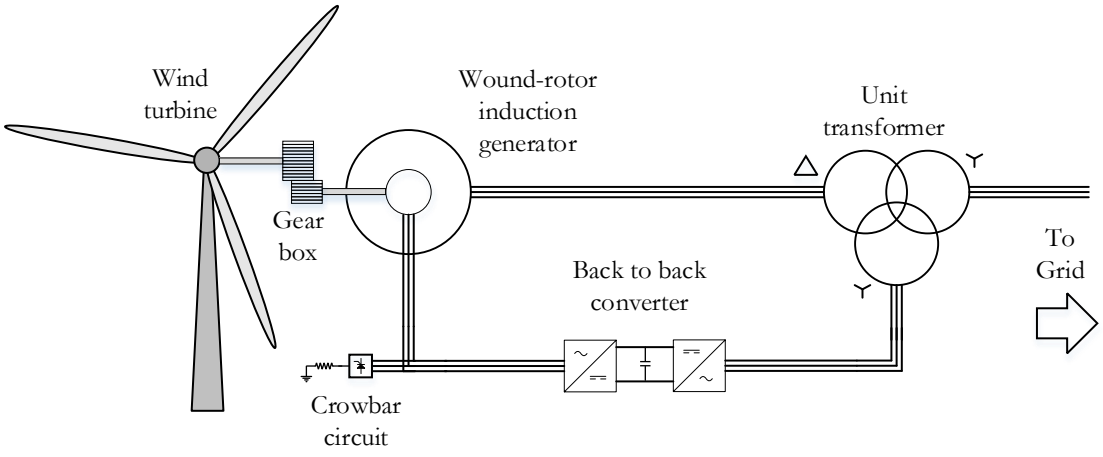

Figure 1.1 Type III wind turbine generation based IBR unit

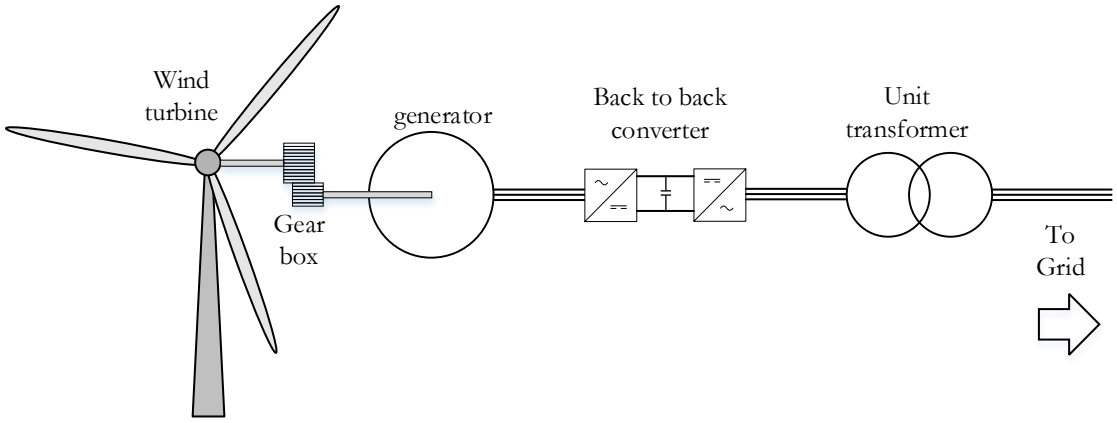

Figure 1.2 Type IV wind turbine generation based IBR unit

1.1.1.2. Solar PV and BESS based Generation

A solar PV system converts sunlight into DC electricity, which in turn is converted into AC electricity to be fed into the electric grid. More recently, large capacity Battery Energy Storage Systems (BESS) are often co-located with other IBRs (such as solar PV) to increase grid resilience and meet interconnection requirements. Standalone BESS facilities (without any RES) are also becoming increasingly common in modern power systems. Both Solar PV generation and BESS plants also require full-rated a DC-AC frequency converter to be interfaced. However, their behaviour (as seen from the power system) is relatively similar to a Type IV wind system as far as power system protection is concerned. All of the abovementioned sources (Type III, Type IV wind systems, solar PV and BESS) require some form of inverter interfacing and thus, commonly referred to as Inverter-Based Resources (IBRs) [23].

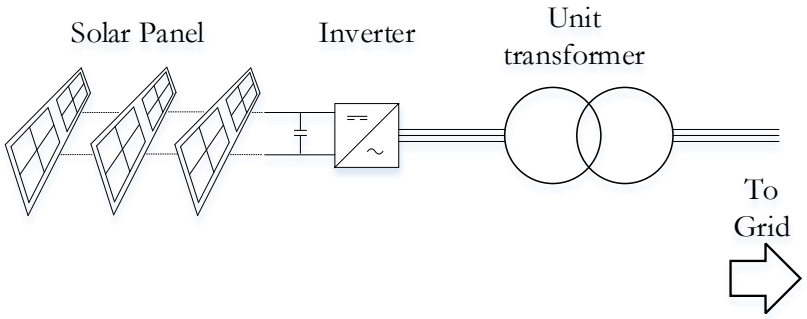

Figure 1.3 Solar PV generation based IBR unit

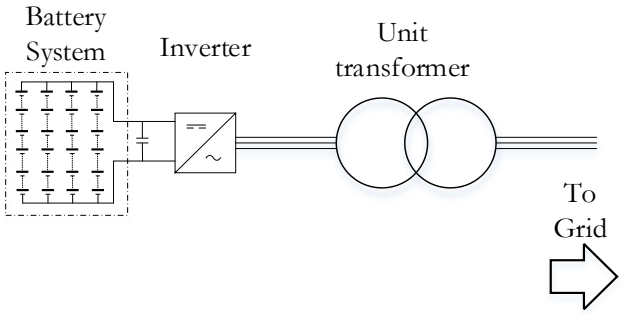

Figure 1.4 BESS based IBR unit

1.1.1.3. IBR Plant

An IBR plant (also known as IBR generating facility) can be viewed as a collection of IBR units (typically multiple units, can be one as well), their supplementary devices and a collector system behind a single reference point (often the HV side of the main power transformer). The overall operation of the plant (all IBR units and supplementary devices) is governed by a common facility-level controller to achieve the applicable performance requirements [3]. Depicted in Figure 1.5 is an example schematic of a typical IBR plant (Solar PV and BESS based).

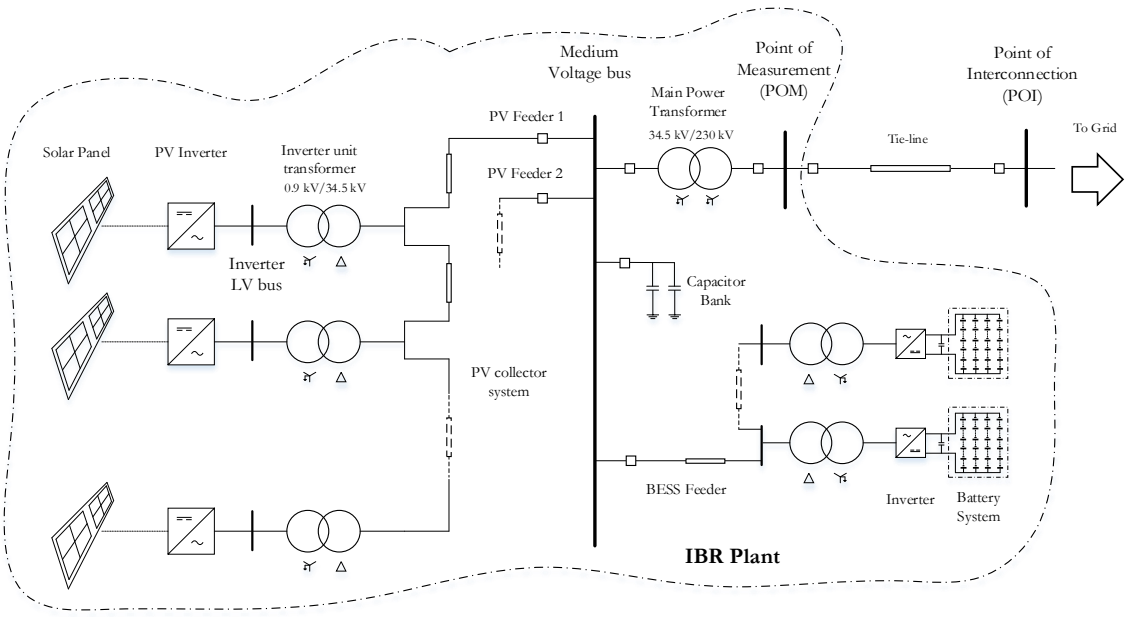

Figure 1.5 An example IBR plant

In its most commonly implemented forms, individual IBR units in a modern IBR plant operate at a lower voltage level (0.5-1.5 kV) and connected to a medium voltage collector feeder system (20-34.5 kV) via a unit transformer. Based on the design, one or more IBR units can be connected via the same transformer. Typical generation capacity of a single IBR unit varies from 1-5 MW. Generally, multiple IBR units are connected to a collector feeder (the exact configuration can vary) and an IBR plant often consists of more than one such collector. Point-of-Connection (POC) is defined as the point at which an IBR unit is electrically connected to a collector system (specified by the IBR owner) [3].

The length of the collector feeders depends on resources type, wind-based generation often requires the longest as it spreads over a larger area. Supplementary IBR devices, which may or may not be inverter-based, are equipment within an IBR plant, and according to IEEE std. 2800, only used to meet some or all of the interconnection requirements. Capacitor banks,

static synchronous compensators (STATCOMs), harmonic filters, protective devices, and plant controllers are examples for supplementary IBR devices [3].

Main power transformer (MPT), or the plant transformer, connects the medium voltage collector bus to the high voltage system. The MPT is usually wye-grounded on the HV side, however, delta connected systems can be found in rare occasions. HV bus of the MPT is generally taken as the Point-of-Measurement (POM) of the IBR plant. The point where an IBR plant connects to the rest of the transmission system (TS) is known as Point-of-Interconnection (POI). The HV transmission line (and associated equipment and systems) that is exclusively used to exchange power from an IBR plant, connecting the POM to the POI is referred to as the IBR tie-line. Typically, IBR tie-line is a short line segment connecting to an exiting switching station in the utility transmission grid. In addition, there are isolated IBR generation plant(s) interconnected to rest of the transmission system via a Voltage Source Converter (VSC) – High Voltage Direct Current (HVDC) transmission facility, and similar performance requirements are applicable to such facilities as IBR plants [3][4]. Their behaviour during faults (on AC system) is generally comparable to regular IBR plants as well.

1.1.1.4. Control and Protection Related to IBR Plants

There are numerous control and protection functions to ensure the safe and reliable operation of an IBR plant. These exist and operate at different levels and are designed to achieve coordinated operation. Note that control and protection functions of a typical IBR plant are discussed only at a high-level in this subsection. It, however, does not cover lower level, power electronic converter controls (such as inner and outer loop current controls),

which are well-established in industry and documented in literature [25],[26]. Controls related to an IBR facility can be broadly divided into two categories as plant-level controls and inverter-level controls. Plant-level controls are generally facility-level controls that govern steady state behavior of the plant as a whole. Examples include plant's active power control (for RES, typically set to extract the maximum amount of available power, for BESS a bi-directional set-point), reactive power control (based on mode of operation, can be a reactive power set-point, voltage control, power factor control etc.). Dynamic behaviour of an IBR plant can be influenced to a certain degree by plant-level controls as well. Typically, plant-level controls are implemented in a separate high-level controller, often referred to as the Power Plant Controller (PPC), which takes measurements at the POM and accordingly, sets control inputs to be fed into the inverters. Even when there is more than one generation source (such as in a hybrid facility), the PPC is responsible for the overall control of the plant as a whole.

On the other hand, inverter-level controls typically dominate the dynamic behavior of an IBR, specially during large transients such as faults. Controls related to fault ride-through (RFT) such as reactive current injection (for voltage support), active power injection (to arrest frequency excursions) and asymmetrical or negative-sequence current injection (to support protection functionality) are generally implemented at inverter level based on measurements at its local terminal. It should be noted that negative-sequence current injection is also a fairly recent development in IBR technology, and only incorporated into newer systems (most existing IBRs in power systems do not have negative-sequence current injection capability).

In addition, IBRs can be also broadly divided into two categorized based on their inverter's control architecture, namely, grid-following (GFL) or grid-forming (GFM). Grid-

following inverters operate in synchronism with the AC grid voltage (and therefore frequency and phase angle) by means of a Phase-Looked Loop (PLL). From a high-level system perspective, grid-following inverters can be viewed as current sources with a regulated power output. By design, they do not attempt to actively control the frequency of their output, but merely follows the grid reference. Grid-following IBRs operate well when connected to relatively strong AC systems, however, can perform poorly in weaker grids. On the contrary, grid-forming inverters are capable of independently regulating the voltage and frequency of their output (operates as voltage source from a high-level perspective). Therefore, they can deliver better performance in weaker AC grids or even form its own grid in an islanded system. Grid-forming architecture also allows implementation of other advanced control features such as providing virtual inertia. As more and more conventional rotational generation being replaced by IBRs (which in turn makes the AC grids weaker), there is a growing demand for IBRs to acquire grid-forming capabilities. Note that a majority of exiting IBRs in present power systems are operating in grid-following mode, although a considerable portion of newly commissioned IBRs have grid-forming capabilities (they all may not be operating in grid-forming mode, however). It should also be emphasized that both types of inverters are based on VSC-HVDC technology. However, note that while they share a similar high-level control architecture, there may be differences in hardware and implementation of some of the control functionality and performance requirements between IBRs and generic VSC-HVDC converters connecting two points in a transmission system.

In addition to their control operation, inverter systems often come with integrated protection functions to protect itself from abnormal system conditions. A good example of

this is VRT protection function, which is basically a set of the time-delayed over and under voltage elements meant to protect inverter hardware from temporary over/under voltages. A similar form of protection is often implemented for over/under frequency as well. Some inverters also come with fast-operated (or instantaneous) overvoltage elements to protect against transient over-voltages. In addition, there may also be embedded overcurrent protection elements as well. When these protection elements are triggered, the inverter is either tripped off using an internal circuit breaker or driven into momentary cessation (stop injecting power) until the system recovers. Additionally, the electrical substation that contains the IBR plant also has its own protection system, which often comprises of feeder protection relays to protect IBR collector feeders (usually overcurrent and overvoltage protection) and a transformer differential relay to protect the MPT.

All of the protection elements above-mentioned need to be coordinated with each other as well as inverter ride-through settings (current injection thresholds), and applicable interconnection requirements [24].

1.1.1.5. Regulatory Bodies and Applicable Standards

This subsection presents a very brief introduction to some of the key regulatory bodies and applicable industry standards governing the interconnection and operation of IBRs (focusing on North America only). North American Electric Reliability Corporation (NERC), also the national Electric Reliability Organization (ERO) of the United States, is a key player in the development of standards for power system operation (including those related to IBRs) and enforcing their compliance. For example, NERC standard PRC-029-1 defines frequency

and voltage ride-through requirements for IBRs and enforces its compliance in facilities in its jurisdiction [24]. Moreover, there are several other reginal regulatory bodies that define specific requirements for interconnection and operation in their own region.

IEEE Std. 2800-2022 (IEEE Standard for Interconnection and Interoperability of Inverter-Based Resources (IBRs) Interconnecting with Associated Transmission Electric Power Systems), released in 2022, standardized most of the common practices and prevailing requirements for interconnection of IBRs in the industry. It has presented a consistent set of minimum requirements for interconnection, capability, and performance of IBRs connected to power transmission (or sub-transmission) systems [3]. Although its adaptation is voluntary, most entities have adopted or planning on adopting IEEE Std. 2800-2022 (at least in part) in foreseeable future.

1.1.2 Behaviour of IBRs during Faults on the AC Transmission System

Dynamic behaviour of IBRs generally is significantly different from conventional synchronous generators-based power plants, particularly during faults on the AC system. In a power system protection study, a synchronous generator can be accurately modeled as voltage source behind an impedance (typically using sub-transient values), and therefore, the fault currents fed into the fault can also be accurately estimated. In contrast, fault current contribution from an IBR is not solely governed by electrical characteristics of its generators. As mentioned above, most of the modern IBRs, due to their variable frequency outputs, require power electronic converters to interface with the transmission system. Control systems of these converters have a major effect on the dynamic behavior of the plants during disturbances [4]. It is

worth noting that in the context of this Thesis, the behaviour of IBRs during faults is viewed at a high level (as seen from the bulk AC power system) as the work presented in this Thesis focuses on transmission level protection of the AC system.

Traditionally, IBRs are perceived to provide very little reactive power support to the system and have weak fault ride-through capabilities. Disconnecting IBRs from the grid during faults has also been a prevailing practice in some systems (particularly for interfacing at distribution level) as a protective measure [9]-[11]. In recent years, this behavior has largely changed due to the enforcement of gird-codes throughout the world, which demand a minimum level of Fault Ride-Through (FRT) capability from IBRs [4], [3]. The manner in which the minimum fault ride-through capability is defined vary from one gird-code to another and IBRs use different control techniques to meet these requirements [3], [34].

The fault current contribution of modern IBRs is heavily dependent on its terminal voltage and has a non-linear relationship with the voltage magnitude [5]. Under reduced terminal voltages during a fault, an IBR might have to increase its current output up to its maximum, (typically around 1.1 pu), in order to meet the real and reactive power requirements enforced by the grid-code. However, should the terminal voltage drop below a certain threshold, the IBR control system may completely shut down its operation. In addition, delta connected interconnection transformers can alter the terminal voltage of the IBR for grid-side faults, which in turn further reduces the fault current contribution from the IBR.

Moreover, conditions of the system prevailed before the inception of the fault also can have a bearing on the fault current contributions of an IBR. For example, terminal voltage, input level of the source (wind speed, solar irradiation etc.), power output and power factor

of an IBR prior to a fault can affect nature of the fault current of an IBR. In certain cases, such as with Type III wind systems, the severity of the disturbance can also dictate the behaviour of fault currents due to the operation of auxiliary controls such as the crowbar system.

Conventionally, synchronization systems (for example, synchronous reference frame (SRF) based SRF-PLL) of grid-connected IBRs are designed to detect the positive-sequence component of the fundamental frequency grid voltage. These systems (i.e. PLLs) are often equipped with workarounds such as filtering to track the positive-sequence grid voltage even during unbalanced grid conditions (for example, the double frequency oscillations in d-axis signals during unbalanced conditions can be filtered out using a low-pass or a notch filter) [25]. As such, IBRs with conventional synchronization systems and controls inherently inject balanced currents, since their references are generated using a balanced measurement, even during unbalanced grid conditions. Note that some VSC-HVDC controls may even actively supress negative-sequence current injection using more sophisticated decoupled double synchronous reference frame based (DDSFR-PLL) controls. Due to various power system protection related issues (some of which are covered in subsequent sections), capability to inject negative-sequence currents (replicating a synchronous machine to a certain degree) during unbalanced conditions has been incorporated into newer generation of IBRs. However, it is worth noting that most existing IBRs in power systems are from previous-generations, which usually do not have negative-sequence current injection capability. Even in newer systems, negative-sequence current injection feature is often disabled unless specifically demanded by a regulatory requirement, which at the time of this writing, is not common in North American systems (it has been mandated in other parts of the world, however [35]). In addition, injection

of negative-sequence currents from control actions takes time (detection of an un-unbalance, controller delays etc.) and its coordination with other control objectives of the system may not be straightforward. For example, even if an IBR is equipped with unbalanced current injection during faults, related control functions of the IBR may not respond fast enough to be relied upon for primary transmission level system protection functions (applicable IEEE 2800 VRT performance requirements are '*step response time ≤ 2.5 cycles'* and '*setting time ≤ 4 cycles'*, with provisions for even greater values if the system warrants them [3]). Moreover, making decisions based on currents injected by IBRs before its controls has settled down (i.e. while still in a dynamic state) may compromise reliability of protection. Hence, the dynamic behaviour of an IBR (with respect to its sequence current injection) may be significantly different than a synchronous machine (especially during the first cycle following fault inception, in which protection functions of transmission relays typically operate).

Conventional phasor-based protection algorithms often exploit and rely on the fact that the currents during faults invariably exhibit certain characteristics such as higher magnitudes (in comparison to load currents), being highly inductive and asymmetrical (for asymmetrical faults). In contrast, fault currents from IBRs are lower in magnitude and do not exhibit a universal behavior (potentially non-inductive and symmetrical) [4]. Reliance on such assumptions compromise the reliability of conventional protection algorithms in the presence of IBRs. In addition, weather conditions can introduce significantly large and intermittent changes in IBR outputs, which could further increase the vulnerability of protection schemes. Table 1.2 summarizes characteristics of fault currents from conventional synchronous generators and IBRs.

Table 1.2: Comparison of fault currents from conventional synchronous generators and IBRs

Fault currents from synchronous machines	Fault currents from IBR
▪ High in magnitude	▪ Low in magnitude
▪ Uncontrolled	▪ Highly controlled
▪ Characterized by electrical parameters of the synchronous machine and the short circuit path	▪ Characterized by control strategy of the power electronic converters and applicable grid codes
▪ Highly inductive	▪ Can be non-inductive
▪ Asymmetrical (for asymmetrical faults)	▪ Symmetrical (for asymmetrical faults)

In addition, the impact of IBRs on electromechanical dynamics of power systems is significantly different from that of a traditional synchronous generator. This is primarily due to limited rotational inertia contribution from IBRs, due to the decoupling caused by power electronic inverters (specially IBRs using full-frequency conversion such as Solar PV and Type IV wind). Furthermore, their electrical behaviour during an electromechanical transient is also different from that of a synchronous machine. As a result, power swing characteristics (both trajectory and speed) of a power system may change significantly with IBR penetration [4].

1.2 Challenges to Traditional Protection Philosophy

Previous generations of renewable energy-based resources (and IBRs) were smaller in size and primarily connected to distribution networks. With the emergence of active distribution systems, integration of small-scale wind and solar PV units into the power system became a realizable prospect and, having a few small-scale RES as distributed generation resources (DER) is commonplace in modern electric power distribution systems [36]. Effective means of protecting microgrids with a number of DERs is a challenging task and has been one of the most studied areas in power system protection in recent years. Protection issues caused by DERs integrated to microgrids are also well-documented [37]-[41].

However, as technology matured, integration of large-scale IBRs to transmission networks became viable and an ever-increasing number of large-scale IBRs are being connected to transmission networks around the world. Although there is no clear definition, renewable energy sources-based power generation with a power generation capacity greater than 1 MW is considered utility-scale (or large scale). Power system protection challenges caused by high penetration of IBRs is a well-discussed topic in recent literature [4]-[18], while finding remedies to them continues to be a prevalent area of research [17]-[33].

Figure 1.6 illustrates typical IBR interconnections to a contemporary transmission network (loosely based on examples given in [4] and [13]). Here, a conventional synchronous generation plant is delivering power to a strong remote grid via transmission lines 13 and 35 (*Line 13* and *Line 35*). As can be seen, this segment of the network has a large IBR (wind and solar PV) integration as well. *Line 34* connects two wind generation plants to the rest of the network at *Bus 3* while *Line 12* delivers power from a solar PV plant to *Bus 1*. Protection relays

(denoted by Rxy) are installed at either end of each transmission line. It is apparent that some of those relays will have to operate on fault currents dominated by IBRs depending on the location of the fault and other system operation conditions (for example, when a synchronous generation based plant is out-of-service).

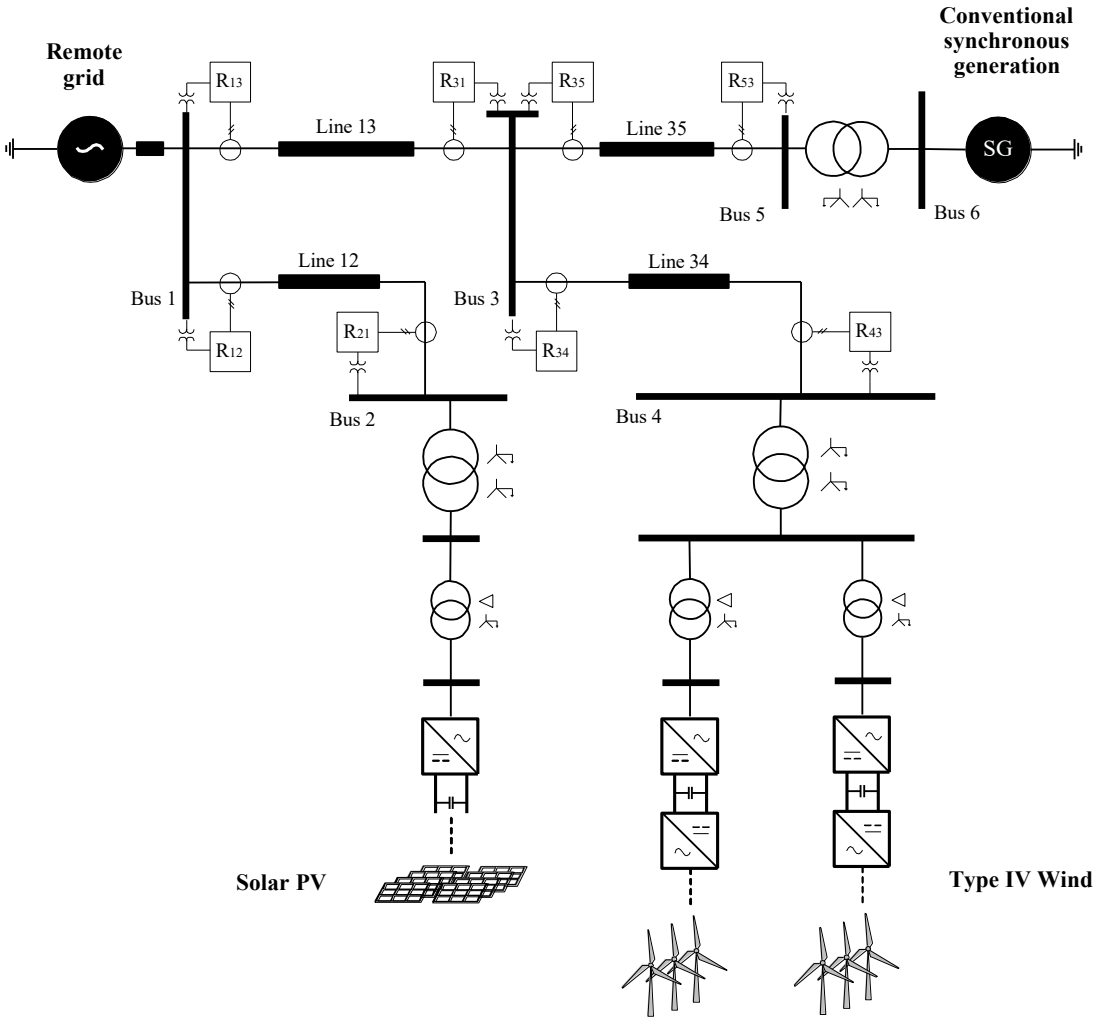

Figure 1.6 Typical IBR interconnections to a transmission network

Following basic protection functions are vulnerable when operating on IBR injected currents and voltages,

- Overcurrent protection
- Fault location/directionality
- Distance protection
- Faulted phase identification/phase selection
- Power swing protection

1.2.1 Impact on Overcurrent Protection and Directional Elements

The control system design in IBRs is often manufacturer specific. One of the main objectives of such a control system during a grid fault is to maintain the magnitude of currents injected within thermal withstand limits of power electronic switching devices (for example, IGBTs). Adhering to applicable grid code requirements is another control objective of such control systems. As a result, fault currents magnitudes produced by IBRs rarely go beyond 2.0 p.u. (typically 1.0-1.2 p.u.) and, in some scenarios, even decay down to zero within several cycles [4]. Due to lower magnitude fault currents, dependability of all overcurrent functions and supervisory elements are potentially compromised, and their usability for backup protection is severely restricted.

1.2.2 Negative-Sequence Quantities-based Protection Algorithms

In symmetrical component theory, it is a well-established fact that conventional sources (synchronous machine based) inject significant amount of negative-sequence currents

into the system during all types of unbalanced faults. Conversely, their abundant presence in the system measurements is a good indication of a fault. Consequently, negative-sequence quantities are commonly used in modern digital relaying algorithms for applications such as fault detection, phase selection and identification of fault location and direction. Typically, negative-sequence elements have very good sensitivity to unbalanced faults and provide dependable fault identification. In addition, they are often used to supervise other protection functions due to their elevated sensitivity to unbalanced fault conditions. Therefore, vulnerability of negative-sequence elements affects the reliability of an entire protection scheme [4], [16], [15].

As motioned in subsection 1.1.2 above, most of the contemporary IBR control designs are known to suppress negative-sequence currents and inject only positive-sequence currents under all fault conditions. This violates the fundamental assumption the negative-sequence protection algorithms are based on for identification of system faults.

1.2.2.1. Negative-Sequence Overcurrent Element (51-2)

Similar to all overcurrent elements, a negative-sequence overcurrent element also operates when the magnitude of the negative-sequence current seen by the relay exceeds a prescribed threshold. As discussed earlier, IBRs with full-scale back-to-back frequency convertors (full-frequency convertors) such as Type IV wind generation and solar-PV generation are known to inject very little negative-sequence currents into the system. Literature on the subject claims negative-sequence current magnitudes can be as low as 0.1 per-unit (p.u.) [4].

These levels of negative-sequence currents are typically well-below the pick-up currents of the corresponding elements, and are even below typical threshold settings used for negative-sequence current supervision. Moreover, since IBR fault currents are unpredictable and time decaying, setting overcurrent elements, particularly time-delayed overcurrent elements become even more challenging.

1.2.2.2. Negative-Sequence Directional Element (67-2)

Most modern numerical relays include some form of negative-sequence quantities-based element in the overall directional identification logic [16]. It is a common practice to prioritize the negative-sequence element when determining the directionality of a fault due to its enhanced sensitivity to unbalanced faults [4], [42], [43].

Generally, directional elements require a preset minimum magnitude of corresponding sequence voltage and current to be activated. Contemporary IBRs usually do not produce enough negative-sequence currents to activate the corresponding directional element. However, if the thresholds for negative-sequence elements are not set with care, a relay fed with an IBR could make decisions on directionality based on available negative-sequence voltages and currents, which are highly controlled and time varying, in addition to being very low in magnitude. Simulations and field events have shown that relay algorithms tend to produce unreliable decisions under such circumstances [4], [13].

1.2.3 Impact on Distance Protection

1.2.3.1. Phase Current Supervision

Impedance based elements in modern line protection relays are supervised by a system current (phase-phase current, phase-ground current or residual current). Impedance elements will not assert if this supervision current is below a minimum threshold. Scenarios where the fault current is largely made-up with contributions from IBRs puts distance protection schemes at risk of not operating for in-zone faults due to not satisfying the current supervision logic. This is true for all types of impedance elements irrespective of them detecting the fault correctly. The dependability of zones 2 and above, for which there are added time delays, is of particular interest in this regard as fault current magnitudes from IBRs tend to decay rapidly after few cycles [4].

1.2.3.2. Polarization Voltage

It is a very common practice in distance relaying to use cross or sequence voltage polarization for implementing impedance-based protection elements. It is also understood that the use of such voltage polarization results in dynamic expansion of the protection zone. For example, a positive-sequence voltage polarized Mho element would dynamically expand into the third quadrant for a forward fault in a conventional system with highly inductive source impedances. The amount of expansion is directly related to the magnitude of the source impedance behind the relaying point [4].

When the source feeding the fault is an IBR, the apparent impedance seen by the relay is dictated by the control system of the IBR. Low fault current magnitudes produced by IBRs generally results in high source impedances, which in turn expand the relay's Mho circle considerably. Due to highly controlled nature of the post-fault IBR current, the apparent source impedance (impedance behind the relay) can be non inductive as well. The unpredictable and constantly varying nature of the IBR fault current exacerbates the issue further. Similar issues are seen for elements with other polarizing quantities like negative-sequence voltage. These affect reliable operation of the relay, as the expansion of the voltage polarized Mho circle depends on the source impedance [4], [22].

1.2.3.3. Faulted Phase Identification

The accurate identification of the faulted phase is an integral part of typical line protection schemes and becomes particularly important when single-pole tripping is desired [42],[44],[45]. Compared to conventional synchronous generators, IBRs inject significantly small and unpredictable unbalanced currents. As a result, most conventional faulted phase identification methods, which often rely on the relative phase angle of fault currents and voltages, perform poorly in the presence of IBRs [4],[16]-[18]. In general, faulted phase identification methods based on a phasor quantities do not perform well in systems with IBRs as they depend on either the existence of reliably detectible amounts of sequence components (negative and zero) or/and the relative phase angle of fault currents and voltages. There are straightforward workarounds to some of the issues caused by unreliable operation of faulted phase identification, such as the use of phase undervoltage elements (for faulted phase identification)

to supervise distance elements in system with IBRs to prevent them from overreaching [16],[17]. For example, a phase distance element can overreach for a resistive LG fault and faulted phase identification is used for supervision to prevent this from occurring (similarly, a ground distance element can overreach for an LLG fault). However, applying the same solution for other applications such as single-pole tripping is not discussed in literature. In addition, since phasor-based methods can approximately take up to one (1) power frequency cycle to operate, they may not be able to cater strict stability margins and critical clearing times of some systems due to reduced system inertia [45]. A more through review of existing faulted phase identification methods is presented in Section 2.2.

1.2.4 Impact on Power Swing Protection Schemes

Power swings origin due to major system disturbances such as loss of large generation/ load that cause abnormal variations in power flow. Power system protection devices (impedance-based relay, in particular) are prone to interpret these events as faults, prompting undesired tripping. Line protection relays are often provided with power swing protection schemes in order to counter for such eventualities. Functionality of a power swings protection scheme is twofold; namely power swing blocking (PSB) and out-of-step tripping (OST). Power swing blocking is used for distinguishing power swings from faults and out-of-step tripping is used for separating stable power swings from unstable ones. Both types of swing protection are based on swing impedance. PSB is measuring the time taken for the impedance observed at relaying point to travel from one threshold value (referred to as blinders) to another. The principle behind this is that the rate of change of swing impedance is slugging as it is restrained

by the system inertia. In comparison, impedance change during a fault is almost instantaneous with signal processing in the relay adding a delay of around one cycle for detection. On the other hand, OST is triggered when the swing impedance enters a predefined zone, which is based on the least stable power swing characteristic [4], [6].

IBRs, particularly those with full-frequency conversion (such as Solar PV and Type IV wind) do not contribute rotational inertia to the connected power system, due to the decoupling caused by power electronic inverters (or the inherent lack of rotating masses). As a result, power swing characteristics of a power system may alter with IBR penetration in two primary ways. Firstly, swing impedances moves faster due to the lack of inertia of the system, and power swing protection timer settings calculated without accounting for this fact may not be able to discriminate between a fault and a stable power swing [4]. Secondly, since the control behaviour and response times of IBRs are significantly different than conventional synchronous machines, their presence may alter the impedance trajectories during power swing conditions. However, several recently published work in literature have already explored the effects system inertia (or lack thereof) on the rate-of-change of the apparent impedance during a power swing, while their bearings on the actual impedance trajectories (on R-X plain) have not been scrutinized to the same extent. Therefore, a through evaluation of the effect of IBRs on power swing characteristics is warranted.

1.2.5 Objectives of the Thesis

With the background provided above, the primary objectives of the work that resulted in this Thesis are summarized below. The work was focused on the protection of radially-connected terminals of AC transmission systems with IBRs. It mainly considered full frequency converted, grid-following IBRs such solar PV, Type IV wind and BESS generation facilities without negative-sequence current injection capabilities, for which IBR-related power system protection issues are at their worst.

- Objective 1: Analyzing the impact of IBRs on conventional faulted phase identification algorithms, validating theoretical expectations through simulations and testing of commercial relays, and development of improved solutions for faulted phase identification.

- Objective 2: Investigating the effects of IBRs on conventional fault direction identifications, development of an enhanced protection algorithm to correctly identify the fault direction in system with heavy IBR penetration and evaluation of its performance.

- Objective 3: Studying the effects of IBRs on electrical trajectories of power swing protection using theoretical analysis and investigation of potential impacts on power swing protection.

1.2.6 Theis Overview

What follows is a very brief overview of each subsequent Chapter of this Thesis. Chapter 2 presents a detailed literature review of each of the objectives identified in subsection 1.2.5. Reviews on each specific area under investigation are provided with relevant work in literature, identified research gaps and specific research objectives. Discussed in Chapter 3 is the research on studying the impact of IBRs on faulted phase identification algorithms and development of improved solutions. Chapter 4 covers the investigation on direction identification of transmission line faults connecting IBRs and development of an improved protection algorithm to identify fault direction in such systems. Investigation on the effects of IBRs on electrical trajectories of power swing protection using theoretical analysis is presented in Chapter 5. Chapter 6 follows with overall conclusions, contributions and potential future work of this Thesis.

Chapter 2

Challenges Posed by IBRs to Traditional Power System Protection

2.1 Introduction

As mentioned in Chapter 1, power system protection issues related to IBRs are a common area of research in power systems engineering in recent times. However, many of the issues discussed are case-specific and often presented without adequate information to be reproduced by an independent party. Furthermore, conclusions made in some literature is entirely based on simulated relay models thus their validity and implications on real-world power system applications are uncertain. This chapter lays out detailed reviews for each of the IBR-induced power system protection related issues identified in above subsection 1.2.5. Each specific subtopic under investigation is provided an independent literature review identifying research gaps and specific research objectives.

The proposed research in this Thesis, firstly, intend to investigate a selected set of power system protection issues related to IBRs mentioned in literature and validate them using detailed EMT type simulations and also by testing commercial protection relays in a hardware-

in-the-loop setup, when applicable. Secondly, further investigations on the identified issues will be carried out, and improved protection techniques will be introduced to overcome some of the complications posed by IBR penetration.

Based on the literature review and preliminary investigations carried out in Section 1.2 of Chapter 1, a few functions related to power system protection were identified as specific areas of focus of this Thesis. Each of the following subsections is dedicated to a specific area of interest, providing an overview of the research gap(s) identified and the reasons that warranted their further investigation.

2.2 Faulted Phase Identification

In conventional power system protection, determining the faulted phases involved in a fault is a critical aspect of transmission line protection schemes. Many other protection functions including distance protection and fault location are often supervised by some form of faulted phase identification (phase selection). Furthermore, faulted phase identification is indispensable for single-pole tripping and reclosing schemes, where only the faulted phase must be operated for a single-phase-to-ground faults while operating all three phases for multi-phase faults [6], [8], [46]-[47].

2.2.1 Conventional Methods

In contemporary power system relaying, several different algorithms are being used for faulted phase identification and phase selection. These methods, designed for synchronous machine-based generation, generally produce accurate results over a variety of conditions for conventional systems. Many commercial relay manufacturers use a symmetrical component-based technique for faulted phase identification [42]-[44], [48], [49]. Implementation details of this method vary slightly from relay manufacturer to manufacturer, but all of its variants essentially determine the phase(s) involved in a fault based on the measured the phase angles between sequence currents and/or voltages during a fault. The key aspects of such relaying algorithms are explained below.

In its most generally realised form, faulted phase identification using symmetrical components use the phase angle signature of '*Phase A*' sequence currents to determine the phases involved in a fault. The symmetrical component theory and the boundary conditions at the

fault dictate that the phase angle difference between negative and the zero-sequence currents lies within a distinct region for particular types of faults. As depicted in Figure 2.1-(a), '*Phase A*' negative and zero-sequence currents reside within specific regions, when the fault is one of two types (indicated on the diagram). For example, angle difference between '*Phase A*' negative and zero-sequence current phasors during a bolted (low impedance) BG fault is theoretically −120°. And, the same relationship holds true for a CAG fault. It is worth noting that a different, yet distinct phase angle relationship also exists between the negative and the positive-sequence current phasors during ground faults, as shown in Figure 2.1-(b).

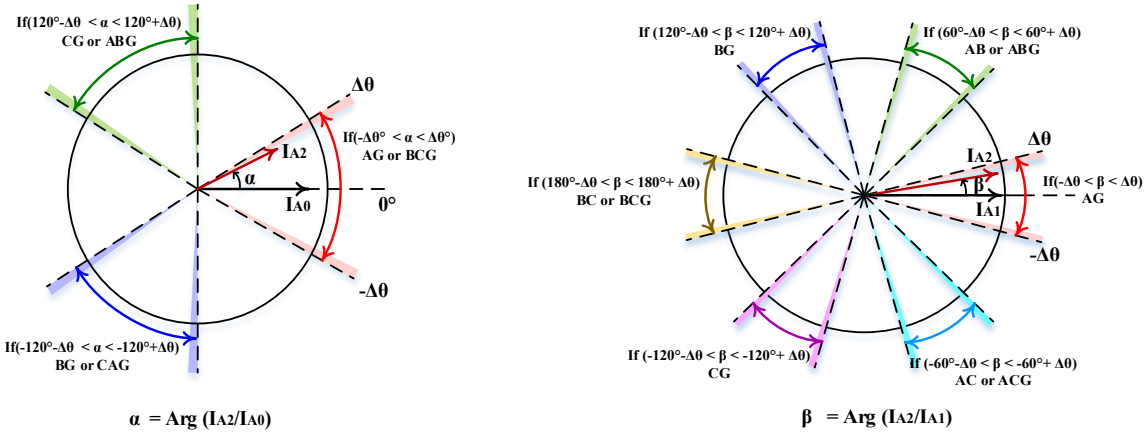

(a) (b)

Figure 2.1 a) Angle difference between 'Phase A' negative and zero-sequence current phasors during bolted faults (i.e., α), (b) Angle difference between 'Phase A' negative and positive-sequence current phasors during bolted faults (i.e., β).

Several methods are being employed by manufacturers to choose between the two possible fault types with the same phase angle signature (BG or CAG). One such example is to select the fault type with the lower (impedance) reach from the corresponding impedance element. This is rooted on the understanding that the actual faulted loop would have a much lower impedance estimation than the un-faulted one [44]. For example, for a phase-A-to-

ground fault, the AG impedance element would yield a much lower reach than the BG or CG elements. Certain other vendors measure phase angle signatures of all three phases and use a combined logic to identify the faulted phase [43]. Combining both phase angle signatures (α and β) to determine and verify the faulted phase has been used by others. It is also noteworthy that phase angle signatures of sequence voltages provide similar information about the faulted phase and can be used in faulted phase identification.

In addition to sequence components-based fault phase identification techniques above-mentioned, there are somewhat older methods that entirely rely upon impedance elements to determine the faulted phase [42]-[44]. These methods use overreaching impedance zones to develop a phase-phase-ground signal that supervises the respective distance Zone 1 phase and ground elements, while issuing trip commands accordingly. Here, discrimination between phase-phase-ground and phase-phase faults is achieved using a zero-sequence pickup signal. A simplified schematic of the logic used in such a method is given in [42]. Furthermore, line current differential relays typically employ phase-segregated differential elements and determine the faulted phases based on the operated elements [18]. As mentioned in subsection 1.2.3.3, the time-varying and unpredictable nature of phase angles of the currents produced by IBRs during faults has rendered most of the above-mentioned methods unreliable. This is further exacerbated by the lack of sequence currents produced by IBRs. Generally, conventional phase angle-based methods perform poorly in system with IBRs, and are seldom used as the primary method of faulted phase identification in such systems.

Although it has been mentioned in the relevant literature that conventional faulted phase selection algorithms can be vulnerable in the presence of IBRs, their performance has

not been rigorously analyzed by most of them [17], [27]. The work conducted in [27] analyzes one of the methods used for faulted phase selection and proposes an improved technique. It also evaluates the performance of commercial relays under IBR currents, but it is unclear what portion of mis-operations presented in the results directly resulted from inaccurate phase selection.

2.2.2 Transient-based Methods

Transient-based faulted phase identification methods can deliver very fast results compared to phasor-based methods (typically under 1 ms as opposed to 12-16 ms), allowing much faster fault clearing times [50]-[56]. More pertinently, they also fare better in the presence of IBRs as they extract information from higher frequency components of system measurements, which are less dependent on the source. This is due to the fact that the transient (high frequency) behaviour of the system is largely oblivious to the steady state and dynamic response of the source (in this case, an IBR and its controls). However, several noticeable drawbacks accompany transient-based methods. By their very nature, transient-based methods are sensitive to Fault Inception Angle (FIA), fault impedance and discontinuities in line impedance. In particular, they have been shown to be ineffective for high-impedance faults occurring at specific FIAs (such as those occurring close to zero-crossing of the voltage waveform). Unreliable performance during line-line-ground faults had also been reported in literature [50]. Furthermore, a majority of transient-based techniques proposed in literature requires computationally intensive signal processing and advanced decision-making processes such as machine learning techniques. Implementation of such methods in the real-world demands high-bandwidth

transducers (specially for voltage), and very high sampling rates to facilitate high-fidelity signal processing. In addition, extensive testing and reliable data are needed to train and optimize these systems. All of the above amounts to significantly higher costs and effort in engineering and can render transient-based faulted phase identification unfeasible to implement at scale. There are few studies on using fault-induced transients for faulted phase selection [50]-[56], however, their applicability has not been tested in the presence of IBRs for most of them.

2.2.2.1. Incremental (superimposed) Quantities based Methods

In many aspects, incremental quantities (also known as superimposed quantities) based methods of faulted phase identification offer the middle ground between those using phasor and transient quantities. They offer faster results than phasor-based methods, but are slower than transient based ones. On the other hand, they deliver better overall reliability than transiens based methods, while performing comparably to phasor-based methods (for general applications). Both phasor and incremental quantities based methods are less resource intensive than their transient-based counterparts. Table 2.1 presents a general comparison of faulted phase identification methods using phasor, transient and incremental quantities. Note that this is a generalized comparison considering all applications and it doesn't not compare specific algorithms (moreover, aspects like reliability are heavily dependent on the individual algorithms, their implementation and application). As can be seen from the comparison presented in Table 2.1, incremental quantities based methods offer a compromise between several important aspects including reliability, speed of operation and cost. A comprehensive review on different faulted phase identification methods can be found in [57].

Table 2.1: Comparison of faulted phase identification methods

Attribute	Faulted Phase Identification		
	Phasor-based	**Transient-based**	**Incremental quantities based**
Operation	▪ Mostly uses phase angle relationship between current/voltages extracted from a phasor calculation	▪ Based on information extracted from high frequency transients	▪ Based on incremental quantities (i.e. difference between instantaneous voltages/currents and those from the previous cycle)
Reliability	▪ High in regular applications ▪ Low with IBRs (ones dependent on angles), magnitude only methods perform better	▪ Lower than phasor-based methods, in general ▪ Higher than phasor-based methods with IBRs	▪ Comparable to phasor-based methods, in general ▪ Can be implemented to perform adequately with IBRs
Speed	▪ Lowest ▪ Takes 10-16 ms typically	▪ Highest ▪ Takes <1 ms typically	▪ Medium ▪ Takes 4-10 ms typically
Engineering cost	▪ Low ▪ Commonly implemented in commercial relays	▪ High ▪ Often requires higher preforming hardware	▪ Low, Comparable to phasor-based methods ▪ Commonly implemented in commercial relays

Several noteworthy attempts can be found in literature for incremental quantities based faulted phase identification [45], [58]-[64]. In [45], a method based on rate-of-change of incremental current had been proposed to identify fault type. However, it was noted that the method yielded poor performance for IBR generated fault currents. The method proposed in [58] is dependent on phase angles of sequence measurements and the one given in [59] uses relative level of three scalar products between incremental voltages and currents to determine the faulted phase. As a general rule, the use of currents or depending on phase angle measurements is ineffective for faulted phase identification in system with IBRs, due to their fault behaviour being unpredictable [45], [63]. A faulted phase identification method using

incremental voltage is more likely to produce satisfactory performance in such systems, as system voltages are less affected by IBRs compared to currents. Work presented in [60]-[63] have proposed using incremental voltage for identifying faulted phase. In [60], a technique using relative phase-angle relationship between superimposed sequence voltages had been proposed. However, performance in systems with IBRs had not been evaluated in [59] and [60], since they were published in a pre-IBR era. The work presented in [61] offers a technique based on incremental line-to-line voltages for faulted phase identification, however it's analysis lacks in detail (it had not been tested for a variety of system conditions). A selected set of faulted phase identification algorithms including a method that uses superimposed (incremental) voltages had been implemented and tested for systems with IBRs in [62]. While this work had delivered a reasonable depth of analysis and detailed implementation, the algorithms implemented and tested (particularly the one that uses incremental voltages) were only partially successful in identifying faulted phases. Work presented in [63] proposes using the energy signal of incremental voltages and dynamic thresholds to determine faulted phases. While results presented are promising and had yielded a very high success rate, cases for which the proposed method failed are not specified. This information is critical to assess the overall applicability of the method irrespective of the success rate. In addition, incremental voltage based methods presented in [61]-[63] use thresholds of some form, which are vital for the correct operation of the algorithm. These thresholds had been determined mostly based on simulations, which invariably makes them harder to replicate, system dependent and require extensive testing to configure. Moreover, most methods in literature were not tested for a wide range of fault inception angles, to which some faults types are highly sensitive.

Based on the information provided in above subsections, it was deemed necessary to evaluate and compare the performance of faulted phase identification algorithms of contemporary relays in the presence of IBRs and investigate possible improvements as necessary. The main emphasis of this investigation is summarized below,

- Although there is a theoretical understanding of the reasons behind the faulted phase identification problems due to IBR penetration, the extent of the issue is not well understood. The phase selection performance of commercial relays under presence of IBRs is not well documented. Firstly, a simulation-based analysis is carried out to validate theoretical explanations and demonstrate deficiencies of conventional faulted phase identification algorithms in the presence of IBRs. Secondly, a few samples of commercial relays are tested in a hardware-in-the-loop (HIL) simulation setup using an electromagnetic-transient (EMT) type digital real-time simulator (DRTS) to assess the performance and further validate theoretical expectations.
- Although alternative phase selection algorithms have been proposed in the recent literature to overcome the deficiencies of conventional phasor-based techniques, most of them are only verified by using offline simulations. In order to investigate the real-time applicability of such methods, a transient-based faulted phase identification method proposed in literature is implemented in hardware and tested using HIL simulations. The work also highlights practical considerations that require special attention while implementing transients-based algorithms in real hardware.
- As can be seen from the comparison presented in Table 2.1, it is clear that incremental quantities based methods of faulted phase identification offer a compromise between

several important aspects including reliability, speed of operation and cost. Therefore, it was deemed that faulted phase identification methods based on incremental quantities warrants a more detailed investigation. Firstly, the effectiveness of using incremental voltages for faulted phase identification shall be evaluated using theoretical analysis of fault loop equations. Secondly, based on the theoretical analysis, an attempt shall be made to develop an effective faulted phase identification method for systems with high IBR penetration. Moreover, the prospective algorithm shall be tested exhaustively in an EMT simulation environment, including for a wide range of fault inception angles, to which some faults types are highly sensitive. This is a deficiency in most of the work presented in literature, as most of them had only been tested for a few inception angles, whereas testing for the full range of fault inception angles is often required to reveal potential failures.

2.3 Identification of Fault Direction

Identifying the direction of a fault is one of the most critical aspects of a line protection scheme and, one that is severely affected by the increased presence of IBRs in power systems. The following subsections provide a brief overview of existing standard methods for fault direction identification, their behaviour and challenges in systems with IBRs and, some of the recent attempts made to resolve the aforementioned challenges.

2.3.1 Conventional Fault Direction Identification Methods

In transmission protection schemes, the most common application of negative-sequence quantities is their use in determining the directionality of faults. Operation of conventional directional elements are depicted in Figure 2.2. As previously stated, most modern numerical relays employ some form of negative-sequence quantities-based method to identify fault direction [16]. Typically, most directional algorithms use a combination of all three sequence impedances (alternatively, the relationship between sequence voltages and currents) seen at relaying location to determine the direction of the fault. If the calculated impedance (phasor) resides within a predefined area (for example, $\pm 90^0$ of the respective line impedance angle), the fault is identified as either in the forward or reverse direction, as shown in Figure 2.2-(b). It is a common practice to prioritize the negative-sequence element when determining the direction of a fault due to its enhanced sensitivity to unbalanced faults. In such schemes, if the negative-sequence voltage and current magnitudes are too low to make a reliable decision, relay's directional algorithm will instead use zero and positive-sequence quantities [4], [42], [43].

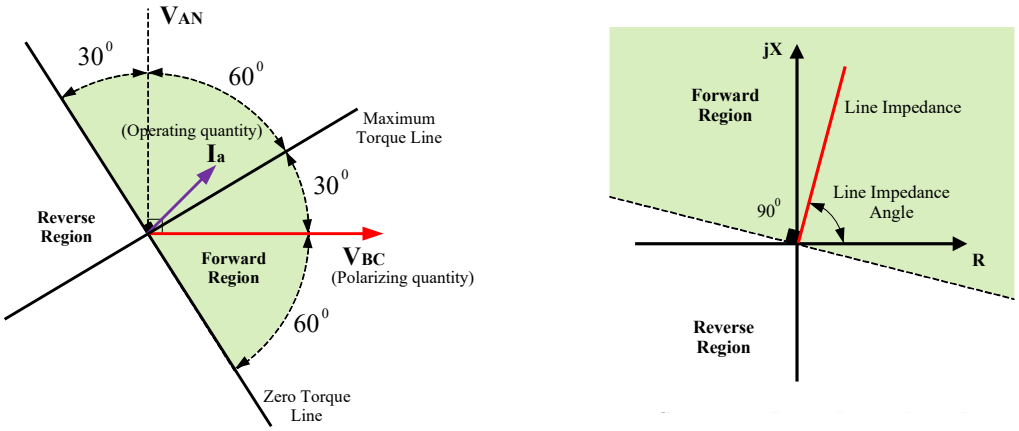

(a) (b)

Figure 2.2 Conventional directional elements (a) 90-60directional element and (b) sequence impedance based directional element

Typically, directional elements have a predetermined minimum magnitude of voltage and current (in sequence domain) to be activated. As most existing IBRs in the system usually do not produce enough negative-sequence currents to activate the negative-sequence directional element, decisions on direction have to be taken based on other components (zero and positive-sequence). However, if the negative-sequence directional elements are not intentionally disabled (or the activation thresholds are set too low), a relay fed with an IBR is likely to make incorrect decisions on directionality by relying on IBR-generated negative-sequence currents (which are highly unpredictable and unconventional even though very low in magnitude). Simulation studies and field events have shown that relay algorithms are prone to produce unreliable decisions on fault direction under such circumstances [4], [13].

In summary, the above discussion underlines the fact that if the relay settings are not precisely set, misbehaved negative-sequence quantities produced by IBRs can compromise the reliability of relay algorithms. Reliable operation of these elements demands attention during relay configuration, especially for the selection of pickup currents and element characteristic

angle (ECA) for the affected relay elements. This solution, however, is case specific and requires extensive and detailed simulation studies of the system.

2.3.2 Recent Work on Fault Direction Identification with IBRs

The applicability of directional relay algorithms under IBR heavy systems has been explored in recent literature. Some of them have proposed using zero-sequence quantities for determining fault direction as an alternative to negative-sequence directional elements [4], [17]. While this may produce satisfactory results for ground faults, finding fault direction for ungrounded faults (line-to-line faults) remains a challenge (where there is no zero-sequence). In addition, there are IBR plant configurations with transformer vector groups that does not provide a zero-sequence path (for example, grounded Wye-Wye connected MPT and delta-grounded Wye connected inverter transformer is a common configuration as shown in Figure 1.5), where the use of zero-sequence quantities is infeasible. In such cases, direction identification of all fault types is based on positive-sequence quantities, which depending on the implementation, may not deliver the most efficient performance (as demonstrated later in subsection 4.2).

Over the years, several noteworthy attempts have been made to develop new techniques to correctly identify the fault direction and, some of them are specially designed to work with IBRs [65]-[74]. The work presented in [69] proposed a method based on comparison of the amplitude of sequence currents or the comparison of the phase angle between the sequence voltage and the sequence current for direction identification. This analysis was largely based on DFIG based IBRs and the method still relies on phase angles of currents, which can

be problematic in most types of IBRs with full converter interface (without DFIG). In [70], a technique based on comparison of power frequency sequence voltages to determine the fault direction had been proposed. While the premise presented in this work is promising, the investigations carried out lacked depth and detail, in general. The authors of [71] proposes a scheme where high-frequency impedance components are used to determine the fault direction, which is relatively complex and resource intensive to execute. In [72], a technique based on the waveform correlation of phase transient voltage has been proposed. The work presented in [74] introduces a technique based on sequence impedance employing a different impedance measurement (using superimposed quantities) and a novel criterion than conventional directional elements to identify the fault direction.

Most of the above-mentioned techniques, while producing acceptable results, are complex to set up or/and expensive to implement in hardware. In addition, some of the above-mentioned techniques have limited scope and the applicability of them has not been thoroughly tested under different system configurations and conditions.

Key goals of this research are as follows,

- Verifying the claims in literature regarding the impact of IBRs on directional elements using detailed EMT simulations. This study will then be extended to further investigate the impact on misbehaved directional elements on a transmission system protection scheme as a whole.
- Developing a new protection algorithm to correctly identify the fault direction in system with heavy IBR penetration and evaluate its performance against existing techniques.

2.4 Power Swing Protection

As mentioned in subsection 1.2.4, power swings originate due to major system disruptions such as loss of large-scale generation or load that cause abnormal oscillations in the power flow. Protection devices are susceptible to these events as they can interpret them as faults, prompting undesired tripping. This is a significant concern for impedance-based relays in particular. In a majority of line protection relays, out-of-step (OOS) protection functions are based on impedances seen at the relaying location (apparent impedance). Power swing blocking (PSB) generally measures the time taken for the impedance observed at the relaying point to travel from one region on the R-X (Resistance-Reactance) plane to another, and commonly referred to as blinder schemes. This is based on the principle that the rate-of-change of swing impedance is slugging during a power swing as it is restrained by the system inertia (it is an electro-mechanical dynamic phenomenon). In comparison, impedance change during a fault is almost instantaneous, however, signal processing in the relay adds a delay of around one cycle for detection. Once a power swing is detected, OST is triggered if and when the swing impedance enters a predefined zone, which is based on a predetermined least stable power swing characteristic [75]-[78].

Typical IBRs provides limited contribution to rotational inertia of the connected power system, due to the decoupling caused by power electronic converters [4], [18], [79]-[81]. Consequently, power swing characteristics of a power system alter with IBR penetration. Studies have shown that due to increased levels of IBR penetration, swing impedances move faster due to the lack of overall inertia of the system, and PSB timer settings calculated without accounting for this detail may be unable (as they are too high) to distinguish between a fault

and a stable power swing [4], [18], [79]-[80]. Using a lower PSB timer setting is the obvious remedy for this issue, but it can be challenging to select this value in a way that the dependability of fault detection is not affected. It is also noteworthy that some of the more recently developed IBR control techniques are capable of providing virtual inertia to the system, hence has a less of an effect on power swings (may even enhance it) than the ones from previous generations. Figure 2.3 illustrates the blinders curves of typical power swing protection scheme and a typical trajectory of the most stable power swing with 100% synchronous generation and with some of that synchronous generation being replaced by IBRs (which do not contribute inertia).

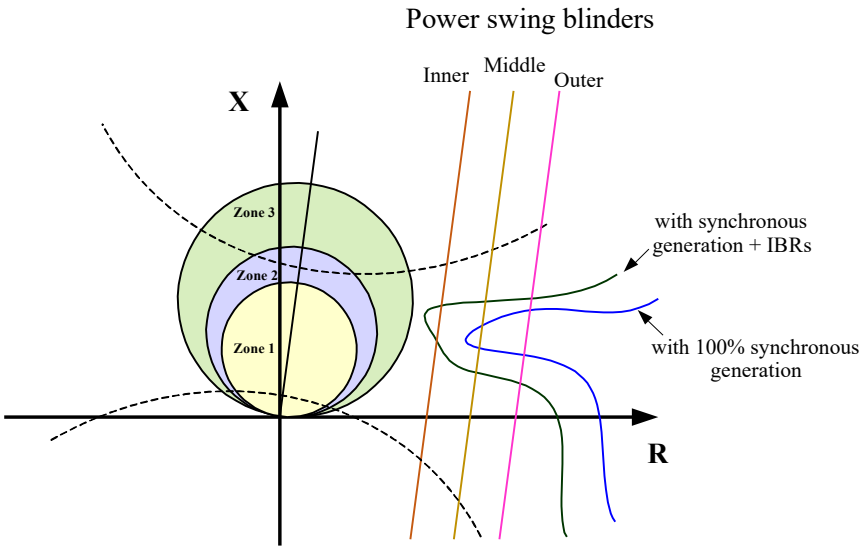

Figure 2.3 Swing impedance trajectory of the most stable power swing, with and without IBRs

Conventionally, dynamics of synchronous machine controls (such as exciters) are ignored during power swing protection calculations as they are considered too slow to react during the first swing [8]. The behavior of an IBR control system during a power swing can be considerably different than that of a synchronous machine [4], and some control functions of a modern IBR, such as those applicable to voltage-ride through (VRT) requirements can

respond in a much quicker time-frame (performance requirements for current injection during VRT mode ≤ 4 cycles as per IEEE Std. 2800-2022 [3]). This is a relatively unexplored topic worthy of further investigation.

A number of recently published work found in literature discusses the impact of IBRs on power swing protection [4], [18], [79]-[84]. However, a majority of them, focuses on the effects of lack of inertia of a system with IBRs on the rate-of-change of the apparent impedance (the speed of the swing trajectory) during a power swing. It was observed that a systematic theoretical analysis of the impact of IBRs on impedance swing trajectories was largely absent in published literature related to this topic. Work presented in [4], [18], [79] analyses, using simulation results, how replacing conventional synchronous generation with IBRs can affect the dynamics of power swing in a system. Reference [82] had developed a dynamic model for power swings for systems with IBRs and in turn, it has been applied in [83] to study practical implications on power swing protection. While this work had produced an in-depth investigation and detailed modelling, it requires complex system models, thus cannot be conveniently adopted for general use. The premise of these studies is that faster moving swing impedances due to diminished system inertia may cause difficulty in discriminating between power swings and system faults. Furthermore, the results presented predict that the installation of IBRs may alter the boundary between stable and unstable power swings, demanding reassessment of power swing protection settings (out-of-step tripping blinders in particular). Reference [79] also briefly mentions the effect of IBR controls on swing trajectories, however, only a very limited details are provided on this matter. The work carried out in [85] presents a theoretical analysis of IBRs' effect on power swing impedance trajectories, also taking control dynamics

of IBRs into account. However, the investigation was carried out on a single-source-to-infinite-bus system, where the source is an IBR. While this represents an important development, the configuration considered does not represent a common situation where power swing protection is critical (as power swing protection is not applicable to an IBR alone as it would for a synchronous generator). Therefore, further investigations for more generic configurations are warranted.

Main Goals of this research are given below,

- Investigate the effects of IBRs on power swing impedance trajectories by generic theoretical examination and determine the impact on existing power swing protection. The focus of this analysis would be to investigate the effects of IBRs on power swing impedance trajectories using a generic circuit equivalent, without resorting to complex dynamic models. Analysis of traditional power swing protection is generally carried out using simplified system equivalents represented in phasor-domain, and the objective of this work is to incorporate IBRs into this type of simple analysis. Therefore, this analysis shall be carried out in phasor-domain, based on well-established principles modified to incorporate IBRs. This type of analysis does not intend to address the effects of IBRs on swing speed due to reduced inertia, which has been adequately investigated in literature. In addition, the proposed analysis is projected to provide a vital point of reference against which results from more detailed simulation can be compared.
- As a secondary objective, the impact of potential changes to swing trajectories on traditional power swing protection shall also be examined.

2.5 Overall System Protection of a System with IBRs

As noted above, power system protection concerns caused by IBRs are most severe at radially-connected terminals of a transmission system. These include, for example, the plant terminal of a tie-line connecting an IBR plant, where a protection relay is fed entirely by IBR generated currents. Note that contingency events (for example, tripping of a line forcing a radial topology or conventional generation) can also cause scenarios in the system, in which protection relays are fed by IBR-generated currents only. Therefore, the work presented in this Thesis mainly focuses on investigating and improving transmission level protection functionality of such systems. This subsection presents a brief summary of prevailing power system protection practices, specially focusing on radially connected IBR facilities [4],[16],[17].

2.5.1 Line Current Differential Protection

It is generally accepted that, among all conventional protection schemes, line current differential protection (ones that compare instantaneous values, in particular) performs the best in the presence of IBRs. This is understandable as nature of the source injecting current does not affect the differential current, which in some form or the other, is the operating quantity of a differential protection scheme. Line current differential protection offers fast and reliable fault detection and 100% coverage of the line. On the other hand, line current differential protection is also the most demanding of the conventional protection schemes to implement as it requires secure and reliable communication channels with a high bandwidth at all times [86]. In addition, by its very nature, the number of tapped loads connected to the line is limited. Furthermore, some implementations of line current differential protection schemes

can be susceptible to phenomena such as current inversion due to series-compensation (resulting in a capacitive source impedance) [16],[17]. Due to technical or economical reasons mentioned above, the use of line current differential protection may not always be feasible for system with IBRs. Even when they are in use, other forms of back-up protection that only uses local measurements are required to cater for contingency situations such as unavailability of communication channels or operate as back-up protection for faults on adjacent lines.

2.5.2 Other Communication-assisted Protection Schemes

Other Communication-Assisted Protection Schemes such as permissive overreaching transfer trip (POTT), directional comparison block (DCB) and direct underreaching transfer trip (DUTT) can also be effectively used to enhance protection reliability in systems with IBRs. Weak infeed protection trip schemes such as echo logic or/and direct transfer trip (DTT), are especially applicable to systems with IBRs due to lack of fault currents.

As an example, Figure 2.4 shows a communication assisted weak-infeed protection trip scheme, where the relay at the IBR plant end, R1, is fed entirely by the IBR whereas that at the POI, R2, is fed by a strong conventional source for an internal line fault. Typically, these schemes use directional mho phase distance relays for phase fault detection and directional ground distance for ground fault detection. However, since dependability of such protection schemes is uncertain in the presence of IBRs, R1 cannot be relied upon to operate on its own, even for internal line faults. Consider an internal line fault close to the IBR terminal, which would be in forward distance zone 2 of R2. Here, R2 would pick up the fault and send a permissive trip to R1. Upon reception of the permissive trip, and if it also sees a forward fault

(may or may not be using the same detection method as R2), R1 would trip and echoes back the permission to R2 to clear the fault at the remote end. In case R1 fails to detect the fault completely, R1 would have to depend on R2 sending a direct transfer trip once it has operated on time delayed zone 2 distance protection alone. To ensure dependability of protection, R2 is usually configured to send a direct transfer trip to R1 whenever it (R2) trips (with or without echo logic) [4].

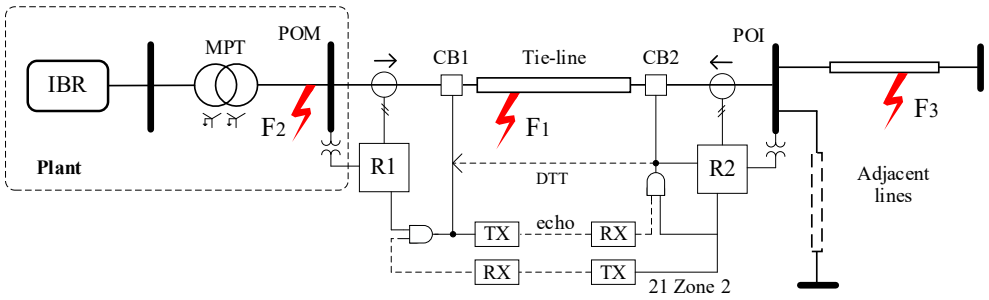

Figure 2.4 Weak Infeed trip scheme

Communication-Assisted Protection Schemes such as POTT require less communication bandwidth compared to line current differential protection. Nevertheless, local back-up protection such as time delayed undervoltage elements are required to manage contingency situations such as failure of communication channels.

2.5.3 Back-up Protection

As noted above, protection functions only dependent on local measurements are required as backup protection even with the use of communication assisted protection such as line current differential or permissive trip schemes. Some form of backup protection also enhances protection reliability for faults beyond the POI of the IBR plant (such as those on adjacent lines). Notwithstanding reliability concerns mentioned in subsection 1.2.3, distance

protection elements with overcurrent supervision set to their lowest reasonable value (often 1.0 pu) can be one option of providing backup protection. In addition, since the HV side of the IBR plant transformer is often wye-grounded (and a delta connection at the low-voltage side), ground faults on the tie-line generates adequate zero-sequence currents for inverse-time zero-sequence overcurrent (directionalized by zero-sequence quantities) to be used for ground fault detection [4].

Undervoltage protection is also an extremely useful tool for providing backup protection for system with IBRs, and often setup as the last bastion of defence when all other means of protection fail. Time-delayed phase-to-phase undervoltage protection is often used to achieve this goa; however, care must be taken to coordinate these elements such that, before operation, they allow faults on adjacent lines to clear on their own protection. Furthermore, they must also be coordinated with applicable interconnection requirements such as low voltage ride through requirements defined in grid codes and standards (for example, North American Electric Reliability Corporation (NERC) standard PRC-024-03, PRC-029-01).

2.6 Known Real-world Incidents in Systems with IBRs

There are real-world incidents in recent times involving IBRs that put in jeopardy the stable operation of power systems and their protection. This section provides information about some of the well-documented and significant such events.

2.6.1 Evolving Ground Fault in BC Hydro System

A Phase B-to-ground fault occurred in the BC hydro system in August 2014, which later evolved into a Phase B-to-C-ground fault (after about three-cycles) [13]. This fault occurred on a segment of the transmission line which is connected to a large hydro generation station on one end but had a system with a high degree of IBR penetration connected to the other. Captured data from the two relays on either end of the line (looking into the line) exhibited significantly different magnitudes and relative phase angles (of voltage and current). More important was the behaviour of forward directional elements of the two relays. The relay connected to the hydro station of the line operated as expected and declared a forward fault whereas the one connected to the IBR heavy end only operated transiently.

2.6.2 Blue-cut Fire Event in Southern California

In August 2016, a fire in a transmission corridor in Southern California caused several faults on 500 kV lines owned by Southern California Edison (SCE), and 287 kV lines owned by Los Angeles Department of Water and Power (LADWP). These triggered some of the PV generation facilities in the system to cease injecting power, without providing fault 'ride though' and remaining in the system. The loss of approximately 1,200 MW of solar PV

generation, resulted in the frequency of the western interconnection dropping to a value of 59.867 Hz.

Two similar types of incidents were reported in October 2017 (the Canyon 2 Fire [10]) and April 2018 (Angeles Forest and Palmdale Roost Disturbances [11]), where a number of solar-PV sources either tripped or driven into momentary cessation in response to faults in the transmission system.

2.6.3 SSCI Event in Texas

Sub-Synchronous Oscillations (SSO) are a class of interactions occurring between two entities of a power system engaging in an energy exchange at a frequency below the nominal system frequency [87]-[89]. Types of SSO are typically classified based on what segments of the power system get involved in the interactions. IBR plants and their control systems too can interact with other entities of the power system, particularly fixed series capacitors in transmission networks, to generate SSO. This type of oscillations is caused purely by electrical interactions between the two entities and commonly referred to as Sub-synchronous Control Interactions (SSCI). Several factors including the type of IBR, its proximity to series capacitors, network topology and other operational conditions can determine the risk of SSCI in a system.

By design, standard power system protection relays operate based only on fundamental frequency components. Off nominal frequencies, including those in the sub-synchronous frequency range, are largely filtered out during signal proceeding (however, depending on effectiveness of signal processing, presence of sub-synchronous frequency components can leave some artifacts or induce small errors in fundamental frequency measurements). Therefore,

regular power system protection relays cannot generally detect SSO conditions. Consequently, evaluation of the risk of SSCI via detailed simulation studies is a common practice when integrating large scale IBRs or installing fixed series capacitors in a modern power system. Risk of SSCI in a power system is reduced and managed primarily by control and operational level countermeasures, while specially designed relaying devices can also be used as an added defence [89]. However, without proper mitigation, poorly damped SSCI can rapidly grow to produce dangerously high currents and voltages in a power system, causing significant damage. A brief description of a real-world SSCI event is provided below.

AEP-Texas system experienced a SSCI event in October 2009, which resulted in damaging turbine and utility equipment [90]-[93]. A fault occurred in one of the two 345 kV, series compensated transmission lines carrying power from two wind farms (Type-3 wind turbine-generators). The fault was cleared in due course by tripping the line, however, this inadvertently resulted in a network topology susceptible to SSCI, in which the two wind farms were radially connected to the other series compensated transmission line.

Data captured from digital fault recorders revealed that bus voltage at the interconnection point (with the wind farms) reached 1.45 pu and the combined magnitude of the current from the two wind farms escalated to 9 times the pre-fault values during the oscillations. Since the dominant component of the fault current (and voltage) was sub-synchronous (at 24 Hz), dedicated protection functions designed to operate at fundamental frequency were oblivious to what had transpired. As a result, the SSCI event remained unchallenged for approximately 1.5 s, caused damage and fatigue to system equipment, until the bypass breaker of the series capacitor bank closed and removed the series capacitor bank from the system [90], [92].

2.7 Concluding Remarks

This chapter presented a detailed literature review of IBR-caused power system protection challenges and prevailing solutions. Main power system protection issues posed by IBRs were briefly discussed in Chapter 1. Three topics were selected from them as main research topics for this Thesis; namely (I) impact of IBRs on conventional faulted phase identification algorithms, (II) effect of IBRs on conventional fault direction identification and, (III) effects of IBRs on electrical trajectories of power swing protection. Systematic literature reviews of the three selected topics were provided in Chapter 2, underlining their real-world challenges, existing work in literature and respective research gaps. Furthermore, a review of the overall system protection of systems with IBRs was also provided for context. The three main research topics discussed in this chapter shall be individually explored and expanded in Chapters 3, 4 and 5, respectively.

Chapter 3

Investigation of Impacts of IBRs on Contemporary Faulted Phase Identification Methods and Techniques for Mitigation

3.1 Effects of IBRs on Faulted Phase Identification Techniques

IBRs impose substantial challenges to traditional faulted phase identification methods, particularly for methods that depend on phase angle signature of sequence currents, as explained in Section 2.1. The key concerns are:

- IBRs inject very little amounts of negative-sequence currents during faults which may not be enough to activate the phase identification algorithms in relays [4].
- Even the small amounts of negative-sequence currents resulting from the imperfections in the converter controls vary with time and fail to exhibit the same relationship with those of the other sequence currents as a conventional source.

3.1 Effects of IBRs on Faulted Phase Identification Techniques

- Distance protection elements produce unexpected impedance trajectories in the presence of IBR [22], [30] affecting the faulted phase selection techniques that depend entirely on impedance measurements, such as the one shown in Figure 3.1.

Most sequence-current-based faulted phase identification techniques, consequently, are susceptible to miss-operate in the presence of IBRs with full converter interfacing. To establish the differences between fault currents from a conventional generation source and an IBR, and their effects on faulted phase identification, the system given in Figure 3.2 was simulated in an EMT-type Digital Real-time Simulator (DRTS, i.e. RTDS®). The simulation was carried out for two scenarios, with only one type of source connected at a time. In the first scenario, a conventional source was connected (to represent a synchronous machine-based system), and it was represented as a voltage source behind an impedance.

In the second scenario, the conventional source was replaced by an IBR model. The IBR was represented in simulation using an averaged model with generic DQ frame current controls. Other peripheral controls such as LVRT (low-voltage ride-through) controls were based on the guidelines outlined in the IEC 61400-27-1 standard [96]. The general behavior of the IBR model was verified with those available in the published literature [4],[5]. In both cases, the generation source was injecting 100 MW of active power at a unity (1.0) power-factor to the AC grid (which is also represented as a voltage source behind an impedance) via a short transmission line (plant tie-line).

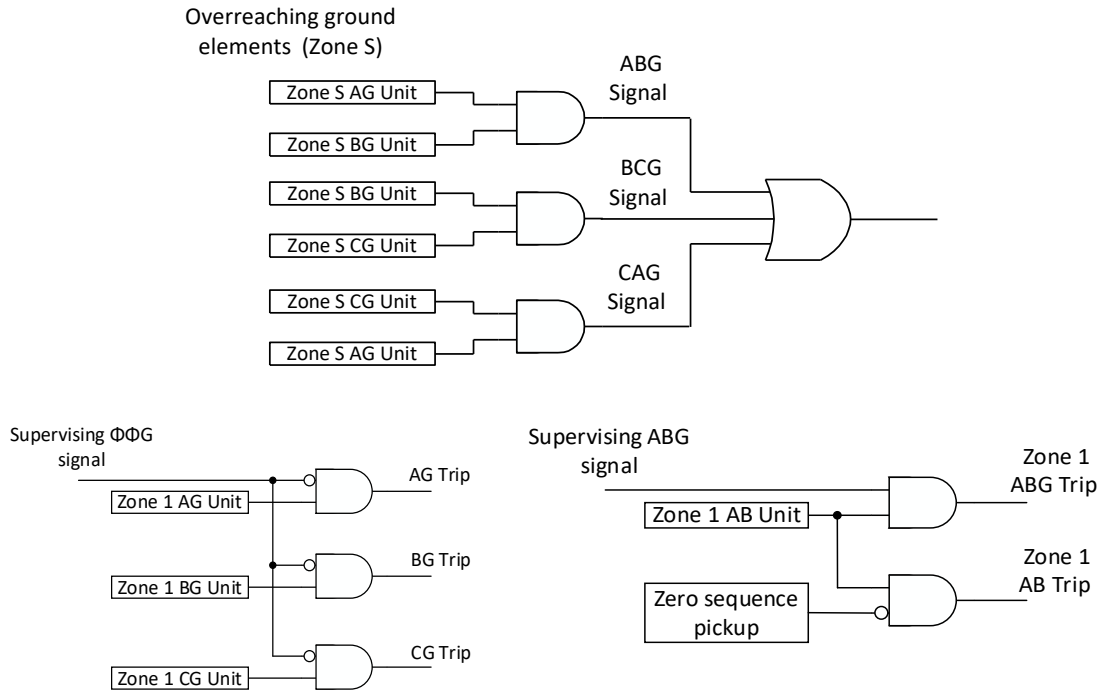

Figure 3.1 Logic diagram of the implemented impedance-based phase identification technique

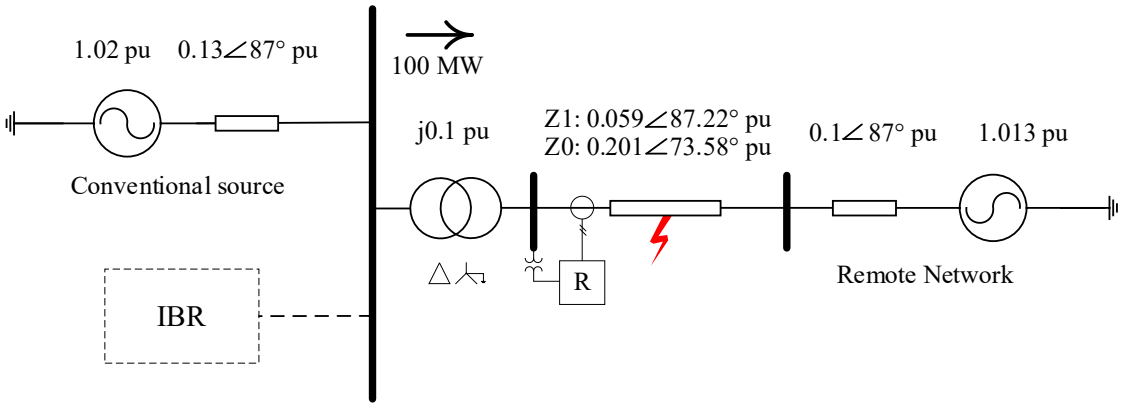

Figure 3.2 Single line diagram of the power system used for comparing a conventional source and an IBR

Figure 3.3 presents the phase currents, the magnitude of the sequence currents, and the angle difference between 'Phase A' negative and zero-sequence current phasors recorded at the relaying location (R) for each case, as indicated. The results shown are for a bolted (low

impedance) BG fault at the mid-point (50%) of the transmission line. Here, the stark difference between fault currents produced by the two sources is evident.

As can be seen, a substantial presence of all three sequence currents, and a phase angle difference of close to −120° between '*Phase A*' negative and zero-sequence currents was observed with the conventional source (as expected). In contrast, fault current injected by the IBR was dominated largely by the zero-sequence current produced by the plant transformer, which has a grounded-wye connection on the grid-side (HV side). The magnitude of the negative sequence current was very small, and that of the positive-sequence current remained essentially unchanged at 1.0 pu. Furthermore, the phase angle difference between '*Phase A*' negative and zero-sequence currents fluctuated with time during first few cycles before finally settling down at a different value from −120° (the theoretically expected). The phase angle of the negative-sequence current, however, has little meaning in this scenario as its magnitude was very low.

The pickup signal from a simple faulted phase identification logic based only on the angle difference between 'Phase A' negative and zero-sequence currents is also presented in Figure 3.3. As expected, the logic identifies the fault as a *'BG'* fault for scenario 1 with the conventional source and does not respond properly in scenario 2 with the IBR.

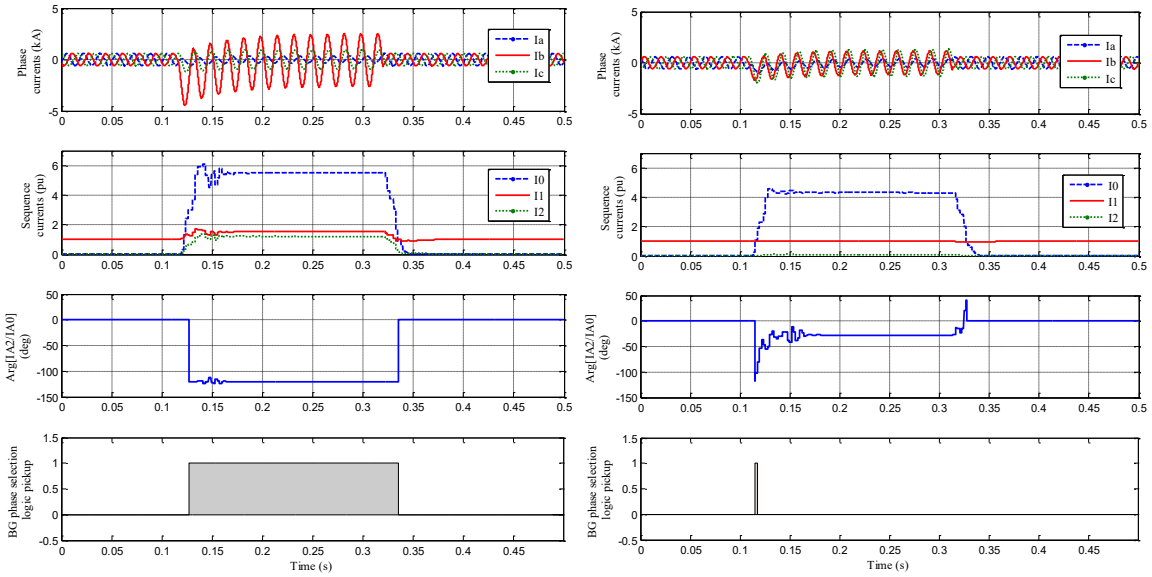

Figure 3.3 (a) Results for faulted phase selection for a BG fault at the mid-point of the line with the conventional source. Results for faulted phase selection of a BG fault at the mid-point of the line with the IBR, (b) Results for faulted phase selection of a BG fault at the mid-point of the line with the IBR.

The method shown in Figure 3.1 was also implemented in the DRTS environment in order to investigate the impact of IBRs on impedance-based fault type identification methods. Its performance was evaluated using the same methodology detailed above. The implemented logic in the simulation yielded accurate and dependable faulted phase identification for conventional sources as expected, while failing to operate reliably with an IBR. However, purely based on the results of simulation studies, impedance-based method fared better than the sequence components based algorithm in the presence of IBRs; the impedance-based method produced a correct fault classification for some fault types under certain conditions, whereas the sequence components-based method was unsuccessful in all tested scenarios.

3.2 Testing and Analysis of Commercial Relays

3.2.1 Performance of Commercial Relays

In order to further establish the premise that the fault identification algorithms in relays were affected by the presence of IBRs, two commercial line protection relays were tested in a laboratory setup. A majority of work available in literature related to protection issues caused by IBRs ground their conclusions based on simple relay functions developed in simulation environments, which can perform differently than commercial relays deployed in the field (work presented in [16], [27] are exceptions). Hence, it is imperative to validate the theoretical expectations in laboratories using a test setup that closely replicates real-world scenarios. Furthermore, the manuals of commercial relays and other examples in the literature available to the public often do not disclose some minor but critical details of internal relay algorithms, such as sensitivity thresholds used for supervising signals. As a result, it is possible that commercial relays perform better than theoretical expectations in the presence of IBRs. This warrants investigation and validation. A controller-hardware-in-the-loop (CHIL) test setup where commercial relays are interfaced with a DRTS is well suited for this task.

3.2.2 Test Setup

For this exercise, a slightly more complex system (AC grid) was modeled to carry out tests in a more comprehensive manner, as shown in Figure 3.4. The IBR model is the same as the one explained in Section 3.1, which is rated at 100 MW and injected power to the AC grid via a short (30 km) 138 kV tie-line. The far (remote) end of this transmission line is connected

to a 230 kV system through a transformer and an adjacent transmission system. A conventional power source, represented in simulation using a synchronous generator model, is connected to the remote bus (*Bus 2*) via another short (50 km) transmission line, as depicted in Figure 3.4. Both line protection relays were interfaced and tested in a CHIL setup and realized using a DRTS (RTDS®). A high-level schematic of the CHIL test setup is presented in Figure 3.5.

As shown in Figure 3.5, the power system in its entirety was simulated in the DRTS, and both commercial line protection relays were interfaced using low-energy analog signals (low-level interface) and the relay's dry contacts. High-fidelity digital waveforms (outputs of voltage and current transformers) produced in DRTS were converted to low-energy analog voltage signals (<±10 $V_{peak\text{-}peak}$) by the analog output card of the simulator. They were then fed to the low-level test interface of the relays, bypassing relay's internal (secondary) instrument transformers. Scaling factors and safety limits for the analog output card must be determined with caution in order to feed precise low-level voltages to the low-level test interface of the relays under test.

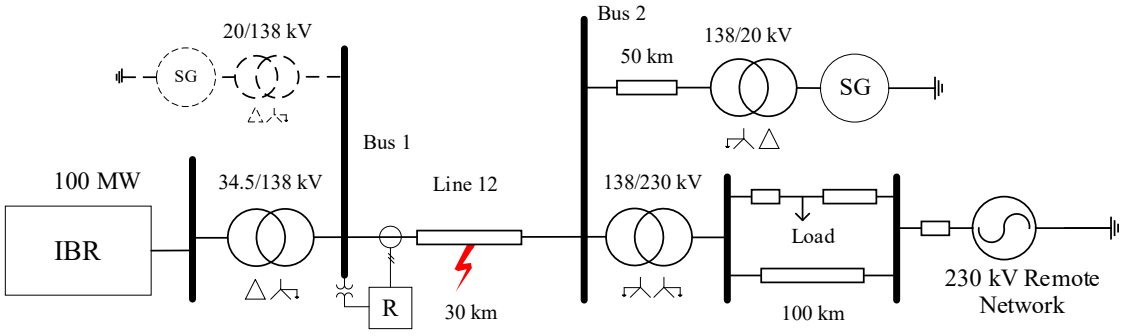

Figure 3.4 Single line diagram of the power system model used for testing commercial relays

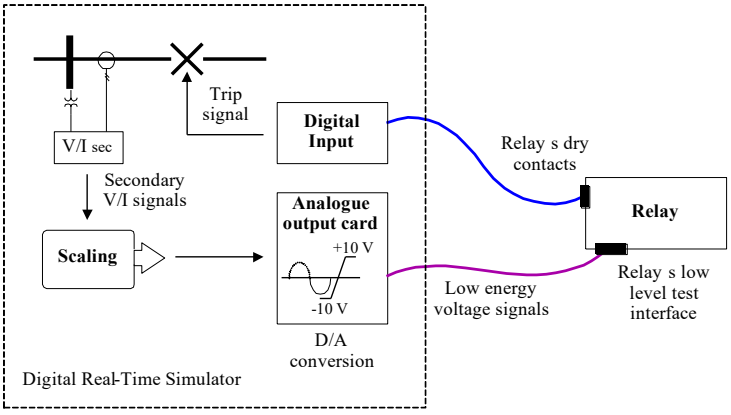

Figure 3.5 Schematic of the test setup

Note that the two relays were tested independently by connecting only one at a time to the test setup. The transmission lines were modeled using Bergeron's line models with realistic data. The positive-sequence and zero-sequence impedances of *Line 12* were 11.3∠87.22° Ω and 38.38∠73.58° Ω, respectively. The current transformers (CT) and voltage transformers (VT) were also modeled using the standard master library components available in the DRTS's software suite. In addition, the synchronous generators were also modeled using the standard library component with typical parameters. However, note that the synchronous generator connected at *Bus 1* (shown in dashed line in Figure 3.4) was kept disconnected for the first part of the experiments. The remote AC grid was represented using a Thevenin's equivalent with a 230 kV source behind an impedance of 20∠87° Ω. A 50 μs simulation time step was used for all simulations. Both relays were configured as distance protection relays looking into *Line 12* at *Bus 1* (**R** in Figure 3.4), with *Zone 1* enabled as a direct tripping element with an 80% reach. Faults of different types were applied along the length of the IBR tie-line, *Line 12,* and the performance of the relays' was recorded.

3.2.3 Test Results and Discussion

Table 3.1 and Table 3.2, present faulted phase identification results for low-impedance faults (R_f = 0.01 Ω) and high-impedance faults (R_f = 50 Ω), respectively. The fault inception angle was fixed at 0° (with respect to the voltage at *Bus 1*). When considering results of the two relays, *Relay 2* failed to identify the faulted phases in all test cases. Moreover, *Relay 2* failed to detect phase-to-ground faults as well. However, for all types of faults, *Relay 2* issued a three-phase trip signal irrespective of the type of short circuit fault applied.

In comparison, *Relay 1* identified a number of faults for all types with a varying degree of consistency. Yet, *Relay 1* failed to detect the existence of a fault in most phase-to-ground faults. However, even when a fault was detected, *Relay 1* was unable to correctly identify the faulted phase in phase-to-ground faults. Table 3.1, Table 3.2 and Table 3.3 summarize the performance of the two commercial relays for applied ground and ungrounded faults. Both low-impedance (short circuit) and high-impedance faults were applied at three fault locations (at 5%, 50%, and 75% of the line length). Multiple simulations were run with the fault inception angle varied from 0° to 180° in one-degree steps.

Table 3.1: Fault type identification of relays for low impedance faults

Applied Fault		Fault Type Identification	
Type	**Location**	**Relay 1**	**Relay 2**
AG	5%	Unreliable	Does not identify *
	50%	Unreliable	Does not identify *
	75%	Unreliable	Does not identify *
BC	5%	BC	Does not identify *
	50%	BC	Does not identify *
	75%	BC	Does not identify *
ACG	5%	ACG	Does not identify *
	50%	ACG	Does not identify *
	75%	ACG	Does not identify *

* The relay issues a three-phase trip signal

Table 3.2: Fault type identification of relays for high impedance faults

Applied Fault		Fault Type Identification	
Type	**Location**	**Relay 1**	**Relay 2**
AG	5%	Does not identify	Does not identify
	50%	Does not identify	Does not identify
	75%	Does not identify	Does not identify
BC	5%	Does not identify	Does not identify
	50%	Does not identify	Does not identify
	75%	Does not identify	Does not identify
ACG	5%	Does not identify	Does not identify
	50%	Does not identify	Does not identify
	75%	Does not identify	Does not identify

Results presented in Table 3.2 indicate that both *Relay 1* and *Relay 2* failed to detect faults with a high fault impedance. As evident from the results presented above, both commercial relays do not consistently and reliably identify the faulted phase with IBR-generated fault currents. It was also observed that the faulted phase identification for the phase-to-ground faults was not only inaccurate in most cases, but also the results were not reproducible with consistency when the same tests were repeated. This is a deficiency of particular

importance, considering the fact that correct faulted phase identification is essential for the reliable operation of certain other protection functions.

Table 3.3: Overall performance of relays for various fault types

Applied Fault	Number of Cases	Correct Identification		Accuracy (%)	
		Relay 1	Relay 2	Relay 1	Relay 2
AG	1086	261	0	24.03	0
BG	1086	373	0	34.34	0
CG	1086	275	0	25.32	0
Total	**3258**	**909**	**0**	**27.9**	**0**
ABG	1086	464	0	42.72	0
ACG	1086	540	0	49.72	0
BCG	1086	542	0	49.90	0
Total	**3258**	**1546**	**0**	**47.45**	**0**
AB	1086	543	0	50.0	0
AC	1086	543	0	50.0	0
BC	1086	543	0	50.0	0
ABC	1086	543	0	50.0	0
Total	**4344**	**2172**	**0**	**50.0**	**0**

Both relays used in this experiment utilize the principle of phase angle signatures of sequence currents to determine the faulted phases (as explained in subsection 1.2.3.3). However, the two vendors use different approaches for singling out the faulted phase(s) from two or more possibilities. One relay vendor uses the phase angle signatures of all three phases with additional logic to single out the faulted phase, while the other uses multiple sequence phase angle signatures (α and β) to determine and verify the faulted phase. However, attributing the differences in the performance of the two relays for low impedance faults to this fact alone is unwarranted, as implementation details such as various internal checks, supervisions and thresholds used can also contribute to different behavior exhibited by the two relays.

Another observation made during testing was the differences between the accuracies in *Relay 1* for the different fault types, which can be attributed to several factors. Firstly,

different fault types produce different system conditions (for example, voltage at the IBR terminal varies depending on the fault type), which in turn can yield different responses from the IBR itself (for example, due to the behavior of the LVRT controls). Secondly, sensitivity of relay algorithms to different faults types may be different, resulting in varying degrees of accuracies. Further inspection of data obtained from *Relay 1* indicated that the protection pickup signals and phase identification signals issued by *Relay 1* were transient in nature (relay pickup signals were triggered transiently). Therefore, it is worth noting that the accuracy results (%) obtained from these tests must only be used to gather a general idea about the relay's behavior, and NOT as a conclusive quantitative account of their performance. Additionally, these results further underline the unreliable and, perhaps more importantly, unpredictable behavior of conventional relays in the presence of IBRs.

The results presented above showed that the fault type identification functions in the relays are severely affected by the presence of IBRs. In an attempt to add an extra dimension to testing, it was deemed necessary to find out the minimum penetration level of the synchronous generation required to successfully operate the fault identification algorithms of commercial relays. To achieve this, the power system model used for previous tests was modified by connecting a small synchronous generator (shown as a dashed line in Figure 3.4) to the IBR POM bus (*Bus 1*). Starting with 10 MVA, the synchronous generator's apparent power rating was increased. Short circuit faults of types phase-A-to-ground, phase-B-to-C-to-ground, and phase-A-to-C at 5 % of the length of the protected line were applied. Results obtained are given in Table 3.4. With the synchronous generator MVA rating (which represents in fault current capability) set to 10 MVA, the performance of *Relay 2* improved compared to the IBR-

only case. *Relay 2* started identifying phase-A-to-ground fault correctly, while the phase-B-to-C-to-ground fault and phase-A-to-C fault were still identified as three-phase faults. Note that *Relay 2* did not identify the faulted phases for all the applied faults (see Table 3.3), when there was no synchronous generator connected to *Bus 1*. In contrast, *Relay 1* did not display any improvement with a 10 MVA rated synchronous machine compared to the IBR-only case. At 15 MVA, *Relay 1* started classifying the type for all three types of faults applied at different fault inception angles, while *Relay 2* also exhibited some improvement by correctly identifying both phase-A-to-ground and phase-A-to-C faults. When the synchronous generator power rating was increased to 20 MVA, however, both relays started to identify the faulted phases accurately for all tested faults. Based on these results, it can be stated that with approximately 20% of the synchronous generation, typical commercial relays are able to accurately classify the fault type when operating in a system with both conventional and IBR based generation.

Table 3.4: Fault type identification of relays with added synchronous generation

Synchronous Generator Apparent Power	**Applied Fault**	**Fault Type Identification**	
		Relay 1	**Relay 2**
10 MVA	AG	Unreliable	AG
	BCG	BCG	ABC
	CA	CA	ABC
15 MVA	AG	AG	AG
	BCG	BCG	ABC
	CA	CA	CA
20 MVA	AG	AG	AG
	BCG	BCG	BCG
	CA	CA	CA

3.2.4 Non-conventional Fault Classification Schemes

In order to provide further perspective to the performance of phasor-based techniques, a non-conventional fault classification algorithm proposed in literature was implemented, tested and evaluated under similar conditions. The implemented method is based on transient quantities as presented in [50]. Given in Table 3.5 is the overall performance of the transient-based method, obtained using the same test setup as in above subsection 3.2.2. Note that the transient based algorithm was implemented as a real-time process on a different DRTS unit and interfaced to the DRTS unit running the power system using real IEC 61850 (SV and GOOSE) communication. More details about the implementation of this method, its applicability and validation can be found in [94],[95].

Table 3.5: Fault type identification of transient quantities-based faulted phase identification algorithm

Applied Fault		**Fault Type Identification (Transient-Based)**	
Type	**Location**	**Bolted Fault**	**High Impedance Fault**
AG	5%	AG	AG
	50%	AG	AG
	75%	AG	AG
BC	5%	BC	BC
	50%	BC	BC
	75%	BC	BC
ACG	5%	ACG	ACG
	50%	ACG	ACG
	75%	ACG	ACG

As with commercial relays, low-impedance faults were applied at three different fault locations (5%, 50%, and 75% of line length), while varying the fault inception angle from 0° to 180° in one-degree steps. These tests were repeated with a high fault impedance as well. It was observed that the transient-based method identified the type of the applied faults with an

accuracy of more than 95% for most fault types (see Table 3.6). However, it was observed that this method yielded a lower accuracy in identifying the faulted phases of phase-to-phase-to-ground faults compared to other fault types. Even in this scenario, it delivered a higher accuracy (over 70%) than the commercial relays (which had an accuracy below 50% under the same conditions). Moreover, the transient-based scheme identified the faulted phase within 1 ms of fault inception, which is faster than any conventional phaser-based technique. Therefore, a compromise needs to be made between speed, accuracy, and computational efficiency when selecting the best method to be implemented while also considering the requirements of different applications.

Table 3.6: Overall performance of transient-based faulted phase identification algorithm

Applied Fault	Number of Cases	Transient Based Method	
		Correctly Identified Cases	Accuracy (%)
AG	1086	1062	97.79
BG	1086	1067	98.25
CG	1086	1062	97.29
Total	3258	3191	97.94
ABG	1086	796	73.29
ACG	1086	813	74.86
BCG	1086	811	74.67
Total	3258	2420	74.28
AB	1086	1079	99.36
AC	1086	1080	99.44
BC	1086	1080	99.45
ABC	1086	1028	94.66
Total	4344	4267	98.22

3.3 Improved Faulted Phase Identification in Systems with IBRs using Incremental Voltages

As established in subsection 2.2.2.1, incremental (superimposed) quantities-based methods strike a more acute balance between aspects of system protection such as reliability, speed and economy of implementation, when compared with its counterparts. A few significant attempts made in literature for incremental quantities based faulted phase identification can be found in [12], [20]-[23]. It can be reasoned that the use of incremental currents is futile in systems with IBRs for faulted phase identification since the fault currents generated are low in magnitude and unpredictable [12],[24]. Conversely, system voltages are less affected by IBRs compared to currents, and therefore, the use of incremental voltages for faulted phase identification has more potential to yield satisfactory performance in such systems.

The work presented in this subchapter, firstly, evaluates the effectiveness of using incremental voltages for faulted phase identification using theoretical analysis of fault loop equations. Secondly, based on the theoretical analysis, it presents an effective faulted phase identification method based on integrated incremental voltages for systems with high IBR penetration. The proposed algorithm is based on six coefficients reflecting the relative strength of incremental voltages hence requires minimum configuration. Advantages and applicability of the proposed method are discussed in more detail in subsection 3.3.6. The proposed method was tested and verified using extensive Electromagnetic Transient (EMT) simulation studies.

3.3Improved Faulted Phase Identification in Systems with IBRs using Incremental Voltages

3.3.1 Theoretical Derivations

Presented in the following subsection is derivation of theoretical formulation for incremental voltages of a 3-phase power system during a line fault, as seen by a relay at a line terminal. The system under consideration is a generalized representation of a power system where two electrical networks are connected by a transmission line. The two networks are represented by equivalent voltages sources behind impedances and the transmission line using a lumped series inductance. All system resistances, charging currents and travel-time of the transmission line are neglected in this analysis for simplicity.

Illustrated in Figure 3.6 are the general fault circuit for the system under investigation and corresponding incremental fault circuit in phase (abc) domain with all self and mutual inductances between phases considered. The equations governing general behavior of the system, which are applicable for all fault types, are derived using this general representation. Fault type specific incremental circuits shall be considered at a later stage. Note that this representation accounts for mutual inductances exist in all segments of the systems (including within the sources) and are considered in the equations. All voltages and currents mentioned are time domain, instantaneous values.

3.3Improved Faulted Phase Identification in Systems with IBRs using Incremental Voltages

(a)

(b)

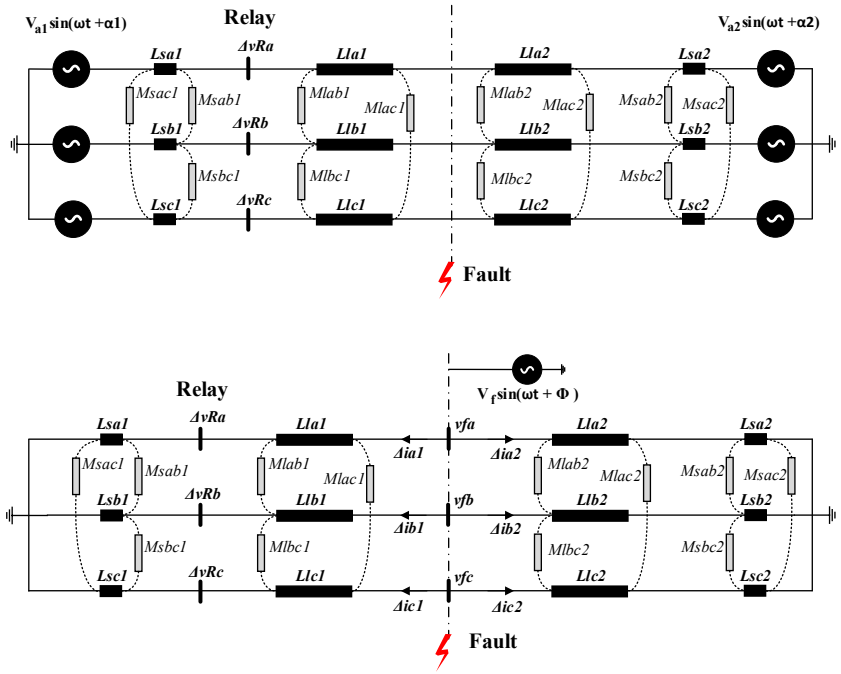

L_{sp1}: Local source self impedance (rectance) - phase p
M_{spq1}: Local source mutual impedance (rectance) - phase p to q
L_{lp1}: Line self impedance from local end (relay) to fault - phase p
M_{lab1}: Line mutual impedance from local end (relay) to fault - phase p to q
L_{sp2}: Remote source self impedance - phase p
M_{spq2}: Remote source mutual impedance (rectance) - phase p to q
L_{lp2}: Line self impedance from fault to remote end - phase p
M_{lpq2}: Line mutual impedance from fault to remote end - phase p to q
Δv_{fp}: incremetal voltage at the fault location - phase p
Δv_{Rp}: incremetal voltage at the realying location - phase p
Δi_{p1}: incremetal current flowing into the local source end - phase p
Δi_{p2}: incremetal current flowing into the remote source end - phase p
Note 1: (p → phases a,b or c)

Figure 3.6 (a) General fault circuit for the system under investigation and (b) the circuit corresponding to incremental quantities

Writing time-domain circuit equations for the voltage drops on the local source end of the fault loop for the incremental quantities (assuming all self and mutual line reactance among phases are equal, i.e. $L_{la1} = L_{lb1} = L_{lc1} = L_{l1}$ line self reactance, $M_{lab1} = M_{lac1} = M_{lbc1} = M_{l1}$ line mutual reactance between each pair of phases),

3.3Improved Faulted Phase Identification in Systems with IBRs using Incremental Voltages

$$\begin{bmatrix}\Delta v_{Ra}\\ \Delta v_{Rb}\\ \Delta v_{Rc}\end{bmatrix} = \begin{bmatrix}\Delta v_{fa}\\ \Delta v_{fb}\\ \Delta v_{fc}\end{bmatrix} - \begin{bmatrix}L_{l1} & M_{l1} & M_{l1}\\ M_{l1} & L_{l1} & M_{l1}\\ M_{l1} & M_{l1} & L_{l1}\end{bmatrix}.\frac{d}{dt}\begin{bmatrix}\Delta i_{a1}\\ \Delta i_{b1}\\ \Delta i_{c1}\end{bmatrix} \quad (3\text{-}1)$$

$$[\Delta v_{Rabc}] = [\Delta V_{fabc}] - [Z_{l1}].\frac{d}{dt}[\Delta \mathrm{i}_{1abc}] \quad (2\text{-}1a)$$

A similar equation can be written for the voltage drop across the local end source (similar assumptions are made for self and mutual reactance of the sources, L_{s1} local source self-reactance, M_{S1} local source mutual reactance for all phases),

$$\begin{bmatrix}\Delta v_{Ra}\\ \Delta v_{Rb}\\ \Delta v_{Rc}\end{bmatrix} = \begin{bmatrix}L_{s1} & M_{s1} & M_{s1}\\ M_{s1} & L_{s1} & M_{s1}\\ M_{s1} & M_{s1} & L_{s1}\end{bmatrix}.\frac{d}{dt}\begin{bmatrix}\Delta i_{a1}\\ \Delta i_{b1}\\ \Delta i_{c1}\end{bmatrix} \quad (3\text{-}2)$$

$$[\Delta v_{Rabc}] = [Z_{s1}].\frac{d}{dt}[\Delta \mathrm{i}_{1abc}] \quad (2\text{-}2a)$$

Substituting $\frac{d}{dt}[\Delta \mathrm{i}_{1abc}]$ from (3-2) in (3-1),

$$[\Delta v_{Rabc}] = [\Delta V_{fabc}] - [Z_{l1}].[Z_{s1}]^{-1}.[\Delta v_{Rabc}]$$

$$[\Delta v_{Rabc}] = \{I + [Z_{l1}].[Z_{s1}]^{-1}\}^{-1}.[\Delta V_{fabc}] \quad (3\text{-}3)$$

$$\begin{bmatrix}\Delta v_{Ra}\\ \Delta v_{Rb}\\ \Delta v_{Rc}\end{bmatrix} = \frac{1}{D}\begin{bmatrix}K_L & K_M & K_M\\ K_M & K_L & K_M\\ K_M & K_M & K_L\end{bmatrix}.\begin{bmatrix}v_{fa}\\ v_{fb}\\ v_{fc}\end{bmatrix} \quad (3\text{-}4)$$

Where, $D = \frac{P_1}{P_2.P_3}, P_1 = {L_{s1}}^2 + L_{s1}.M_{s1} - 2{M_{s1}}^2$

$P_2 = [L_{l1}(L_{s1} + M_{s1}) + M_{s1}(M_{l1} - 2M_{s1}) + {L_{s1}}^2 + L_{s1}.M_{s1}]$,

$P_3 = [L_{l1}(L_{s1} + M_{s1}) - 2M_{s1}(M_{l1} + M_{s1}) + {L_{s1}}^2 + L_{s1}.M_{s1}]$,

$K_L = [L_{l1}.L_{s1} + M_{l1}.L_{s1} - 2M_{l1}.M_{s1} + {L_{s1}}^2 + L_{s1}.M_{s1} - 2{M_{s1}}^2]$ and

$$K_M = [M_{l1}.M_{s1}]$$

Looking into the network from the fault location, the two parallel segments of the network (local and remote ends) can be reduced into one equivalent, for which another set of circuit equations can be written,

3.3Improved Faulted Phase Identification in Systems with IBRs using Incremental Voltages

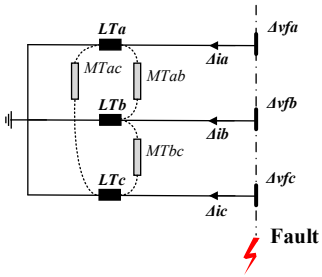

L_{Tp}: Total equvelent self impedance (rectance) - phase p
M_{Tpq}: Total equvelent mutual impedance (rectance) - phase p to q

Figure 3.7 Equivalent incremental fault circuit

System impedance matrix, $[Z_T]$, of the equivalent incremental fault circuit can be determined by considering that the two fault loops are in parallel, each of which has respective source and line impedances connected in series.

$$[Z_1] = \begin{bmatrix} L_{s1}+L_{l1} & M_{s1}+M_{l1} & M_{s1}+M_{l1} \\ M_{s1}+M_{l1} & L_{s1}+L_{l1} & M_{s1}+M_{l1} \\ M_{s1}+M_{l1} & M_{s1}+M_{l1} & L_{s1}+L_{l1} \end{bmatrix} = \begin{bmatrix} L_1 & M_1 & M_1 \\ M_1 & L_1 & M_1 \\ M_1 & M_1 & L_1 \end{bmatrix} \quad (3\text{-}5)$$

$$[Z_2] = \begin{bmatrix} L_{s2}+L_{l2} & M_{s2}+M_{l2} & M_{s2}+M_{l2} \\ M_{s2}+M_{l2} & L_{s2}+L_{l2} & M_{s2}+M_{l2} \\ M_{s2}+M_{l2} & M_{s2}+M_{l2} & L_{s2}+L_{l2} \end{bmatrix} = \begin{bmatrix} L_2 & M_2 & M_2 \\ M_2 & L_2 & M_2 \\ M_2 & M_2 & L_2 \end{bmatrix} \quad (3\text{-}6)$$

$$[Z_T] = [[Z_1]^{-1} + [Z_2]^{-1}]^{-1} = \begin{bmatrix} L_T & M_T & M_T \\ M_T & L_T & M_T \\ M_T & M_T & L_T \end{bmatrix}$$

$$L_T = \frac{L_2\{(L_1 - M_1).(L_1 + 2.M_1)\} + L_1\{(L_2 - M_2).(L_2 + 2.M_2)\}}{\big((L_1 - M_1) + (L_2 - M_2)\big).\big((L_1 + 2.M_1) + (L_2 + 2.M_2)\big)}$$

$$M_T = \frac{M_2\{(L_1 - M_1).(L_1 + 2.M_1)\} + M_1\{(L_2 - M_2).(L_2 + 2.M_2)\}}{\big((L_1 - M_1) + (L_2 - M_2)\big).\big((L_1 + 2.M_1) + (L_2 + 2.M_2)\big)}$$

3.3Improved Faulted Phase Identification in Systems with IBRs using Incremental Voltages

3.3.1.1. Line-to-Ground (LG) Fault

For a Phase A-to-ground fault the flowing initial conditions apply,

$$\begin{gathered}\Delta v_{fa} = V_f sin(\omega t + \phi) \\ \Delta i_a = \Delta i_{a1} + \Delta i_{a2} \\ \Delta i_b = \Delta i_{b1} + \Delta i_{b2} = 0 \\ \Delta i_c = \Delta i_{c1} + \Delta i_{c2} = 0\end{gathered}$$

Considering the equivalent incremental fault circuit, the following equation can be written for a Phase A-to-ground fault,

$$\begin{bmatrix}\Delta v_{fa} \\ \Delta v_{fb} \\ \Delta v_{fc}\end{bmatrix} = \begin{bmatrix}L_T & M_T & M_T \\ M_T & L_T & M_T \\ M_T & M_T & L_T\end{bmatrix} . \frac{d}{dt} \begin{bmatrix}\Delta i_a = \Delta i_{a1} + \Delta i_{a2} \\ \Delta i_b = 0 \\ \Delta i_c = 0\end{bmatrix} \tag{3-7}$$

Since we are considering a Phase A-to-ground fault, the incremental phase A voltage at the fault is assumed to be known and represented in a generic manner $[V_f sin(\omega t + \phi)]$, where V_f represents the pre-fault voltage at the fault location and ϕ the Fault Inception Angle (FIA). With Δv_{fa} and L_T known, $d/dt\ [\Delta i_a]$ can be determined, which in turn enables determination of the incremental phase B and C voltages at the fault.

$$\begin{gathered}\Delta v_{fa} = L_T . \frac{d}{dt} \Delta i_a \\ \frac{d}{dt} \Delta i_a = \frac{1}{L_T} . V_f sin(\omega t + \phi) \\ \Delta v_{fb} = Z_{T21} . \frac{d}{dt} \Delta i_a = M_T . \frac{d}{dt} \Delta i_a \\ \Delta v_{fb} = \frac{M_T}{L_T} . V_f sin(\omega t + \phi) = \Delta v_{fc}\end{gathered} \tag{3-8}$$

Now with ΔV_{fabc} known, the incremental phase voltages at the relaying location $[\Delta v_{Rabc}]$ can be calculated using (3-4).

3.3Improved Faulted Phase Identification in Systems with IBRs using Incremental Voltages

$$\begin{bmatrix}\Delta v_{Ra}\\ \Delta v_{Rb}\\ \Delta v_{Rc}\end{bmatrix}=\frac{1}{D}\begin{bmatrix}K_L & K_M & K_M\\ K_M & K_L & K_M\\ K_M & K_M & K_L\end{bmatrix}.\begin{bmatrix}V_f sin(\omega t+\phi)\\ \frac{M_T}{L_T}.V_f sin(\omega t+\phi)\\ \frac{M_T}{L_T}.V_f sin(\omega t+\phi)\end{bmatrix} \tag{3-9}$$

$$\begin{aligned}\Delta v_{Ra}&=\frac{1}{D}\left[K_L+\frac{2.K_M.M_T}{L_T}\right].V_f sin(\omega t+\phi)\\ \Delta v_{Rb}=\Delta v_{Rc}&=\frac{1}{D}\left[K_M+\frac{(K_L+K_M).M_T}{L_T}\right].V_f sin(\omega t+\phi)\end{aligned} \tag{3-10}$$

From the formula given in (3-10), it is obvious that all incremental phase voltages at the relaying location are in-phase. By considering typical relative magnitudes of self and mutual reactance(s) of the real-world power systems (such as self-impedance is 2 times the respective mutual impedance), it can also be shown that Δv_{Ra} is several times higher in amplitude than Δv_{Rb} and Δv_{Rc} (which are equal).

3.3.1.2. Line-to-Line-to-Ground (LLG) Fault

For a Phase A-B-to-ground fault with zero fault resistance, the following initial conditions apply,

$$\Delta v_{fa}=V_f sin(\omega t+\phi),\ \ \Delta v_{fb}=V_f sin(\omega t+\phi-\pi/3)$$
$$\Delta i_a=\Delta i_{a1}+\Delta i_{a2}$$
$$\Delta i_b=\Delta i_{b1}+\Delta i_{b2}$$
$$\Delta i_c=\Delta i_{c1}+\Delta i_{c2}=0$$

Considering the equivalent incremental fault circuit, the following equation can be written for a Phase A-B-to-ground fault,

3.3Improved Faulted Phase Identification in Systems with IBRs using Incremental Voltages

$$\begin{bmatrix}\Delta v_{fa}\\ \Delta v_{fb}\\ \Delta v_{fc}\end{bmatrix}=\begin{bmatrix}L_T & M_T & M_T\\ M_T & L_T & M_T\\ M_T & M_T & L_T\end{bmatrix}.\frac{d}{dt}\begin{bmatrix}\Delta i_a=\Delta i_{a1}+\Delta i_{a2}\\ \Delta i_b=\Delta i_{b1}+\Delta i_{b2}\\ \Delta i_c=0\end{bmatrix} \tag{3-11}$$

When a Phase A-B-to-ground fault is considered, the incremental phase A and B voltages at the fault are assumed to be known and have equal amplitudes with phase angles 120^0 apart. They can be represented in a generic manner $[\Delta v_{fa}=V_f sin(\omega t+\phi)]$, $[\Delta v_{fb}=V_f sin(\omega t+\phi-\pi/3)]$. This allows determination the incremental phase C voltage at the fault.

$$\Delta v_{fc}=\frac{M_T}{L_T+M_T}V_f sin(\omega t+\phi-\pi/6)$$

Similar to the previous case of a LG fault, with ΔV_{fabc} known, the incremental phase voltages at the relaying location $[\Delta v_{Rabc}]$ can be determined using (3-4).

$$\begin{bmatrix}\Delta v_{Ra}\\ \Delta v_{Rb}\\ \Delta v_{Rc}\end{bmatrix}=\frac{1}{D}\begin{bmatrix}K_L & K_M & K_M\\ K_M & K_L & K_M\\ K_M & K_M & K_L\end{bmatrix}.\begin{bmatrix}V_f sin(\omega t+\phi)\\ V_f sin(\omega t+\phi-2\pi/3)\\ \frac{M_T}{L_T+M_T}.V_f sin(\omega t+\phi-\pi/3)\end{bmatrix}$$

$$\begin{aligned}\Delta v_{Ra}&=\frac{K_M}{D}\left[\left(\frac{K_L}{K_M}\right).V_f sin(\omega t+\phi)+V_f sin(\omega t+\phi-2\pi/3)\right.\\ &\qquad\left.+\left(\frac{1}{L_T/M_T+1}\right).V_f sin(\omega t+\phi-\pi/3)\right]\\ \Delta v_{Rb}&=\frac{K_M}{D}\left[V_f sin(\omega t+\phi)+\left(\frac{K_L}{K_M}\right).V_f sin(\omega t+\phi-2\pi/3)\right.\\ &\qquad\left.+\left(\frac{1}{L_T/M_T+1}\right).V_f sin(\omega t+\phi-\pi/3)\right]\\ \Delta v_{Rc}&=\frac{K_M}{D}\left[V_f sin(\omega t+\phi)+V_f sin(\omega t+\phi-2\pi/3)\right.\\ &\qquad\left.+\left(\frac{K_L}{K_M}\right)\left(\frac{1}{L_T/M_T+1}\right).V_f sin(\omega t+\phi-\pi/3)\right]\end{aligned} \tag{3-12}$$

Formula given in (3-12) suggests that incremental phase *abc* voltages at the relaying location are not in-phase for a LLG fault. Similar to a LG fault, it can be shown that Δv_{Ra} and Δv_{Rb} are several times higher in amplitude than Δv_{Rc}, by making reasonable assumptions for the relative magnitudes of self and mutual reactance(s) of the system. However, since

incremental phase *abc* voltages are not in-phase, a simple amplitude comparison at an instant in time (i.e. instantaneous values) will not always indicate their relative scale.

3.3.1.3. Line-to-Line (LL) Fault

For a Phase A-B fault the flowing initial conditions apply,

$$\begin{gathered}\Delta v_{fa} = V_f sin(\omega t + \phi), \qquad \Delta v_{fb} = -V_f sin(\omega t + \phi) \\ \Delta i_a = \Delta i_{a1} + \Delta i_{a2} \\ \Delta i_b = \Delta i_{b1} + \Delta i_{b2} \\ \Delta i_c = \Delta i_{c1} + \Delta i_{c2} = 0 \\ \begin{bmatrix}\Delta v_{fa} \\ \Delta v_{fb} \\ \Delta v_{fc}\end{bmatrix} = \begin{bmatrix}L_T & M_T & M_T \\ M_T & L_T & M_T \\ M_T & M_T & L_T\end{bmatrix} . \frac{d}{dt} \begin{bmatrix}\Delta i_a = \Delta i_{a1} + \Delta i_{a2} \\ \Delta i_b = \Delta i_{b1} + \Delta i_{b2} \\ \Delta i_c = 0\end{bmatrix} \\ \Delta v_{fc} = 0\end{gathered} \tag{3-13}$$

For a Phase A-B fault, the incremental phase A and B voltages at the fault is assumed to be known (equal in amplitude and 180^0 apart). They are represented in a generic manner as $[\Delta v_{fa} = V_f sin(\omega t + \phi)]$, $[\Delta v_{fb} = -V_f sin(\omega t + \phi)]$, which allows determination of incremental phase C voltage at the fault. As in the previous cases, with ΔV_{fabc} known, the incremental phase voltages at the relaying location $[\Delta v_{Rabc}]$ can be determined using (3-4).

$$\begin{gathered}\begin{bmatrix}\Delta v_{Ra} \\ \Delta v_{Rb} \\ \Delta v_{Rc}\end{bmatrix} = \frac{1}{D}\begin{bmatrix}K_L & K_M & K_M \\ K_M & K_L & K_M \\ K_M & K_M & K_L\end{bmatrix} . \begin{bmatrix}V_f sin(\omega t + \phi) \\ -V_f sin(\omega t + \phi) \\ 0\end{bmatrix} \\ \Delta v_{Ra} = \frac{K_M}{D}\left[\left(\frac{K_L}{K_M}\right) . V_f sin(\omega t + \phi) - V_f sin(\omega t + \phi)\right] \\ \Delta v_{Rb} = \frac{K_M}{D}\left[V_f sin(\omega t + \phi) - \left(\frac{K_L}{K_M}\right) . V_f sin(\omega t + \phi)\right] = -\Delta v_{Ra} \\ \Delta v_{Rc} = 0\end{gathered} \tag{3-14}$$

It can be seen from the formula given in (3-14) that incremental phase C (un-faulted phase) voltage at the relaying location is zero for a LL fault and those of phases A and B are

equal and opposite. Therefore, in theory, Δv_{Ra} and Δv_{Rb} are infinity larger than Δv_{Rc} for a LL fault. A real system, however, will produce a small, non-zero incremental phase C voltage for a LL fault as a result of effects of capacitances of the network, which are not considered in this analysis.

3.3.2 Proof-of-Concept Simulations

In an attempt to further examine the behavior of incremental voltages in power system using the above derived formula, a set of theoretical calculations were performed on a simplified power system with typical impedances in MATLAB®. Figure 3.9 presents the single line diagram of the simplified 3-phase power system used for theoretical calculations, which is identical in configuration to the system used for the derivations. Note that impedances in the system are defined using self (L) and mutual (M) impedances for each element (as opposed to sequence impedances) and, the ratio between the self to mutual impedance in each element is chosen to yield typical positive and zero-sequence impedance values in a power system.

L_{s1}=0.05 pu, M_{s1}= L_{s1}/1.6=0.0312 pu
L_{s2}=0.04 pu, M_{s2}= L_{s2}/1.5= 0.0267 pu

L_{l1}=0.02 pu, M_{l1}= L_{l1}/2.75= 0.0073 pu
L_{l2}=0.08 pu, M_{l2}= L_{l2}/2.75= 0.0291 pu

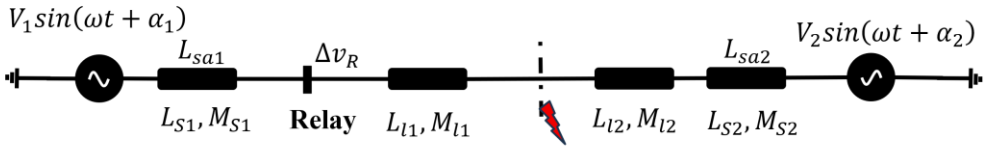

Figure 3.8 Single line diagram of the simplified power system used for theoretical simulations

Concise set of simulation results are presented in Figure 3.9. Here, the incremental voltages seen at the relaying location for (a) AG fault, (b) ABG fault and (c) AB fault produced by theoretical calculations are plotted. All resistances were neglected and the pre-fault voltage

at the fault location was taken to be 1.0 pu. Results for the first 60 Hz cycle following the fault are presented with the fault inception angle (ϕ) was set to 0.0^0.

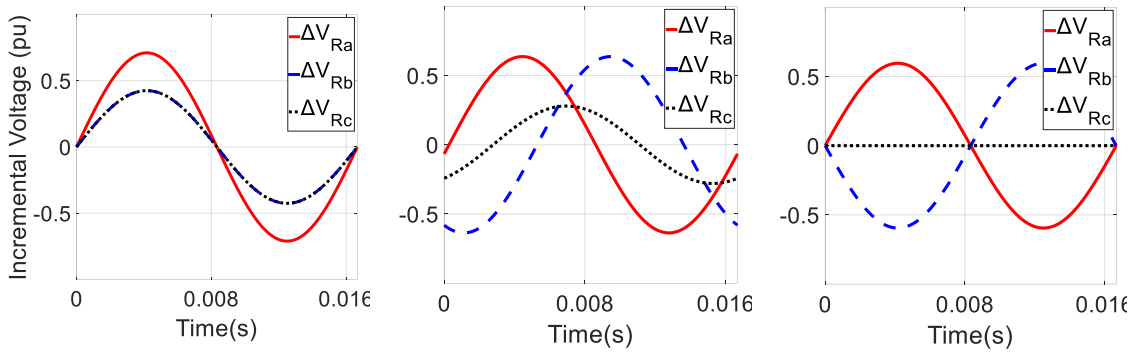

Figure 3.9 Incremental voltages seen at the relaying location for (a) AG fault, (b) ABG fault and (c) AB fault

Figure 3.10 presents results for incremental voltages seen at the relaying location for ABG faults with fault inception angle (a) 45^0, (b) 90^0 and (c) 135^0. Results presented in both Figure 3.8 and Figure 3.10 agree with the theoretical analysis in previous subsections. As predicted by the theoretical analysis, all three incremental voltages are in-phase for the LG faults and 180^0 out-of-phase for LL faults (un-faulted phase is zero for LL faults). By contrast, incremental voltages for LLG are out-of-phase, which also agrees with theoretical analysis. Furthermore, theoretical formulae derived above also suggests that the relative phase angles of the incremental voltages for LLG faults are also dependent on system impedances. These sensitivities of LLG faults to fault inception angle and system impedances make their discrimination considerably more problematic than other fault types in comparison. This also explains the challenges experienced by previous researchers in categorizing LLG faults [50].

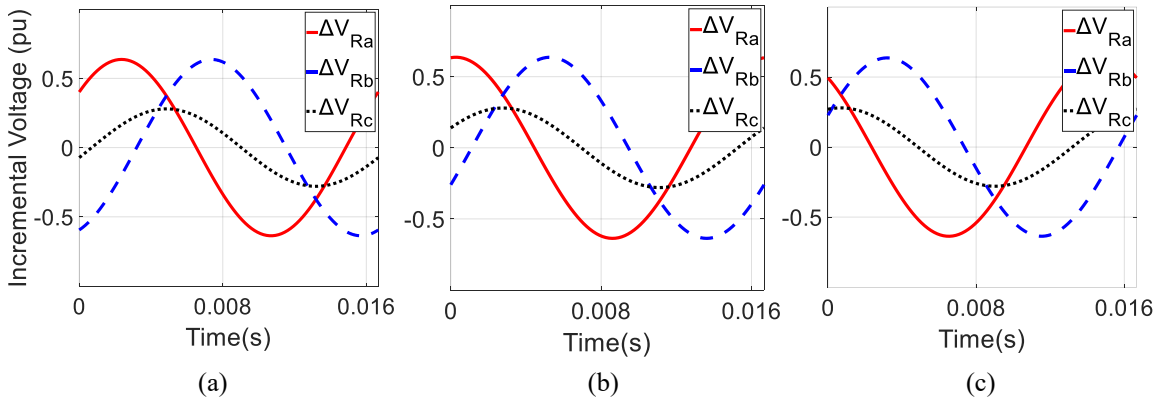

Figure 3.10 Incremental voltages seen at the relaying location for ABG faults with fault inception angle (a) 45^0, (b) 90^0 and (c) 135^0

3.3.3 Proposed Faulted Phase Identification Algorithm

Based on the theoretical derivations for incremental phase voltages and the proof-of-concept calculation results presented in subsection 3.3.2 (see Figure 3.9 subplots (a) and (c)), it can be observed that the incremental voltages of the three phases for line-ground (LG) faults are in-phase and those for line-line (LL) faults are 180° out-of-phase (with un-faulted phase being zero). This essentially means that relative strength of incremental voltages for these fault types can be determined by a simple time-domain (instantaneous) comparison of amplitudes.

3.3.3.1. Use of Integrals for Detecting LLG faults

However, since incremental voltages are not in-phase for a line-line-ground (LLG) faults as shown in Figure 3.10, a simple amplitude comparison in time-domain will not always indicate their relative strength. Comparison of instantaneous values can produce unreliable results for some inception angles. In addition, it can be shown that even the relative strengths of the incremental voltages are dependent on fault inception angle (ϕ) and system impedances.

3.3Improved Faulted Phase Identification in Systems with IBRs using Incremental Voltages

Theoretically, faulted phase identification can be obtained by detecting and holding the maximum value of the incremental voltages (or a ratio of them), which yields reasonable results for LG and LL faults. However, since the voltages are out-of-phase for LLG faults, the maximum value occurring in a predefined period (for example, half-a-cycle) must be considered. Algorithms without a similar security measure tend to transiently mis-operate for some fault inception angles (in particular, this can cause mis-classification of LLG as LG faults). In addition, methods dependent on a single reading (such as a maximum values) are also more prone to mis-operate due to one abnormal sample such as a poorly filtered voltage transient (note that system voltages comprise more transient components in comparison to currents). Moreover, the capacitive (and resistive) effects of the network can impose additional dynamics on system voltages (such as high frequency oscillations, time constants etc.), which can further complicate a method depending on a single reading. In this context, the use of the integral of the incremental voltages over a period is much more robust than depending on a single reading to overcome these security concerns.

3.3.3.2. Fault Indices

This subsection presents a pairwise comparison of ratios of integral of incremental phase voltages to identify the strength of the incremental voltages, and thereby the faulted phases as well. Voltage measurements are preferred over current (or power) due to unreliable and unpredictable nature of IBR injected currents during faults. As mentioned earlier, use of the integral of incremental voltages improves security of the algorithm.

3.3Improved Faulted Phase Identification in Systems with IBRs using Incremental Voltages

The algorithm proposed in this paper uses six indices as defined in (3-15) to determine the relative strength of incremental phase voltages. The work presented in [45] had proposed a similar indices-based approach for faulted phase identification using rate-of-change of incremental currents ($d\Delta \mathrm{i}/dt$), which did not perform well for system with IBRs, however.

$$F_{pq} = \frac{\int_{t_0}^{t_0+T_w} |\Delta v_{Rp}|}{\int_{t_0}^{t_0+T_w} |\Delta v_{Rq}|}, \quad F_{qp} = \frac{\int_{t_0}^{t_0+T_w} |\Delta v_{Rq}|}{\int_{t_0}^{t_0+T_w} |\Delta v_{Rp}|}, \qquad p, q \in [a, b, c] \tag{3-15}$$

Here, t_0 denotes the time of fault detection and the T_w, the window of integration. The absolute values of incremental phase voltages are integrated over a period of T_w starting from t_0, and respective ratios are calculated. Distinguishing between grounded and ungrounded faults is achieved by detecting the existence of a zero-sequence voltage.

Identification of the faulted phase(s) for unbalanced faults is based on the relative magnitude of the indices, which is summarized in Table 3.7 below. As can be seen, the two largest indices essentially determine the faulted phase(s). Observe that the combination of the two highest indices for LLG faults and LL are identical. However, they can be easily discriminated using the presence of a zero-component voltage ($v_0 = (v_a + v_b + v_c)/3$), which is the method used in this work.

3.3Improved Faulted Phase Identification in Systems with IBRs using Incremental Voltages

Table 3.7: Fault type identification using indices (unbalanced faults), shaded indices are the two largest for each fault type

Fault Type	Index					
	F_{ab}	F_{bc}	F_{ca}	F_{ba}	F_{cb}	F_{ac}
AG	■					■
BG		■		■		
CG			■		■	
ABG/AB		■				■
BCG/BC			■	■		
CAG/CA	■				■	

It can be seen from Table 3.7 that for each fault of a particular fault type, a unique pair of indices become larger than the rest. For example, for a phase A-to-ground fault, phase A incremental voltage is greater than those of phases B and C, which are relatively close, but non-zero. Therefore, the relationship between the indices should be $F_{ab},\ F_{ac} \gg 1,\ F_{bc},\ F_{bc} \approx 1, F_{ba},\ F_{ca} \ll 1$. Similarly, for a phase A-to-B-to-ground fault, incremental voltages of phases A and B are greater than that of phases C, therefore, the relationship between the indices should be $F_{bc},\ F_{ac} \gg 1,\ F_{ab},\ F_{ba} \approx 1, F_{cb},\ F_{ca} \ll 1$. Even though this can be inferred from a general understanding of a power system during faults, a more rigorous, quantitative explanation can be obtained using the theoretical derivation provided in subsection 3.3.1. The theoretical analysis also revealed that the relative relationship between incremental voltages is more nuanced than what the common sense suggests. For example, for LLG faults, since incremental phase voltages are not in-phase, fault indices have a strong sensitivity to FIA (ϕ).

3.3Improved Faulted Phase Identification in Systems with IBRs using Incremental Voltages

In addition, the same six indices can be used to identify three-phase faults as well. During a three-phase fault, the incremental voltages induced in all three phases are theoretically the same resulting in all six indices having a value close to 1. This can be exploited to declare three-phase faults.

3.3.3.3. Implementation

The proposed method was implemented in an EMT type simulation environment for testing and validation. Figure 3.11 illustrates the digital signal processing and implementation of the proposed method in the simulation environment.

First, high frequency components of the voltage measurements are filtered out using a low-pass filter (this represents analog hardware filtering in a real-world relay). Note that this algorithm is based on instantaneous (time-domain) fundamental frequency components of the voltage measurements. The measurements are then re-sampled at 4.8 kHz (since this a digital simulation, the original signals are inherently sampled based on the simulation time-step). The incremental values of the voltages are calculated using the following equation,

$$\Delta V_p(n) = V_p(n) - V_p(n - kN), \quad p \in [a, b, c] \tag{3-16}$$

where k is the delay in number of cycles and N is the number of samples-per-cycle (SPC). In this work, k and N values are set to 1 cycle and 80 SPC. The absolute value of a calculated incremental phase voltage is then fed into an integrator.

3.3Improved Faulted Phase Identification in Systems with IBRs using Incremental Voltages

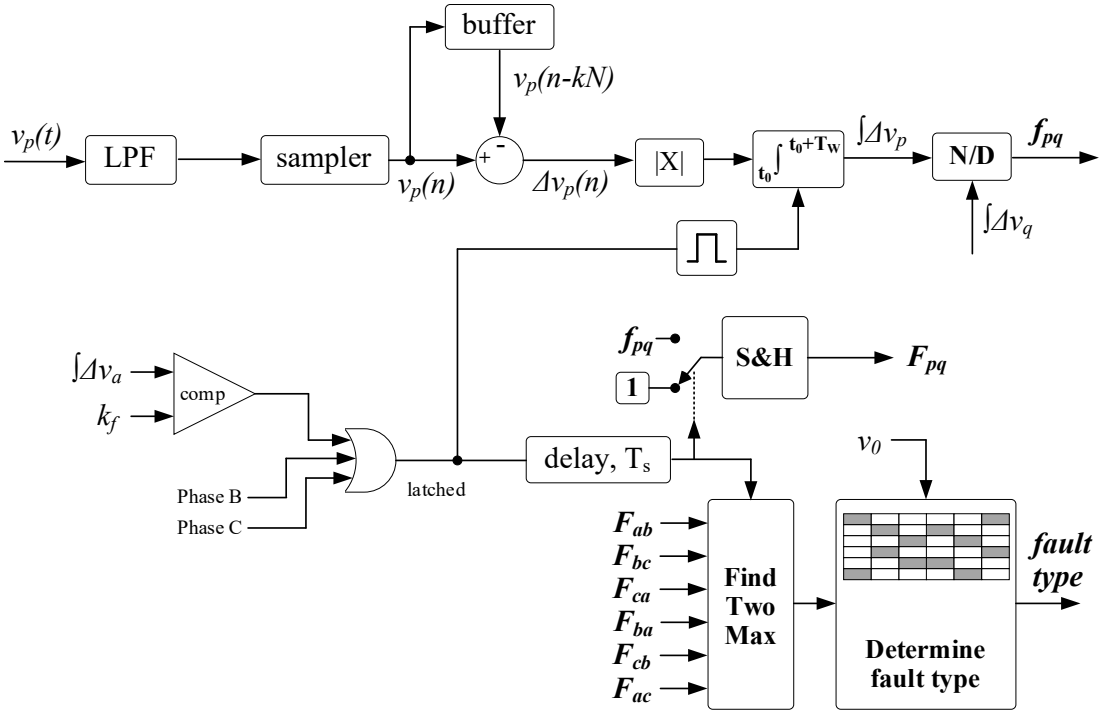

Figure 3.11 Digital signal processing and implementation of the proposed method

As can be seen in Figure 3.11, the process of faulted phase identification is triggered by fault detection. In this exercise, a simple limit-check method is used to detect faults, and a fault is declared when any of the integrated incremental voltages goes above a pre-determined threshold (k_f, set to 10). While this fault detection method complemented the proposed faulted phase identification method (as it requires fast fault detection in addition to reliability) for this work, it is entirely possible to replace it with another fault detection method with adequate reliability and speed of operation.

Once a fault is declared, all integrators are reset and the indices are released from their default pre-fault value of 1. The window of integration, T_w, must be larger than the sample-and-hold trigger, T_s. Shown in Figure 3.12 are the variation of incremental voltages, integrated

3.3Improved Faulted Phase Identification in Systems with IBRs using Incremental Voltages

incremental voltages and calculated fault indices for a ABG fault (with FIA 0.0^0) using the same proof-of-concept calculation presented in above subsection 3.3.2. Figure 3.13 presents variation the fault indices with FIA (ϕ) for different sample-and-hold times (T_s). As can be seen, the variation of fault indices is minimum when T_s is set to 8.33 ms (half-a-cycle at 60 Hz) and fault indices exhibit significant sensitivity to FIA when T_s deviates from 8.33 ms.

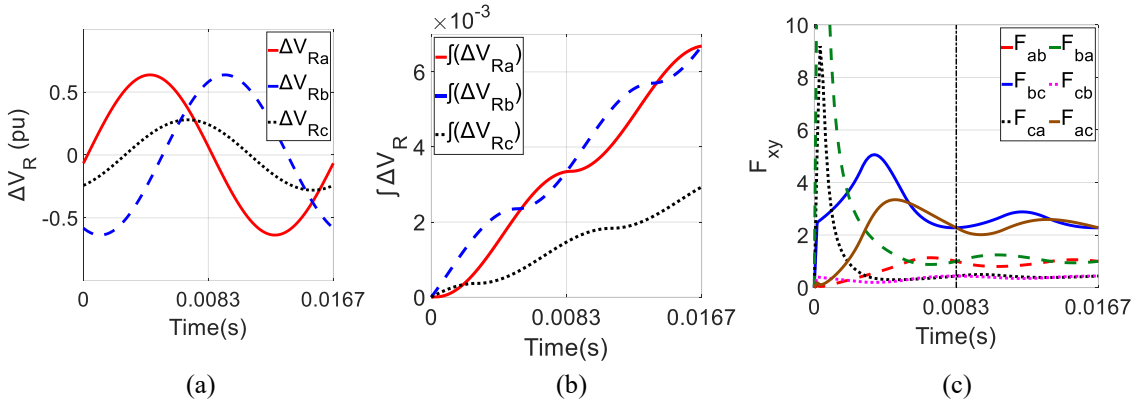

(a) (b) (c)

Figure 3.12 Variation of algorithm parameters with time for a ABG fault (a) incremental voltages, (b) integrated incremental voltages and (c) fault indices

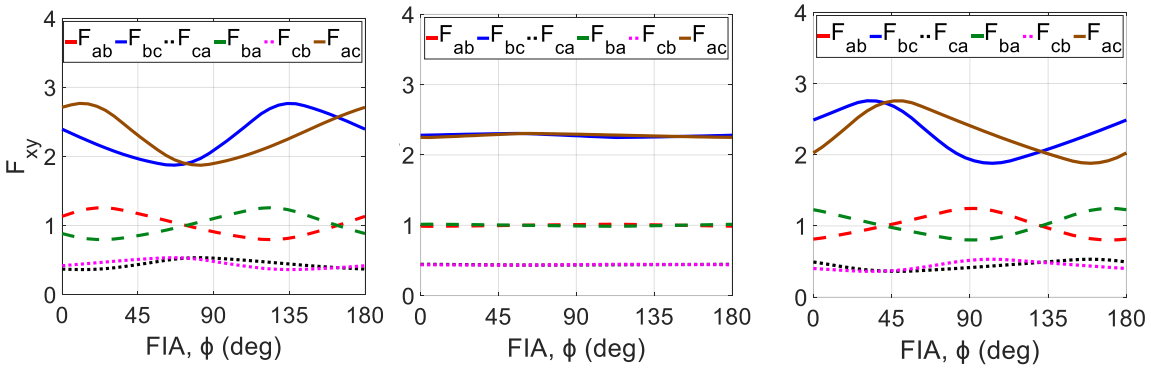

(a) (b) (c)

Figure 3.13 Variation fault indices with fault inception angle (ϕ) for different sample-and-hold times (Ts) (a) Ts=7 ms, (b) Ts=8.33 ms and (c) Ts=10 ms

This agrees with theoretical expectations as integration of any sinusoidal (rectified) wave of a fixed amplitude [$Asin(\omega t + \phi)$] over a half a cycle yields the same result ($2A/\omega$)

irrespective of its phase angle. It is impossible to eradicate this fluctuation and the resulting error with any T_s value below half a cycle (8.33 ms).

In particular, the value of T_s is critical for reliable identification of LLG faults for all FIA. It is possible, however, to achieve reasonable performance for faulted phase identification with a value smaller than 8.33 ms for T_s if faster operation is required. Notice that the choice of T_s is a compromise between speed of operation and security of protection. In this work, T_w of 10.0 ms and T_s of 8.33 ms has been used as it strikes the best balance between speed and security. These settings produced 100 % reliable results (for tests performed in this work) while producing results fast enough for most real-world applications. At the expiration of T_s, the indices are sampled and fed into the rest of the algorithm where faulted phases are identified depending on their relative magnitude. In addition, calculated zero-component voltage (v_0) is also provided to discriminate between LLG and LL faults.

3.3.4 Performance Evaluation

The effectiveness of the above-presented faulted phase identification method was validated by performing detailed EMT simulations in a Digital Real-Time Simulation (DRTS) environment (i.e. RTDS®). Figure 3.14 presents the single line diagram of the test network used for these simulations. The IBR (type IV wind turbine-generator (WTG) system) is rated at 100 MW and pushes power via a short, 138 kV transmission line. The remote end of this line is connected to a 230 kV/60 Hz grid through a transformer and an adjacent transmission system. A conventional power source (a synchronous generator) is connected to the remote bus (*Bus 2*) via another short transmission line as depicted in Figure 3.14. The focus this work is the protection of *Line12*, which connects the IBR to the rest of the power system. The protection method being presented in this work is presumably implemented in the line protection relay (R) of the tie-line, deployed at *Bus 1* looking into *Line12*. Results presented are mainly for faults along *Line12* (forward) and on *Bus 1* (reverse).

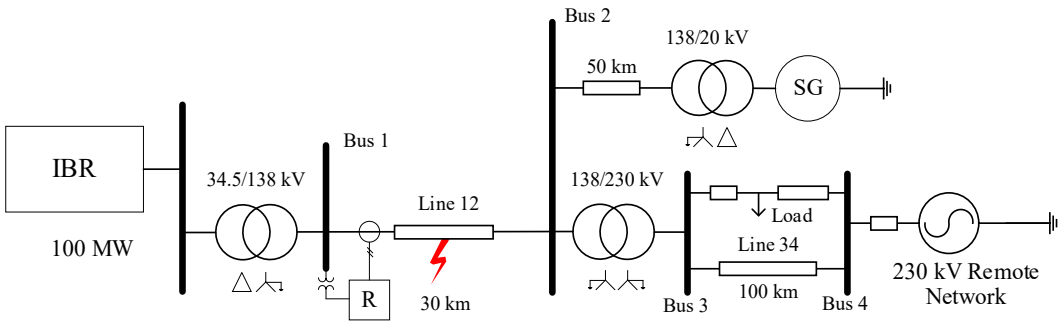

Figure 3.14 Single line diagram of the test network simulated in the DRTS

3.3Improved Faulted Phase Identification in Systems with IBRs using Incremental Voltages

Figure 3.15 presents the voltage measurements and algorithm parameters for a mid-line (50%), short circuit ABG fault. Note that the voltage measurements (primary) given in Figure 3.15-(a) are after signal processing (low-pass filtering and sampling at 80 samples per cycle). Notice that fault detection (and ground fault indication) occurs soon after fault inception (1-2 ms), at which point the calculation of fault indices is started. Half a cycle (8.33 ms) after this, fault indices are sampled and fed into the faulted phase identification algorithm. As can be seem from Figure 3.15-(g), the detection of fault type takes approximately 9-10 ms following fault inception.

3.3Improved Faulted Phase Identification in Systems with IBRs using Incremental Voltages

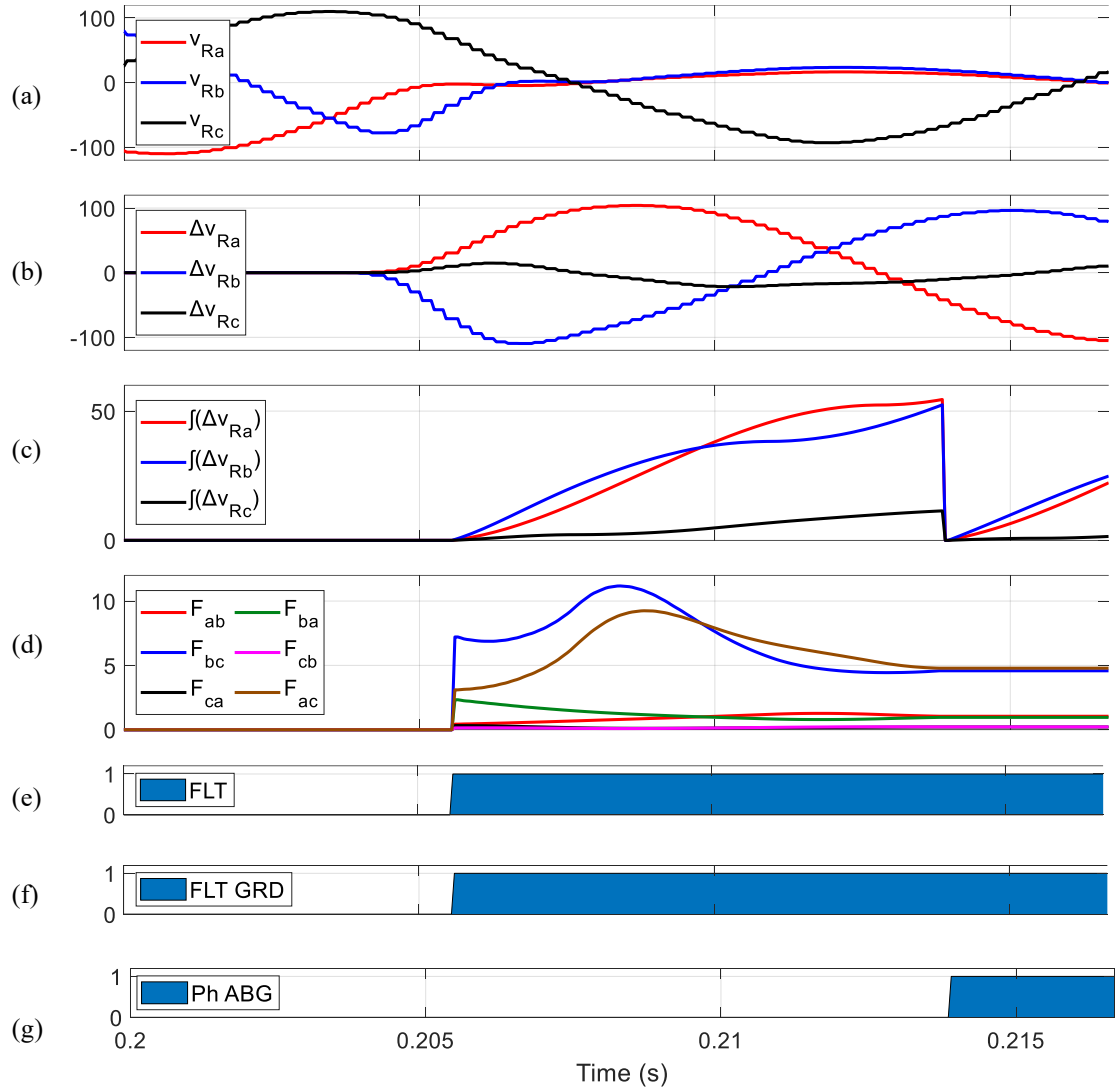

Figure 3.15 Measurements/fault parameters for a mid-line ABG fault (a) Phase-to-ground voltage (b) incremental voltage, (c) integrated incremental voltages and (d) fault indices, (e) fault detection signal (f) ground fault indicator and (g) ABG fault detection

3.3Improved Faulted Phase Identification in Systems with IBRs using Incremental Voltages

3.3.4.1. Impact of Fault Inception Angle

Given in Figure 3.16 is the variation of fault indices (used for faulted phase identification) with fault inception angle (ϕ) for a mid-line, low impedance fault of different fault types (covering all possible unbalanced fault types). Here, ϕ was measured with respect to the phase A voltage at *Bus 1* and varied from $0^{\circ} - 180^{\circ}$ with a resolution of 5°. As predicted by the theoretical equations, the variation of fault indices with ϕ for LG faults was minimal. Indices for LLG faults also did not exhibit a significant amount of variation with ϕ with an optimized sample-and-hold time of 8.33 ms, even though the variation is larger than the theoretical expectations (Figure 3.13-b). Indices for LL faults did produce a considerable variation with ϕ. However, this is inconsequential for faulted phase identification as the two largest indices have significantly higher values than the rest for all values of ϕ. It is also important in this context to note that the values of the two highest fault indices for LL faults are theoretically infinite (as the incremental voltage of the un-faulted phase is zero, see subsection 3.3.2). In a real system, there is a small but a non-zero incremental voltage on the un-faulted phase resulting in greater contrast between fault indices. In general, it can be stated that all fault types produced expected results and the fault inception angle did not affect performance of the algorithm.

3.3Improved Faulted Phase Identification in Systems with IBRs using Incremental Voltages

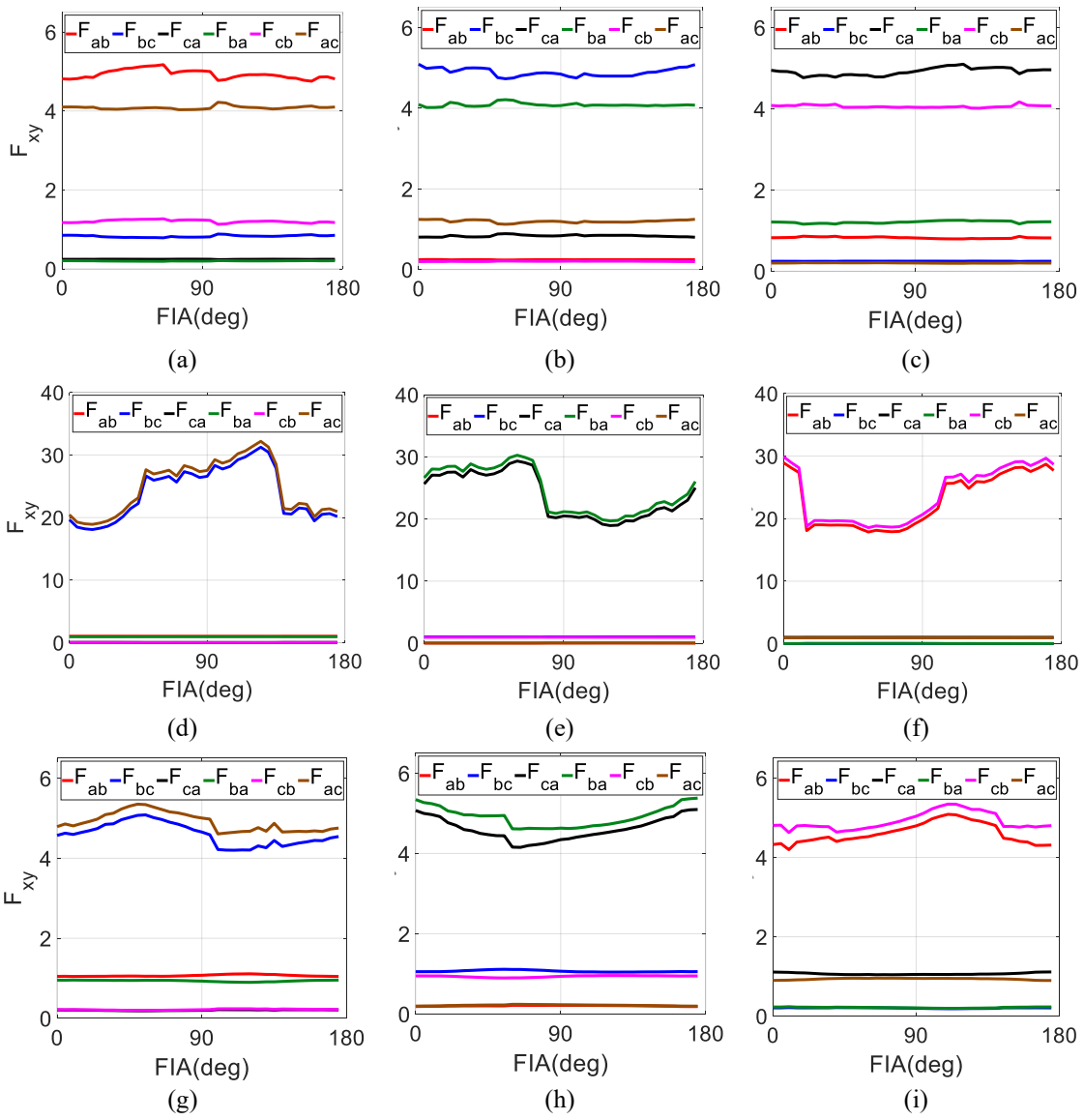

Figure 3.16 Variation fault indices with fault inception angle (ϕ) for different fault types for mid-line faults (a) AG, (b) BG, (c) CG, (d) AB, (e) BC, (f) CA, (g) ABG, (h) BCG, and (i) CAG

3.3Improved Faulted Phase Identification in Systems with IBRs using Incremental Voltages

Figure 3.17 presents a cluster of plots depicting the variation of fault indices with fault inception angle (ϕ) for faults at different locations on *Line 12* (only three fault types are shown).

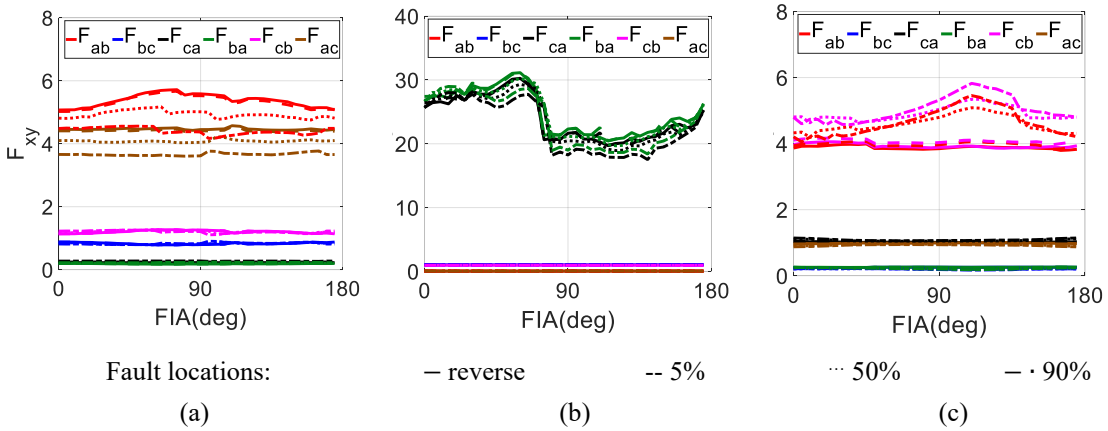

Figure 3.17 Variation of fault indices with fault inception angle (ϕ) for different fault locations (a) AG, (b) BC, and (c) CAG fault

It can be seen in Figure 3.17 that while the values changed slightly with the fault location, the overall characteristic of the fault indices more or less remained the same. Variation fault indices with fault inception angle (ϕ) for 3-phase (to ground) faults on *Line 12* at different locations is given in Figure 3.18. Since all six indices having a value close to 1 during a balanced 3-phase fault, the absolute values of $|F_{ab}-F_{ba}|$, $|F_{bc}-F_{cb}|$ and $|F_{ca}-F_{ac}|$ are checked against a threshold (set to 1.0). And, if all three parameters are less than the threshold, a 3-phase fault is declared. As can be seen from Figure 3.18, the fault parameters $|F_{ab}-F_{ba}|$, $|F_{bc}-F_{cb}|$ and $|F_{ca}-F_{ac}|$ stayed well below the set threshold for all FIA for faults at different locations on the tie-line. Identifying unbalanced faults is more challenging and critical for a faulted phase

identification method. Therefore, the rest of the results presented in this paper focuses on only unbalanced faults in the interest of optimizing space.

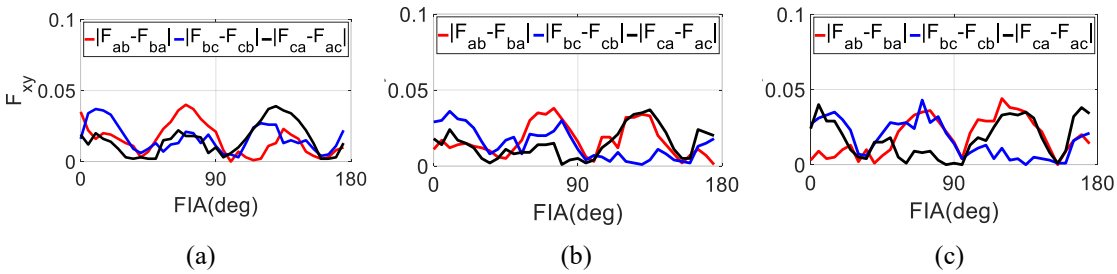

Figure 3.18 Variation of fault indices with fault inception angle (ϕ) for 3-phase faults on Line 12 at different locations (a) 5%, (b) 50%, and (c) 90%

3.3.4.2. Impact of Fault Location

Figure 3.19 shows the variation of fault indices with fault location alone. Here, location of the fault was changed from 5-95% of the line length with a resolution of 5%, while FIA (ϕ) remained unchanged at $0°$ (the default value of FIA). The variations observed were insignificant to affect the proposed faulted phase identification algorithm.

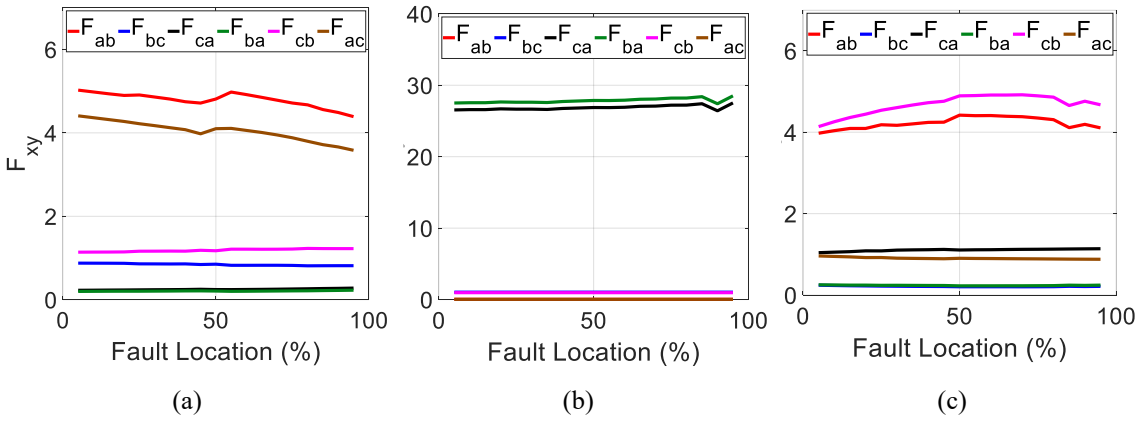

Figure 3.19 Variation of fault indices with fault location (%) along Line 12 for (a) AG, (b) BC, and (c) CAG fault

3.3.4.3. Impact of Fault Impedance

Plotted in Figure 3.20 are the variations of fault indices with fault resistance, which was changed from 0.01-50 Ω, while the FIA $(\phi = 0)$ and fault location (50%) were kept unchanged. The variations observed for LG and LL faults were insignificant.

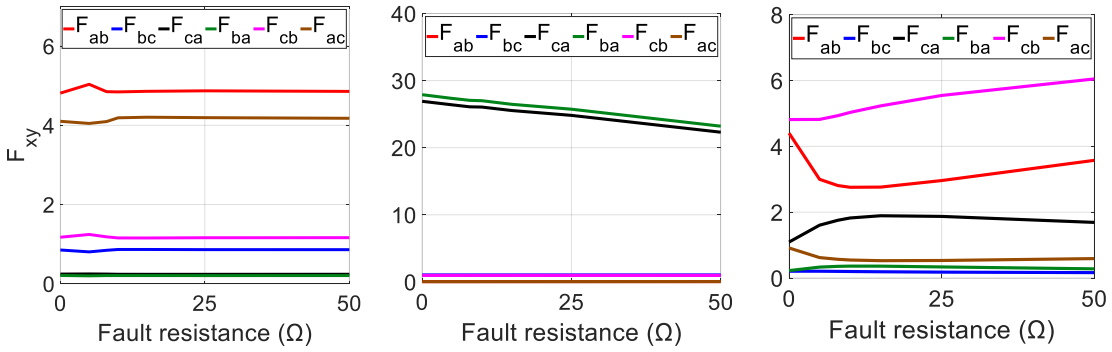

Figure 3.20 Variation of fault indices with fault resistance for mid-line faults (Line 12) (a) AG, (b) BC, and (c) CAG fault

While significant sensitivity to fault resistance was observed for LLG faults (Figure 3.20-(c)), it did not affect reliability of the proposed faulted phase identification algorithm. Results for an even higher fault impedance (of 100 Ω) are given in Figure 3.21, where the variation of fault indices with fault inception angle (ϕ) for a mid-line fault (*Line 12*) is presented. It is observed that the proposed method still produced solid results for all tested FIA even with a very high fault impedance.

3.3Improved Faulted Phase Identification in Systems with IBRs using Incremental Voltages

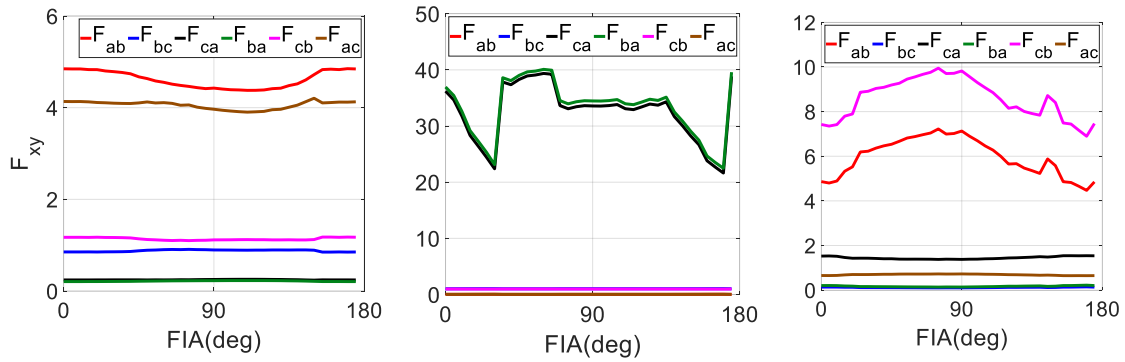

Figure 3.21 Variation of fault indices with fault inception angle (ϕ) for a mid-line fault (Line 12) with a fault resistance of 100 Ω for (a) AG, (b) BC, and (c) CAG fault

In addition, Figure 3.22 shows the variation of fault indices with fault inception angle (ϕ) for a mid-line fault (*Line 12*) with an inductive fault impedance of 7.54 Ω (0.02 H). Presented results in the figure above indicate that the proposed method performs appreciably with a variety of fault impedances.

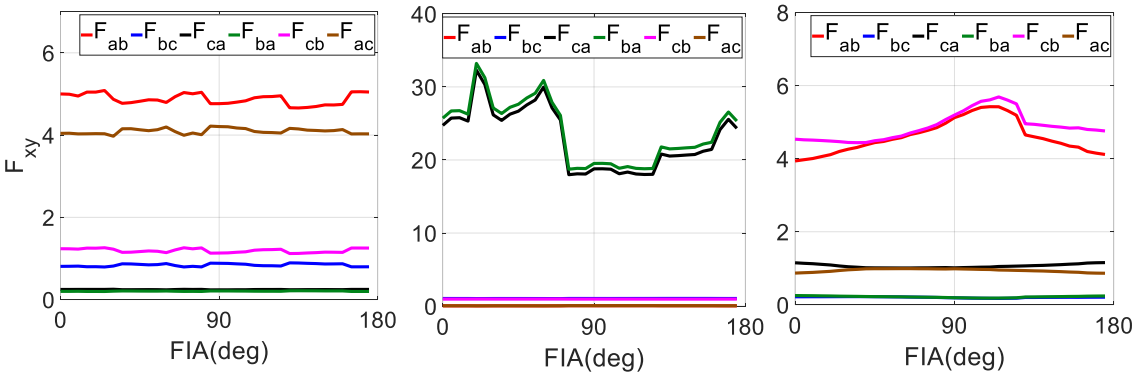

Figure 3.22 Variation of fault indices with fault inception angle (ϕ) for a mid-line fault (Line 12) with an inductive fault impedance of 7.54 Ω for (a) AG, (b) BC, and (c) CAG fault

3.3.5 Further Testing

In order to further evaluate the applicability of the proposed method, it was tested under different conditions by modifying the test system. The following subsections present results obtained during these additional testing.

3.3.5.1. Performance on a Weak AC system

Figure 3.23 depicts the modified test networks simulated, (a) with a weaker AC grid and (b) with a new relay location. Here, the weaker AC grid was realized by disconnecting the SG at *Bus 2* and one of the parallel 230 kV lines from *Bus 3* to *Bus 4* (see Figure 3.23-(a)). The short circuit ratio (SCR) of resulting system was ≈2, which represents a relatively weak grid (the SCR of the original system was ≈6).

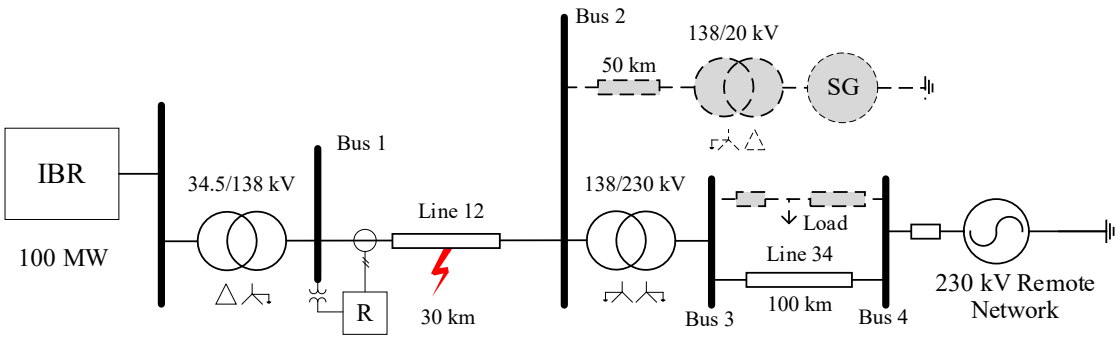

Figure 3.23 Single line diagram of the modified test networks simulated in the DRTS for a weaker AC grid

The variation fault indices with fault inception angle (ϕ) for a mid-line fault (*Line 12*) with a weak AC grid for different fault types is presented in Figure 3.24. It is observed that the proposed method still produced solid results irrespective of the fact that the relative magnitudes of the fault indices were closer than those observed for a stronger grid.

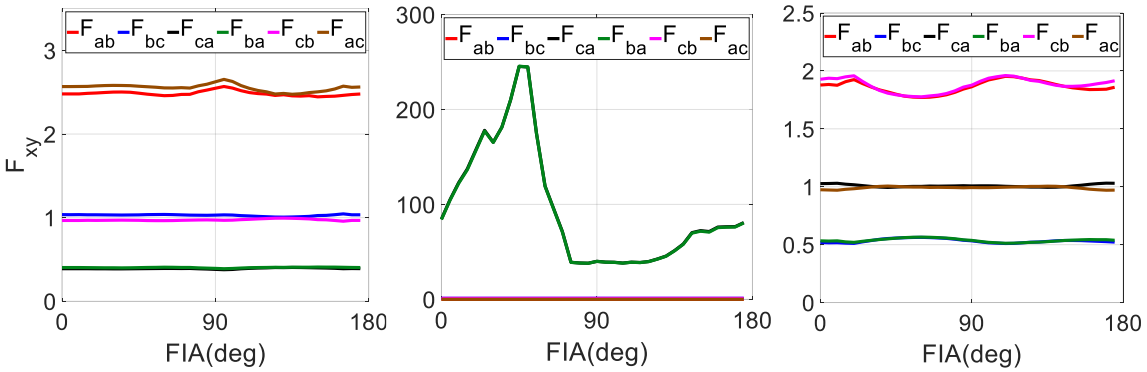

Figure 3.24 Variation of fault indices with fault inception angle (ϕ) for a mid-line fault (Line 12) with a weak AC grid for (a) AG, (b) BC, and (c) CAG fault

3.3.5.2. New Relay Location

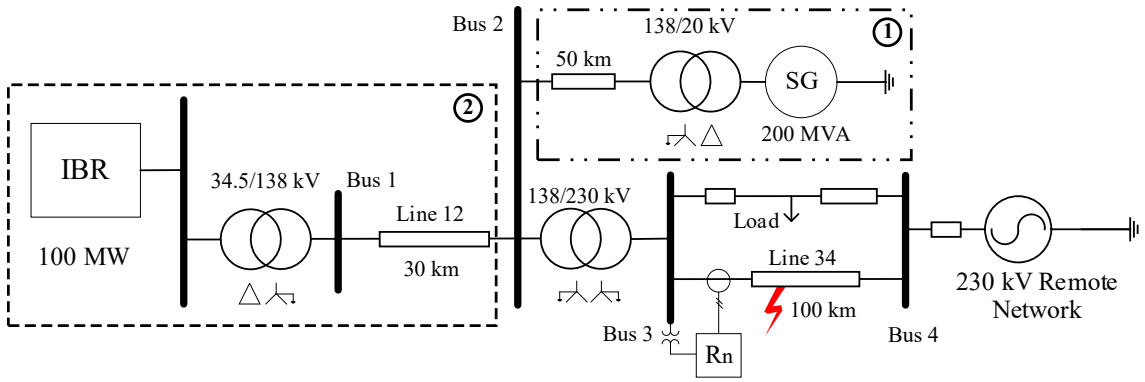

Figure 3.25 Single line diagram of the modified test networks simulated in the DRTS for a different relay location

Here, the relay was deployed at a different location (R_n) at one of the two parallel 230 kV lines from *Bus 3* to *Bus 4* (*Line 34*). Here, two operational scenarios were considered, where only one of the two sources at *Bus 2* was in service (i.e.: scenario 1: only the IBR was in service and, scenario 2: only the SG was in service). The disconnected segment of the system for each scenario is outlined in Figure 3.23.

3.3Improved Faulted Phase Identification in Systems with IBRs using Incremental Voltages

Faults were applied on *Line 34* varying different parameters and the proposed method produced excellent results for all test cases. Figure 3.26 shows the variation of fault indices with fault inception angle (ϕ) for a mid-line (50%) CAG fault for scenarios 1 and 2. Note that these scenarios produced fault indices with greater discrimination (compared to the previous tests done on *Line 12*). These results augment the applicability of this method for systems with varied level of IBR penetration and complex network configurations (such as parallel lines).

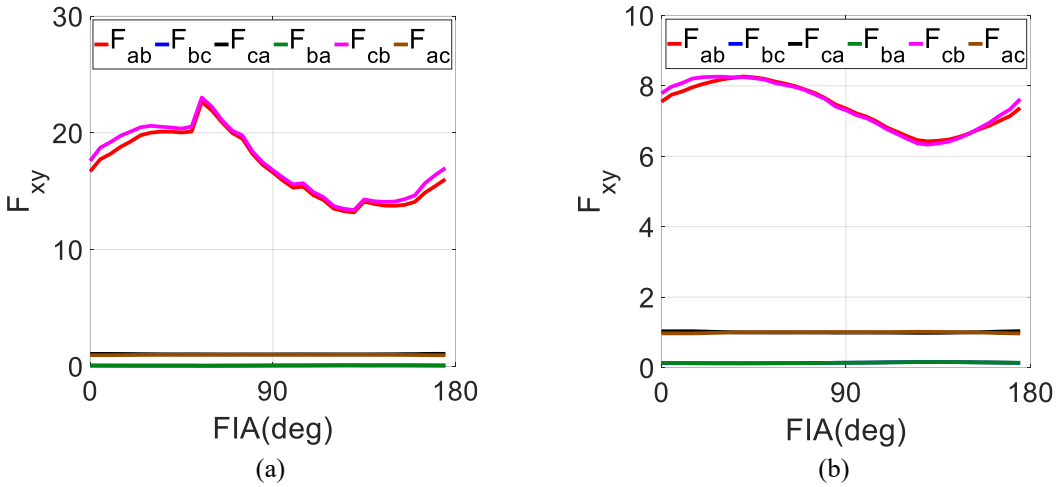

Figure 3.26 Variation of fault indices with fault inception angle (ϕ) for a mid-line (Line 34) CAG fault (a) with only the IBR connected and, (b) with only the SG connected

3.3.5.3. MIL Implementation using Real IEC 61850 communication

In an attempt to put the proposed method under further scrutiny, it was implemented and tested in a more realistic setup. Here, a closed model-in-the-loop (MIL) simulation was performed, where all data for the algorithm was transferred using real IEC 61850 Sampled Values (SV) and GOOSE communication. Given in Figure 3.27 is a schematic of the test system simulated in the DRTS for MIL simulations with real communication (IEC 61850-9-2

Sampled Values and IEC 61850-8-1 GOOSE). Here, the initial power system configuration given in Figure 3.14 was used for testing.

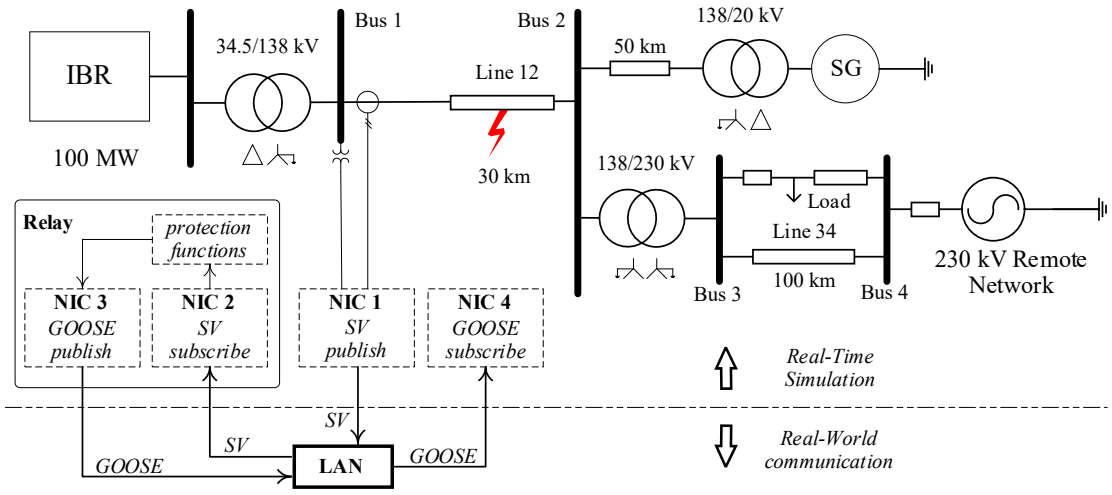

Figure 3.27 Schematic of the test system simulated in the DRTS for Model-in-the-loop simulations with real IEC 61850 communication

Four Network Interface Cards (NIC) of the DRTS was used to achieve communication between the power system and the simulated relay. Both SV and GOOSE packets were connected to a single Local Area Network (LAN) in the laboratory. Figure 3.28 presents the relevant measurements/fault parameters for a mid-line ABG fault (on *Line 12*) recorded using this setup. Note that the voltage measurements received via sampled values, published at 80 S/C, were re-sampled at 16 S/C (which is a more commonly used sampling rate for protection applications). As can be seen from the results given in Figure 3.28, the proposed method produced results consistent with those obtained earlier.

3.3Improved Faulted Phase Identification in Systems with IBRs using Incremental Voltages

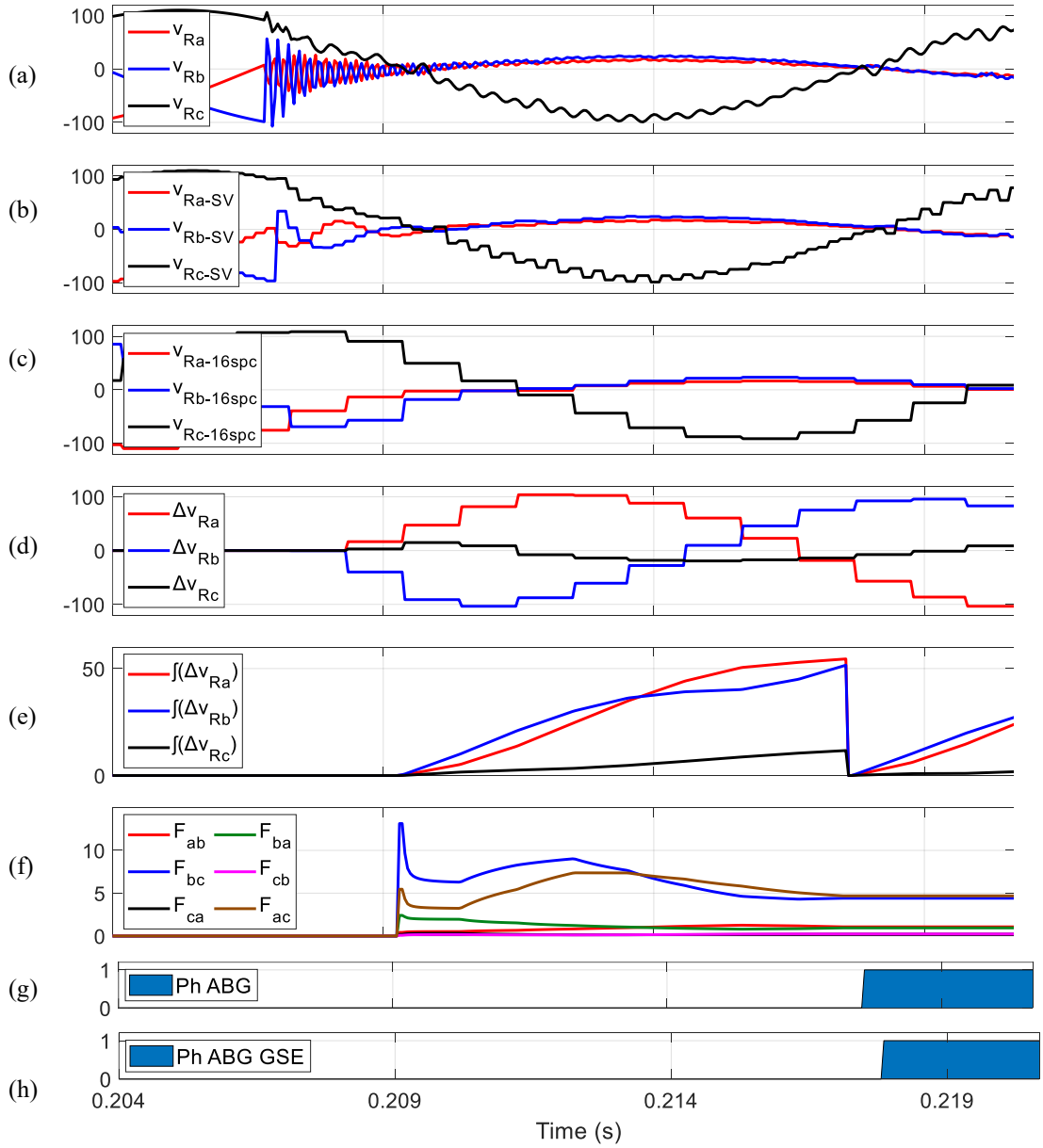

Figure 3.28 Measurements/fault parameters for a mid-line ABG fault (a) Phase-to-ground voltage (b) voltage from subscribed SV, (c) voltage resampled at 16 S/C, (d) incremental voltages, (e) integrated incremental voltages, (f) fault indices, (g) ABG phase selection (h) ABG phase selection sent via GOOSE message

3.3.5.4. Evolving Fault

Figure 3.29 presents results for an evolving fault, where an AG (single phase to ground) fault evolves into an ABG (double line to ground) fault after 4 ms from initial fault inception.

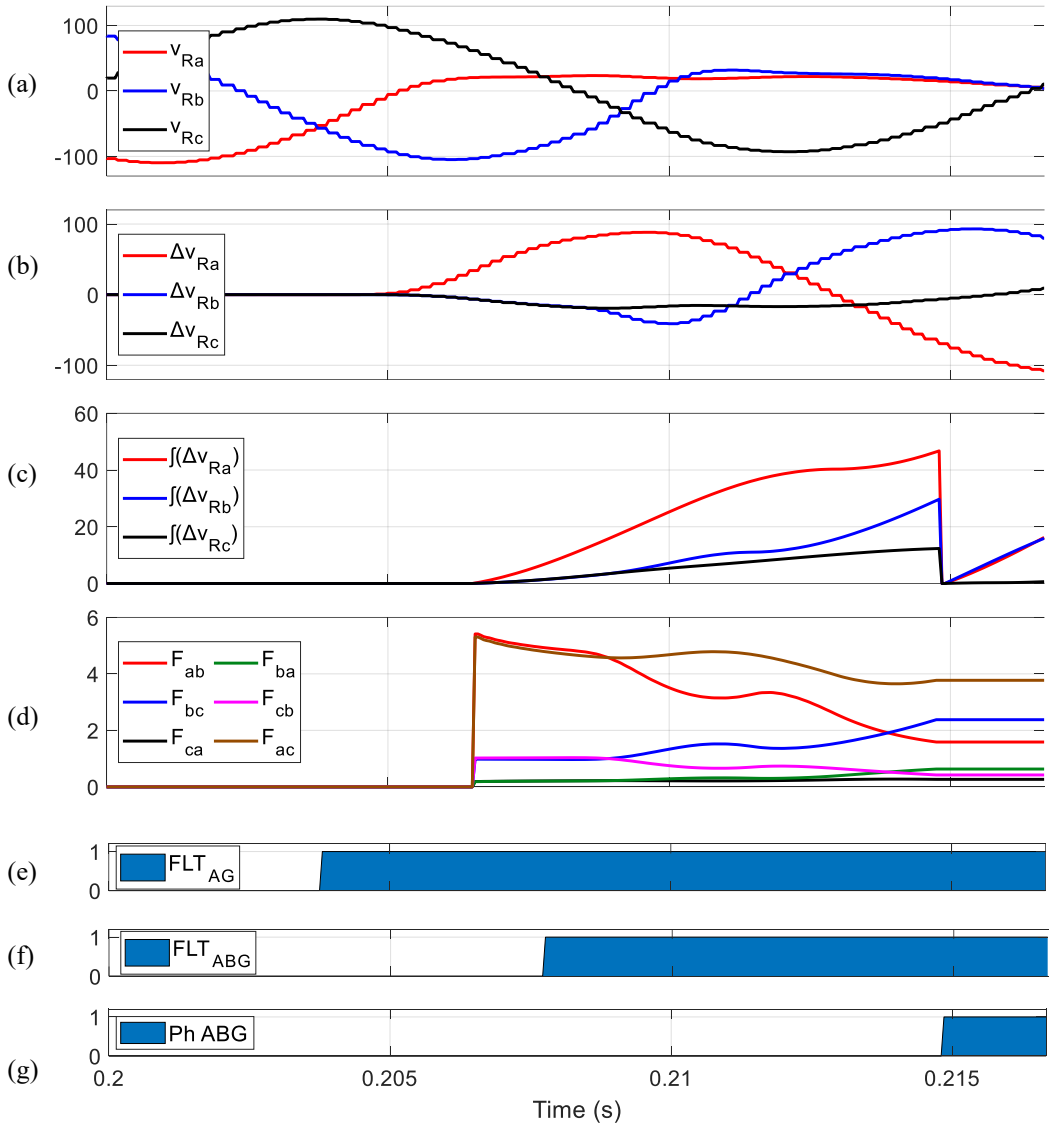

Figure 3.29 Measurements/fault parameters for a mid-line evolving fault, AG to ABG (a) Phase-to-ground voltage (b) incremental voltage, (c) integrated incremental voltages and (d) fault indices, (e) AG inception (f) evolving to an ABG fault and (g) ABG fault detection

As can be seen, the algorithm correctly recognizes conversion of a line-to-ground (AG) fault into a line-to-line-to ground (ABG) fault. In Figure 3.29-(d), observe how the second largest index switch (from F_{ab} to F_{bc}) at a fairly later stage of the detection period as opposed to having two clearly distinguishable maximums from the fault inception (see corresponding plots in Figure 3.16 and Figure 3.28). This, accordingly, indicates that the algorithm may not have sufficient time to reliably detect the change in fault type as the time delay between the initial fault inception and its evolution into a different type gets larger. Testing indicated that the limit for the aforementioned time delay in this system is approximately 5 ms.

3.3.5.5. Performance with Off-nominal Frequency Components

Abnormalities in the system can often result in off-nominal frequencies in voltages measurements. Given in Figure 3.30 is variation of fault indices with FIA for a mid-line fault (*Line 12*) with 15% (0.15 pu of the rated LN voltage) 2nd harmonic component added into the voltage measurement, and as can be seen, the proposed method was unaffected.

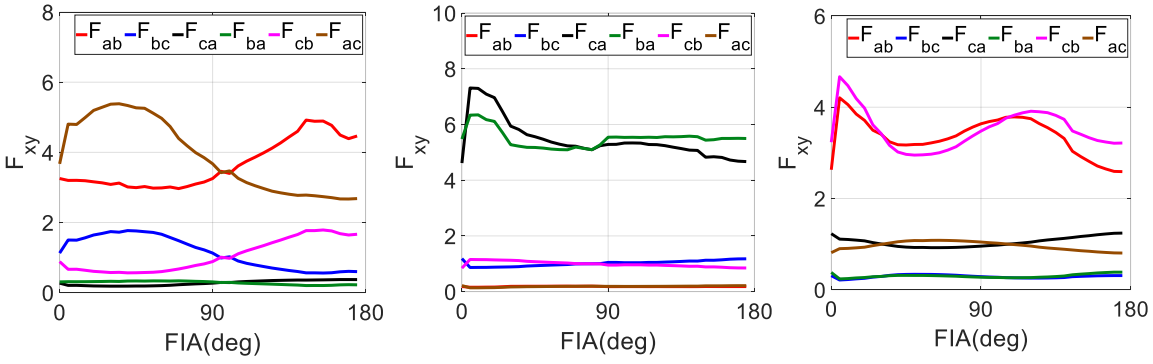

Figure 3.30 Variation of fault indices with fault inception angle (ϕ) for a mid-line fault (Line 12) with 15% 2nd harmonic component

3.3.6 Discussion

Results presented above suggests that proposed method of faulted phase identification yields excellent results in systems with IBRs. It performed well under variety of system conditions and produced 100% accurate results with operating times well-under 1 cycle for all tested scenarios. As can be seen from the results, characteristics of the fault such as fault location, fault impedance and inception angle had no significant impact on the operation of the proposed method. Its performance for LLG faults is particularly noteworthy in this context as some faulted phase identification methods are prone to produce unreliable results for LLG faults when tested for the full range of fault inception angles. The proposed method also performed adequately under different system strengths and different system configurations (i.e. low SCR and with parallel lines). Tests performed with only synchronous generator feeding the relay conformed that the proposed method is also applicable for conventional sources as well.

Another major advantage of this method is that the basic faulted phase identification algorithm requires minimal settings. The only setting required for faulted phase identification portion of the algorithm is the threshold for identifying 3-phase faults. Determination of this setting does not require system specific studies and can be conveniently set to 1.0. The threshold settings required for fault detection and ground fault identification can also be conveniently set and have a large margin of error. Note that they can also be replaced in the algorithm with other appropriate fault detection and ground fault identification methods. Moreover, fault classification is exclusively based on the two highest indices, selection of which does not

dependent on thresholds. Therefore, this method provides better discrimination than any method using thresholds, where there is a built-in margin of error (this applies to both incremental quantities and phasor based methods including an under-voltage element). In addition, the proposed method can be very easily implemented in a modern numerical relay with trivial formulae and little computational burden. It only uses local voltage measurements and does not rely on high frequency transients thus, does not require high-bandwidth voltage transducers or communication schemes. Note that proper selection of the timer T_s is critical to the operation of the algorithm to minimize sensitivity of the indices to FIA (set to 8.33 ms based on insights from theoretical analysis). However, this shall remain a pre-set internal parameter of the algorithm without any user intervention.

By its design, the proposed method takes around 10 ms to process information and produce results (a typical phasor-based protection element takes 1 cycle or 16.67 ms). While this is adequate for most conventional applications, it might not be suitable for applications demanding ultra-high speed operation. As evident from the presented results, LLG faults were the most challenging to identify using this method due to their sensitivity to fault inception angle (LG and LL faults were much more straightforward). While there could be extreme system conditions resulting in abnormal system impedances which can complicate detection for LLG faults at certain inception angles, tests performed in this work did not reveal any failures of the proposed method. The theoretical analysis presented in this paper is useful in further analysis of incremental voltages in system protection in other applications.

3.4 Concluding Remarks

According to literature, faulted phase identification is one of the areas of conventional system protection that is severely vulnerable in the presence of IBRs. The work presented in this chapter investigated the effect of IBRs on the conventional phasor-based faulted phase identification methods widely implemented in contemporary commercial protection relays using both theoretical analysis and simulation results. Moreover, results obtained from purely simulation-based studies were further validated by testing commercial line protection relays using hardware-in-the-loop simulations. This chapter also evaluates the applicability of recently proposed transient quantities-based techniques to overcome the deficiencies of conventional methods to correctly identify the faulted phase in systems with IBRs.

In addition, this chapter presented a theoretical analysis evaluating the effectiveness of using incremental voltages for faulted phase identification using theoretical analysis of circuit equations. Based on the theoretical analysis, it presents a faulted phase identification method based on the integrals of the incremental voltages. This method is suitable for conventional systems as well as ones with high IBR penetration. Performance of the proposed method was evaluated for different operational and system conditions using extensive EMT simulations. The results presented indicated that the proposed method of faulted phase identification performed well in systems with IBRs as well as conventional sources under variety of system conditions.

Chapter 4

Investigation of Impacts of IBRs on Contemporary Fault Direction Identification and an Improved Algorithm

4.1 Introduction

Traditional protection functions such as distance and overcurrent protection are accompanied by an element that independently verifies direction of the fault to improve selectivity of fault detection. As mentioned in subsection 1.2.2.2, most commonly encountered fault direction identification methods are based on negative-sequence measurements. This is due to their heightened sensitivity to faulty conditions, invulnerability to loads [16], and applicability in all unbalanced faults. Conventional negative-sequence directional elements operate based on the relative phase angle relationship of negative-sequence voltage and current (or that of the negative-sequence impedance) seen at the relaying location [16], [43], [91], [97].

Due to unpredictable and highly-controlled nature of IBRs, any protection method reliant on a predefined phase angle relationship (of system currents/voltages) is prone to mis-

operate. This is of particular significance to methods dependent on phase angle of system currents. Method using voltage phase angles can also be affected, although to a lesser degree. It is important in this context to emphasize the fact that the above-mentioned unpredictability of operation is especially prominent during the first few cycles following a major disturbance such as a fault. This is precisely the period in which transmission system protection is typically intended to operate (response times of IBRs controls, including VRT, are generally greater than those of system protection functions).

This this chapter is dedicated to investigation of the impacts of IBRs on prevailing fault direction identification methods and development of techniques for improved performance. This Chapter proposes a new negative-sequence admittance-based fault direction identification method that is specially designed to provide reliable results in systems with high IBR penetration. The work presented in this chapter presents (i) the novel negative-sequence admittance based directional method for system predominated by IBRs, (ii) its validation and analysis of performance through simulations, (iii) implementation of a real-time version and testing using control-hardware-in-the-loop simulations and (iv) discussion on its applicability and advantages against the phase angle based directional algorithms using comparative results.

4.2 Conventional Directional Identification with IBRs

In order to further investigate the operation of conventional direction identification in the presence of IBRs, a simulation study was conducted in an DRTS (RTDS®). Simulated test network is provided in Figure 4.1 (which is similar to the one used in previous chapters). The IBR model is rated at 100 MW and delivers power via a short, 138 kV transmission line (IBR tie-line). The IBR's POI at the remote end of this line (*Bus 2*) is connected to a 230 kV grid through a transformer and an adjacent transmission system. A conventional synchronous generator) is connected to the POI bus (*Bus 2*) via another short transmission line as depicted in Figure 4.1. The line protection relay (R) of the tie-line, deployed at *Bus 1* is looking into *Line12*.

This analysis presents a qualitative comparison of the performance of conventional direction identification with IBRs against synchronous generators. In Figure 4.1, a synchronous generator of comparable ratings is also placed on *Bus 1*, which replaces the IBR accordingly in testing (only one generating source is connected at a time).

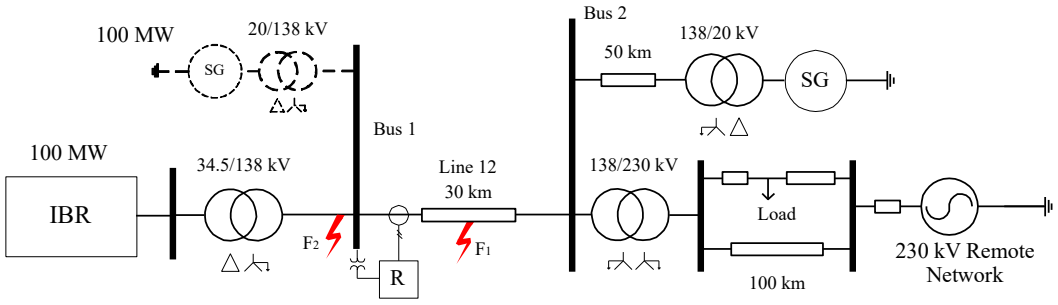

Figure 4.1 Single line diagram of the test network simulated in the DRTS

The line relay is realized using the distance protection relay component available in the master component library in the DRTS (RSCAD®) [98]. This component uses a directional element based on the estimated phase angle of sequence impedances. The priority of sequences used is negative-zero-positive. The negative and zero-sequence elements have settable

current and voltage thresholds for supervision while positive-sequence element has fixed thresholds (elements are used only if these sensitivity thresholds are exceeded). Respective fundamental frequency voltage and current phases are used to calculate negative and zero-sequence impedance. However, the positive-sequence impedance is determined using positive-sequence memory voltage and directly measured current. A forward fault is declared when the sequence impedance angles are within $\pm 90^{\mathbf{o}}$ of respective line impedance (see Figure 2.2-(b)) [98]. Behaviour of this directional element also closely resembles the operation of those implemented in some commercial line protection relays as well [43].

Table 4.1 summarizes the performance of the negative-sequence directional element of the simulated (software) relay for forward, unbalanced faults (Fault F_1 in Figure 4.1) with the two types of generating sources. Faults were low-impedance (fault impedance 0.01 Ω) and applied at three fault locations (at 5%, 50%, and 90% of line length). Multiple simulations were run with the fault inception angle varied from $0^{\mathbf{o}}$ to 180° in $30^{\mathbf{o}}$-degree steps. Note that the current sensitivity threshold was set low-enough for the negative-sequence directional element to be activated by IBR generated negative-sequence currents (which is small).

Table 4.1: Fault direction identification using negative-sequence measurements for forward faults

Applied Fault		**Fault direction Identification**	
Type	**Location**	**IBR**	**SG**
AG	5%	Unreliable*	Accurate
	50%	Unreliable*	Accurate
	90%	Unreliable*	Accurate
BC	5%	Unreliable*	Accurate
	50%	Unreliable*	Accurate
	75%	Unreliable*	Accurate
ACG	5%	Unreliable*	Accurate
	50%	Unreliable*	Accurate
	75%	Unreliable*	Accurate

* Direction identification was incorrect or transient in nature

As expected, the negative-sequence directional element operating on small and unreliable negative-sequence currents generated by the IBR performed poorly during these tests. It did not produce reliable results in any of the 162 tests performed. In most cases, the directional element did not pickup a forward fault at all or operated transiently (for 1-2 ms only) during the transient period immediately following fault inception, where the phase angle estimation varies significantly due to the dynamic behaviour of the DFT algorithm used for phasor estimation. As shown later in subsection 4.4.4, this behaviour of the directional element, which in turn supervises other protection elements such as distance protection can cause the line relay to not respond to line faults on the tie-line. In contrast, the negative-sequence direction element performed accurately for all test cases with the synchronous generator connected in place of the IBR (which is to be expected). On further inspection, it was also observed that for forward faults, the negative-sequence impedance angle estimated by the relay did not lie within $\pm 90^{\mathbf{o}}$ of respective line impedance for the IBR, whereas it was very close to $-90^{\mathbf{o}}$ with the synchronous generator, which was symptomatic of the behaviour of the directional element. Also, note that the IBR model used for these tests did not have active negative-sequence current injection.

The above test was repeated to evaluate the performance of the zero-sequence directional elements and, Table 4.2 summarizes the performance of the zero-sequence directional element of the simulated (software) relay for forward, unbalanced faults. For this test, the negative-sequence current supervision threshold was set very high for the negative-sequence directional element to be bypassed, which effectively gave priority to the zero-sequence directional element.

Table 4.2: Fault direction identification using zero-sequence measurements for forward faults

Applied Fault		Fault direction Identification	
Type	**Location**	**IBR**	**SG**
AG	5%	Accurate	Accurate
	50%	Accurate	Accurate
	90%	Accurate	Accurate
BC	5%	Delayed*	Accurate
	50%	Delayed*	Accurate
	75%	Delayed*	Accurate
ACG	5%	Accurate	Accurate
	50%	Accurate	Accurate
	75%	Accurate	Accurate

* Direction identification took more than 1 cycle to identify a forward fault

As seen from the results presented in Table 4.2, the zero-sequence directional element worked accurately for grounded faults even with the IBR. This was primarily because of the grounded Wye-delta connection of the IBR plant's main power transformer, which provided the source side of the line relay with a strong source of zero-sequence current. On the other hand, during ungrounded faults, for which there is no zero-sequence present, the zero-sequence directional element was rendered inactive. There, the directional identification was achieved using the positive-sequence quantities. However, since the positive-sequence impedance estimation uses positive-sequence memory voltage, a significant delay (often over 1 cycle) was observed before the decision was made (the use of memory voltage is supposed to guard against near-zero voltages during a bolted 3-phase fault at the line terminal). This behaviour can be tolerated, but also not ideal, as it can delay the operation of other protection elements, potentially degrading overall protection reliability. As stated before, there are IBR plant configurations in common use with transformer vector groups that do not provide a zero-sequence path. In such cases, direction identification of all fault types must rely on positive-sequence quantities, even though they do not deliver the most efficient directional

identifications. Moreover, there was no significant change in the behaviour of the zero-sequence directional element with synchronous generators, however, the delay of operation for ungrounded faults was lower (i.e. operation of the positive-sequence element).

In addition, it was observed that both negative and zero-sequence elements produced correct direction identification for reverse faults (Fault F_2 in Figure 4.1). This was also to be expected as the relay was fed by conventional sources at the remote system for reverse faults. Finally, while this analysis provides a general idea about the problems caused by IBRs on convectional directional identification methods (specially ones relying on current and voltage phase angles), it may not fully reflect the performance of all such methods, including those implemented in commercial relays.

4.3 Negative-Sequence Admittance-Based Directional Element

4.3.1 Principle of Operation

The negative-sequence network of a generic power system during an unbalanced fault is illustrated in Figure 4.2. As can be seen from Figure 4.2-(b), the negative-sequence impedance seen by relay, R, for a forward fault (F_1) Z_{2R_F1}, is given by (4-1). The variables in (4-1) are as defined in Figure 4.2.

$$Z_{2R_F1} = \frac{V_{2R}}{I_{2R}} = Z_{2S1} \tag{4-1}$$

I_{2R} : Negative sequence current seen by the relay
V_{2R} : Negative sequence voltage seen by the relay
Z_{2S1} : Negative sequence Impedance of the local source
Z_{2S2} : Negative sequence Impedance of the remote source
Z_{2L} : Negative sequence Impedance of the line
m : fault location as % from the relaying location

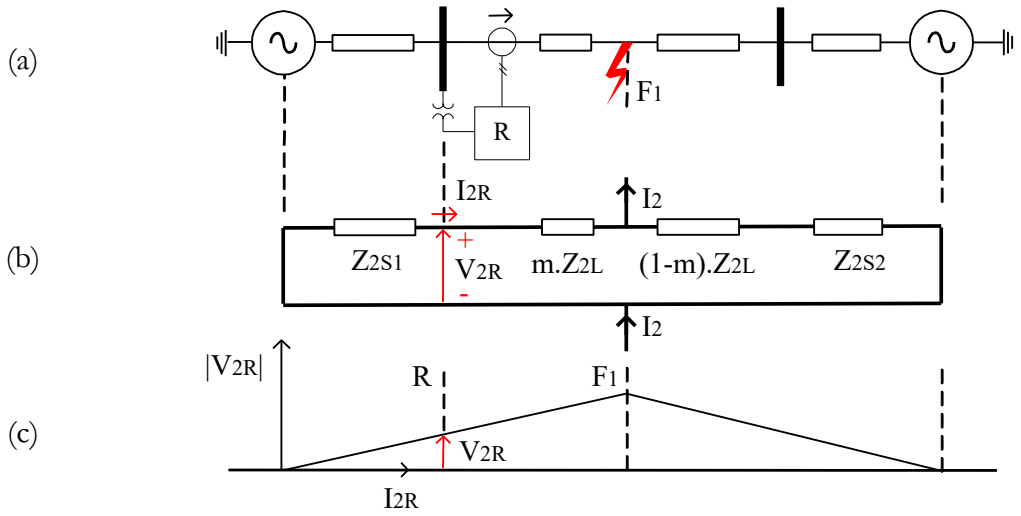

Figure 4.2 (a) Simplified network with two sources connected by a transmission line, (b) Negative-sequence impedance circuit and (c) Negative-sequence voltage magnitude profile for a forward fault

It is understood that the negative-sequence impedance seen by a relay for a forward fault is that from the relaying point back to the local source, as designated in (4-1). Similarly, the negative-sequence impedance seen by the relay for a reverse fault F_2, Z_{2R_F2}, is that of the system in front of the relaying point, as shown in Figure 4.3 (and specified in (4-2)).

$$Z_{2R_F2} = \frac{V_{2R}}{I_{2R}} = (Z_{2S2} + Z_{2L}) \tag{4-2}$$

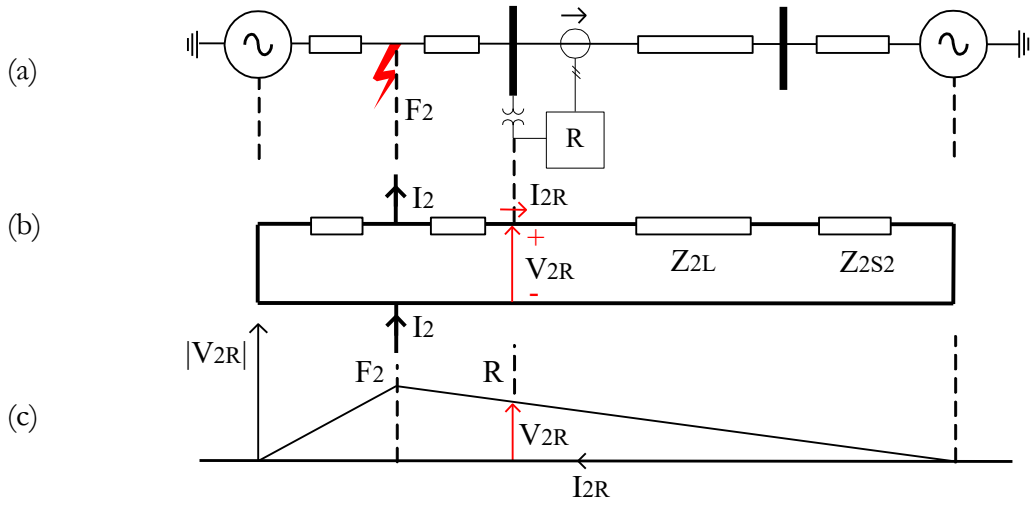

Figure 4.3 (a) Simplified network with two sources connected by a transmission line, (b) Negative-sequence impedance circuit and (c) Negative-sequence voltage magnitude profile for a reverse fault

Given in Figure 4.4-(a) is a simplified illustration of a system where an IBR is connected radially to a grid via a transmission line (a tie-line connecting an IBR to rest of the grid). Figure 4.4-(b) and (c), respectively, depict the arrangement of sequence impedance networks of the simplified power system shown in Figure 4.4-(a) for a single-line-to-ground fault and a line-to-line fault in forward direction. In this representation, source 1 (on the left) represents an IBR and source 2 (on the right) represents a regular non-IBR source. The IBR can also be represented as a current source, which only injects positive-sequence current of approximately

1.0 pu during a fault. As established in the previous subsections, a majority of full-scale IBRs in operation presently inject near-zero negative-sequence current (or a very small current) into the network. This, therefore, can be interpreted as the IBR having infinite (or a very large) negative-sequence impedance. Note that the IBR itself also does not contribute a zero-sequence current. However, the main plant transformer typically a grounded-Wye connection on the HV (gird) side therefore, functions as a source of zero-sequence current for ground faults on the tie-line (as seen by the relay, R).

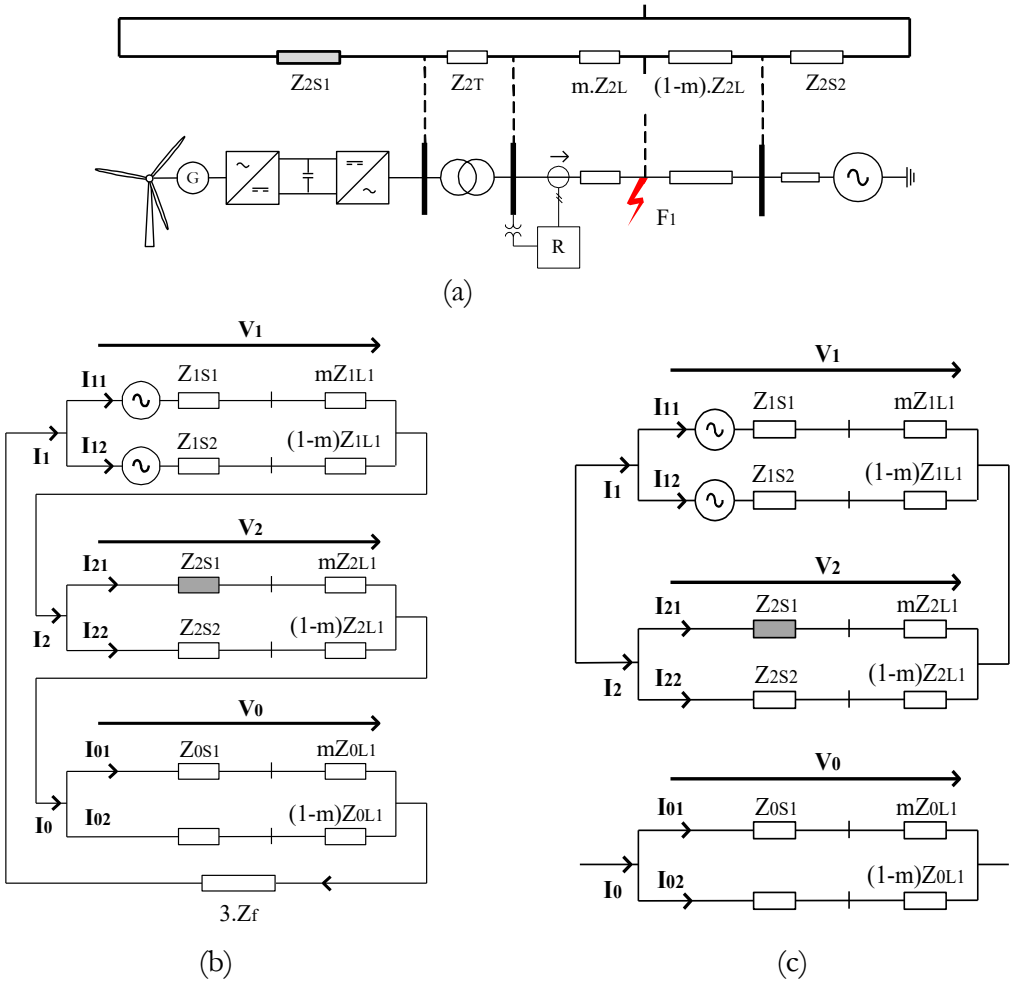

Figure 4.4 (a) Simplified system with an IBR, Sequence networks for (b) a single-line-to-ground fault and (c) a line-to-line fault

4.3 Negative-Sequence Admittance-Based Directional Element

As illustrated in Figure 4.4, the fault splits each sequence network into two sections, which are connected in parallel to each other. Here, the ratio of (sequence) currents flown in the two branches is proportional to the reciprocal of the ratio of (sequence) impedances. Considering the negative-sequence network for a forward fault (F_1), the negative-sequence impedance seen by the relay (R) would be that of its local source, the IBR (in accordance with (4-1)). Due to reasons afore-mentioned, the magnitude of this impedance ($|Z|$) would appear very large. This, in turn, means that the corresponding negative-sequence admittance magnitude ($1/|Z|$) seen by the relay would be very small.

Conversely, for a reverse fault (F_2) according to (4-2), the apparent value of the negative-sequence impedance seen by the relay is the sum of the negative-sequence impedances of the tie-line and rest of the grid, which is typically much smaller than that of the IBR (with the assumption that the rest of the grid is relatively stronger and dominated by conventional generation). The corresponding negative-sequence admittance, therefore, becomes a large value. Noticeable difference between the magnitudes of the negative-sequence impedances (and in turn admittances) of the IBR and the conventional generation can be leveraged to implement a fault directional identification method based on negative-sequence admittance measurements for the protection of lines connecting IBRs to conventional grids. The negative-sequence admittance seen by the relay:

$$Y_{2R} = \frac{I_{2R}}{V_{2R}} = G_{2R} + jB_{2R} \tag{4-3}$$

where G_{2R} and B_{2R} are the apparent negative-sequence conductance and the negative-sequence susceptance, respectively. The basic premise of this method is to determine the direction of the fault (forward or reverse) based on the location of the negative-sequence

admittance seen by the relay on the '*conductance-susceptance'* (B-G) plain. Since the phase angles of IBR-generated negative-sequence quantities (specially the current) are often unpredictable immediately following a fault, it is more secure to make decisions based on magnitude only. Since the magnitude of the negative-sequence admittance becomes considerably reduced when a forward fault occurs, a zone centered on the origin of the B-G plain can be conveniently chosen as the "*forward*" zone. As shown in Figure 4.5, a zone of a desired profile (for example, a circle) in the B-G plain can be prescribed as the "*forward*" zone and the complement of this zone is declared as the "*reverse*" zone, which is conceptually analogous to conventional fault direction identification techniques.

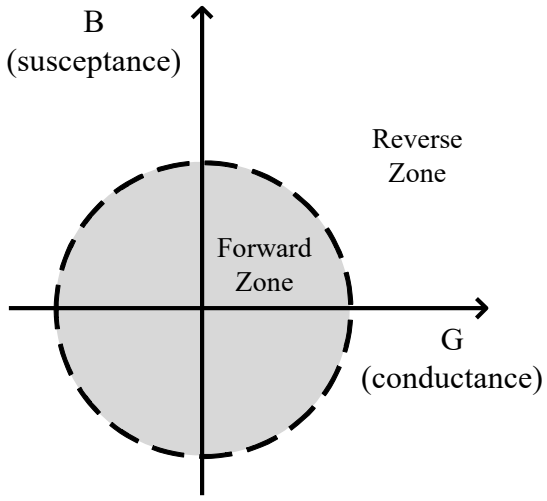

Figure 4.5 Y Plain, forward and reverse zones are indicated

In order to enhance security of the directional element, an appropriately set fault detection element such as the one presented in Appendix A can be optionally used to supervise the proposed admittance element. Alternatively, a negative-sequence voltage element can also be used for the same purpose.

Figure 4.6 shows the flow diagram of the proposed directional element algorithm. As evident form the flow diagram, the proposed method can be expediently implemented on a modern digital relaying hardware platform with standard functions. It is important in this context to note that the proposed directional element can also be realized using the negative-sequence impedance magnitude as well (in this case, forward and reverse zones are interchanged). However, admittance was preferred as it was deemed that the algorithm would be more intuitive if the operating quantity converged into a zone for forward fault.

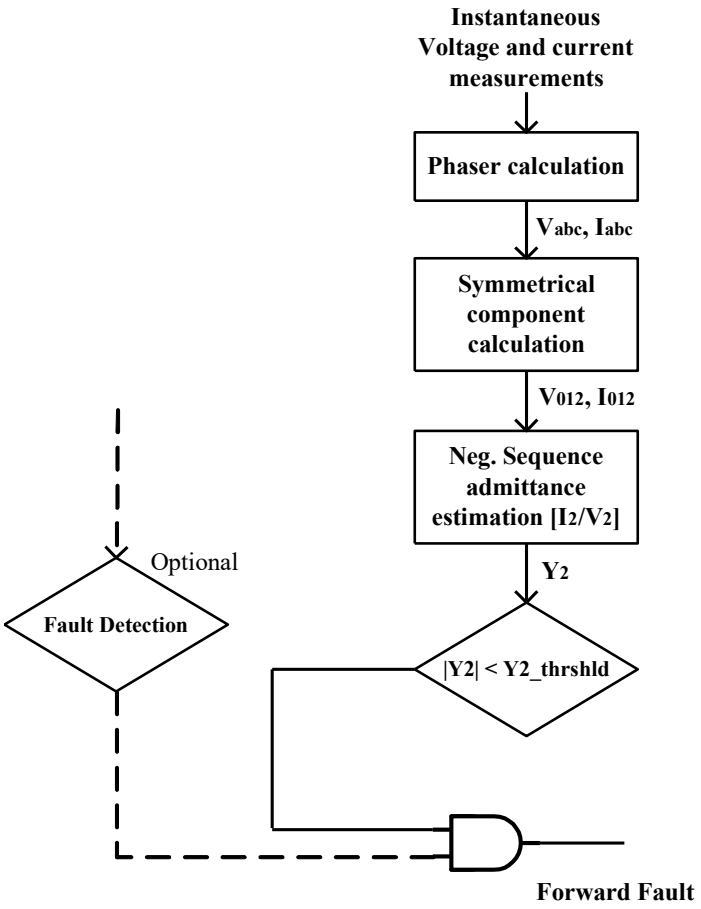

Figure 4.6 Flow diagram of the proposed direction element algorithm

4.3.2 Application of the Proposed Technique

It is critically important to understand that the proposed method depends *only* on the magnitude of the admittance (impedance) estimation since it uses an absolute magnitude comparison. This method does not directly or indirectly depend on the phase angle (or sign) of the calculated admittance unlike most impedance-based conventional directional identification. Some existing techniques, despite being setup as magnitude comparisons [97], have operating quantity(s) that are dependent on the phase angle of the impedance. All protection techniques that are dependent on (or sensitive to) the phase angle of system measurements are potentially susceptible to unpredictable nature of currents injections, negative-sequence currents in particular, of IBRs. This key difference makes the proposed method less vulnerable in the presence of IBRs than conventional methods. Moreover, since both voltage and current are required to determine the operating quantity (i.e. the admittance), this technique is more robust than a function based on a single measurement such as a simple a negative-sequence overcurrent comparison element.

In the context of applicability, it is important to establish the fact that the proposed technique operates under the basic assumption that "the remote AC system is significantly stronger than the IBR of interest". This, however, is not an unreasonable statement regarding most existing IBR plants in operation at present (specially in North America). Importantly, most conventional methods under perform in this very condition, while the proposed method functions effectively, as can be seen from the results shown in subsequent subsections. Furthermore, the analysis performed in this work suggests that this technique can be used in a variety of other "weak infeed" systems as well.

Also relevant in this context is the fact that the proposed technique is not indented to be used in conventional systems, where there is little or no integration of IBRs. If sources at both ends of a relay are relatively strong and produce significant amounts of negative-sequence currents, the proposed technique is less effective and more importantly, not required as conventional directional methods yield acceptable results. The proposed method can be integrated into relays as an optional function in addition to existing direction identification methods and should only be activated when the system of interest demands it.

4.3.3 Calculation of Settings

The admittance setting of the forward zone for this method can be determined considering the system impedance data of the AC network. For example, the equivalent negative-sequence admittance of the AC system in front of the relay (R) can be determined when system data of the AC network are known (or estimated). This can be used as the basis to calculate the reach of the forward zone. Assuming that the IBR under investigation injects no negative-sequence currents, the apparent negative-sequence admittance for forward fault, in theory, should be 0 (i.e. $Z_{IBR} = \infty$). However, real-world IBRs can inject some amount of negative-sequence currents, even though they are significantly smaller than those from the AC network. Moreover, potential errors from instrument transformers and an adequate safety margin must be incorporated into a robust protection setting. On the other hand, it also important to understand that a smaller reach yields better discrimination between forward and reverse faults.

Considering the above factors, it is suggested to use 10-25% of the magnitude of the equivalent negative-sequence admittance of the remote end AC system as the forward reach

to achieve effective discrimination. The above estimation is based on the general assumption that the IBR's negative-sequence current injection is 5-10 times weaker than the AC grid (i.e., the negative-sequence admittance of the IBR is 5-10 times smaller). It is clear that the above assumption must hold, at least to a certain degree, for the proposed method to be effective (therefore, rationalizing the above estimation of the reach settings). When the above assumption is not satisfied due to a strong negative-sequence current injection from the local source, irrespective of it being an IBR or a conventional source, it is highly likely that the conventional negative-sequence directional algorithms would perform adequately and the proposed method is not required. However, notice that even IBRs equipped with unbalanced current injection may not produce negative-sequence currents fast enough to be relied upon for primary transmission level system protection functions. Therefore, mere existence of unbalanced current injection capability in an IBR is not indicative of the adequacy of performance of associated protection functions that depend on negative-sequence currents. Furthermore, when the remote end AC grid is also weak (see subsection 4.4.7 for more analysis) and consists of a high penetration of IBRs, determining a robust setting for this technique requires some analysis, accurate data and a certain degree of engineering judgement, as all protection settings do.

4.4 Performance Evaluation

Performance of the above-presented method of faulted direction identification was validated used detailed simulations conducted using an EMT-type DRTS (RTDS®). One-line diagram of the simulated test network is provided in Figure 4.7 (similar to the one used previously). The IBR model is rated at 100 MW and pushes power via a short, 138 kV transmission line (IBR tie-line). The IBR's POI at the remote end of this line (*Bus 2*) is connected to a 230 kV grid through a transformer and an adjacent transmission system. A conventional power source (a synchronous generator) is connected to the POI bus (*Bus 2*) via another short transmission line as depicted in Figure 4.7. Note that the protection method being presented in this work is implemented in the line protection relay (R) of the tie-line, deployed at *Bus 1* looking into *Line12*.

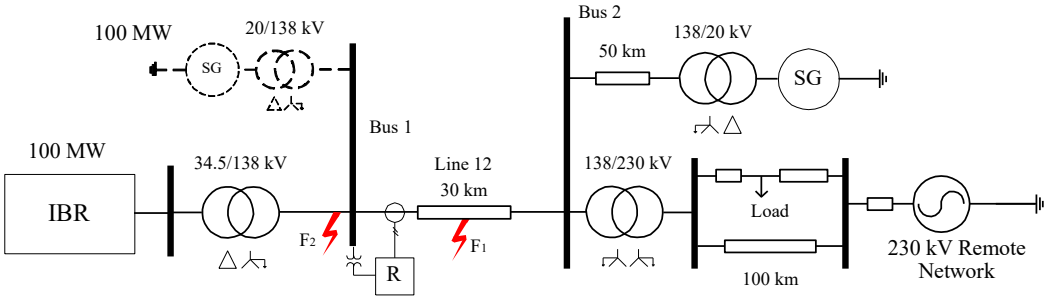

Figure 4.7 Single line diagram of the test network simulated in the DRTS

For this scenario, the area within a circle centered on the origin of the G-B plain (with a radius of 5×10^{-3} S) is chosen to be the forward zone. In the results presented, the radius of the forward zone is chosen approximately as 12.5% of the equivalent negative-sequence admittance (the magnitude of the negative-sequence impedance of the remote equivalent system is about 25 Ω).

A chosen set of simulation results showing the function of the proposed method are presented below. Given in Figure 4.8 is the trajectory of negative-sequence admittance on a G-B plain for a short-circuit (low impedance) AB fault at 50% of the *Line 12* (in the forward direction). Note that all admittances (both real and imaginary) are scaled by a factor of 10^3 in the results presented in this subsection (i.e. axis units are 10^{-3} S). The seemingly abrupt entrance and exit of the admittance trajectory in and out of the plot window are due to negative-sequence voltage supervision of the admittance element (which is a way of confirming a possible fault). As evident from the plot, the trajectory clearly enters and settles inside the designated forward zone, signifying a forward fault and leaves the zone after the fault has been cleared. On the other hand, Figure 4.9 shows how the negative-sequence admittance behaves for a short-circuit AB reverse fault on *Bus 1*. One can observe that the trajectory converges on to a location well outside the designated zone, thus indicating a reverse fault.

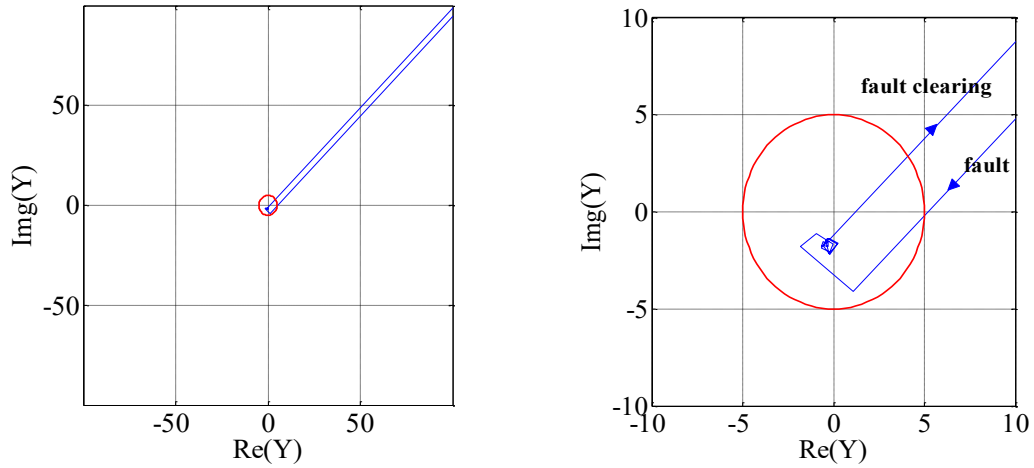

Figure 4.8 Trajectory of negative-sequence admittance on a G-B plain (a) forward short circuit AB fault at 50% of Line 12 (b) magnified view

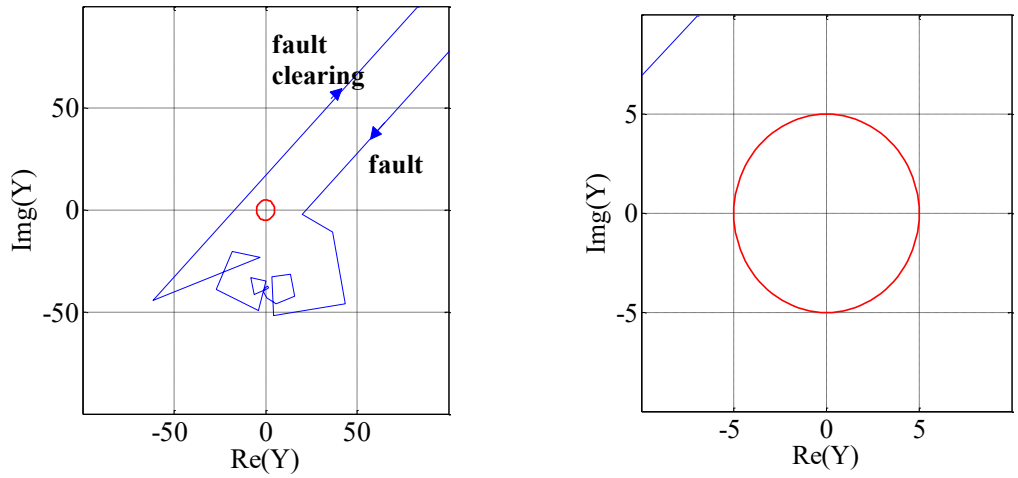

(a) (b)

Figure 4.9 Trajectory of negative-sequence admittance on a G-B plain (a) reverse bolted AB fault at Bus 1 (b) magnified view

4.4.1 Impact of Fault Location

Results for forward faults at different locations of *Line 12* are presented in Figure 4.10. Three different fault locations are considered and all three faults are correctly identified as forward faults verifying that this technique is not affected by the location of the fault. This is to be expected as the negative-sequence impedance seen by the relay for a forward fault is that of the local source behind the relay (in this case, that of the IBR), which is not affected by the location of the fault in the forward direction.

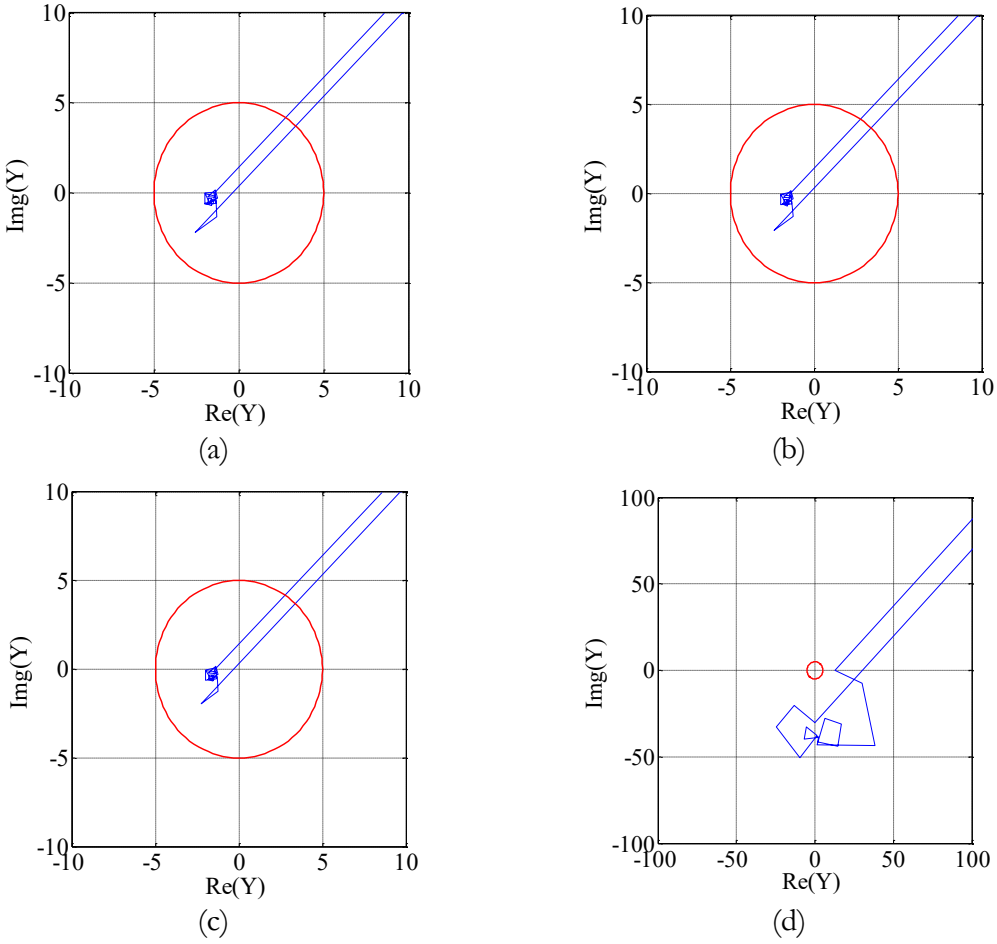

Figure 4.10 Trajectory of negative-sequence admittance on a G-B plain for a forward BC fault at (a) 10%, (b) 50%, (c) 80% of Line 12, and (d) reverse fault at Bus 1

4.4.2 Impact of Fault Impedance

In theory, the proposed method is also not expected to be affected by the fault impedance. This is because the network, including fault impedance, in front of the relay has no bearing on the negative-sequence impedance seen by the relay for a forward fault (i.e. the relay only sees the negative-sequence impedance behind it for a forward fault). Figure 4.11 provides a comparison of results obtained for low and high impedance faults (in both forward and reverse directions). Both scenarios yielded similar admittance trajectories as can be seen from Figure 4.11. Results confirm that the effect of fault impedance on this technique is minimal.

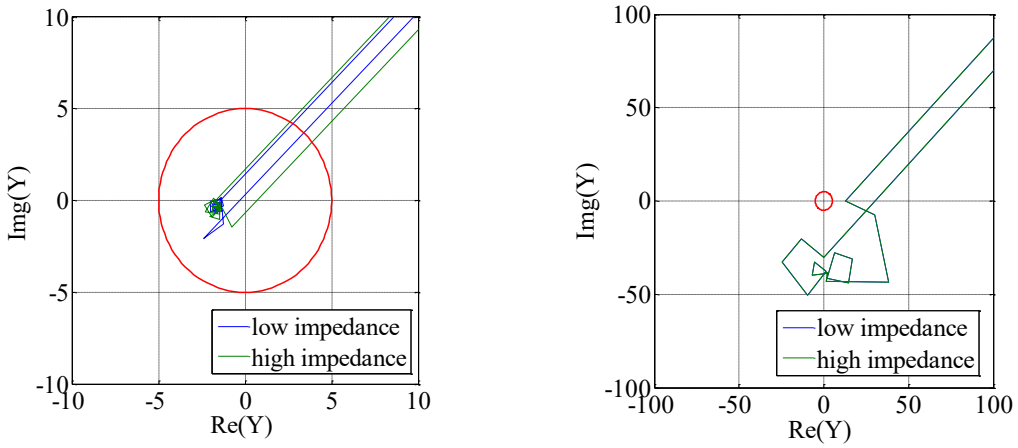

Figure 4.11 Trajectory of negative-sequence admittance on a G-B plain for (a) forward BC fault at 50% of Line 12, short circuit fault and with a fault resistance of 50 Ω and (b) reverse (Bus 1) short circuit fault and with a fault resistance of 50 Ω

4.4.3 Type of Fault

Presented in Figure 4.12 are results obtained for different fault types (single-line-to-ground and a line-to-line) in the forward and reverse directions. As expected, both fault types yielded similar trajectories (again due to the fact the negative-sequence impedance behind the relay is not affected by the type of the fault in the forward direction).

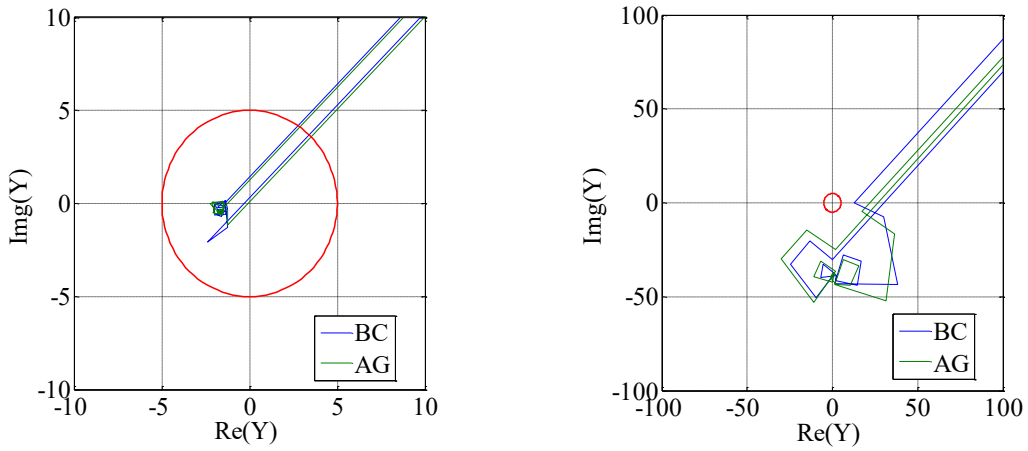

Figure 4.12 Trajectory of negative-sequence admittance on a G-B plain for (a) forward bolted faults at 50% of Line 12, BC and AG and (b) reverse fault (Bus 1) BC and AG

Table 4.3 presents a qualitative summary of the performance of the proposed directional method for a variety of faults on the network. These include faults of three different types (AG, BC and ACG) at four different locations (5%, 50% and 75% of the line and a reverse fault at *Bus 1*). Six iterations of each fault were applied with high and low fault impedance (0.001 Ω and 50 Ω) and at three different fault inception angles (0º, 60º and 150º). These extensive tests showed that the proposed method works 100% accurately, when the relay has an IBR as its local source.

Table 4.3: Fault direction identification for different faults

Applied fault		Fault Direction	
Type	**Location (forward)**	**Forward**	**Reverse (Bus 1)**
AG	5%	Correct	Correct
	50%	Correct	Correct
	75%	Correct	Correct
BC	5%	Correct	Correct
	50%	Correct	Correct
	75%	Correct	Correct
ACG	5%	Correct	Correct
	50%	Correct	Correct
	75%	Correct	Correct

4.4.4 Comparison with a Conventional Direction Element

Figure 4.13 and Figure 4.14 present a scenario where the applicability of the proposed method is emphasised. The results shown are for a forward AB fault at 50% of *Line 12* (given in Figure 4.7). As indicated by the impedance trajectory shown in Figure 4.14-(a) and the *Zone 1*, AB impedance element pickup signal shown in Figure 4.13-(c), the conventional distance relay clearly identifies the fault as a Zone 1 fault. However, the relay is restrained from issuing a trip due to mis-operation of its conventional directional element (DIR_{conv}). In contrast, one can see that the proposed directional element clearly identifies the fault as a forward fault based on the results shown in Figure 4.13-(f) and Figure 4.14-(b).

(a)

(b)

(c)

(d)

(e)

(f)

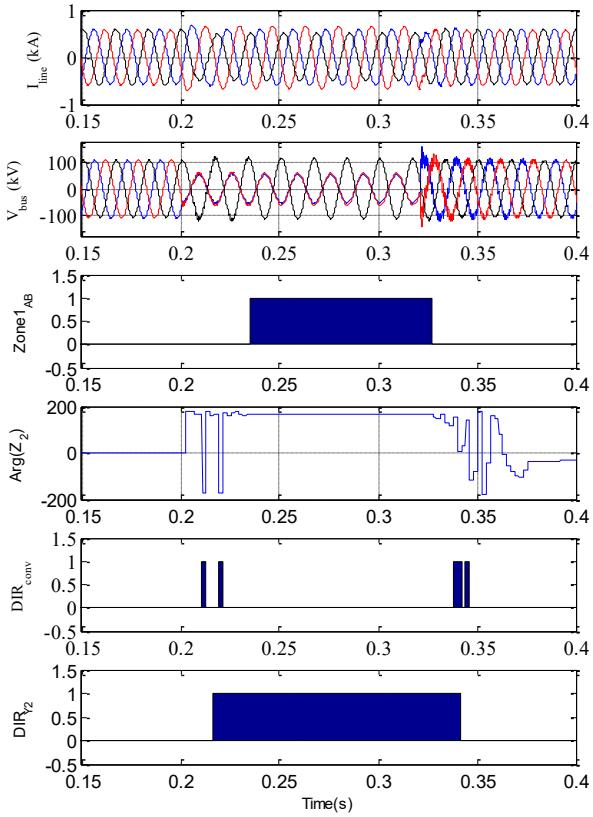

Figure 4.13 Results for a forward bolted AB fault at 50% of Line 12 (a) Line Current, (b) Bus voltage, (c) Zone 1 AB impedance element, (d) Negative sequence impedance angle, (e) conventional directional element pickup and (f) proposed directional element pickup

Notice that the distance relay model used in this exercise is a generic (distance) relay model available in DRTS component library and the results presented in Figure 4.13 for Zone 1, AB impedance element pickup, negative-sequence impedance angle, conventional directional element pickup and AB impedance trajectory are its outputs. It resides in relay R looking into *Line 12*, as shown in Figure 4.7. Note that the relay would have correctly issued a Zone 1 trip, had the above-mentioned AB impedance element been supervised by the proposed directional element.

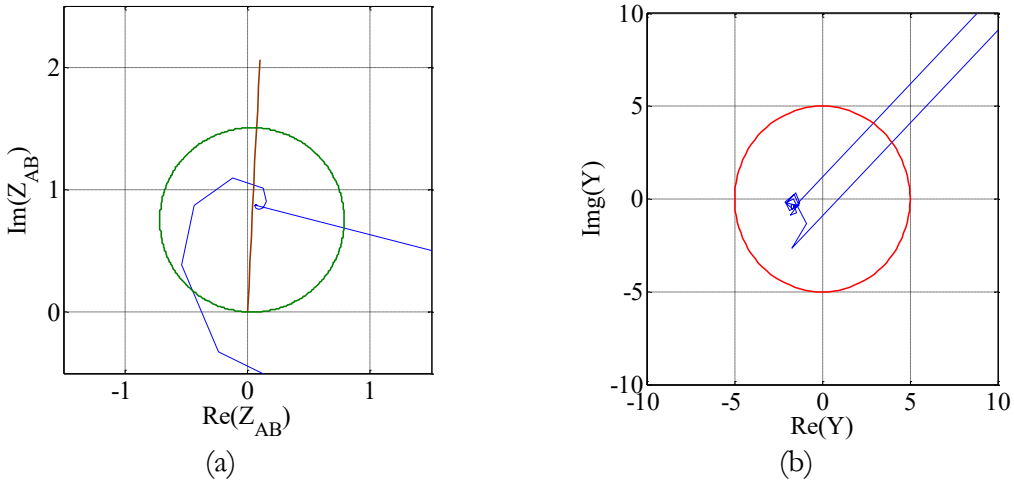

Figure 4.14 Results for a forward bolted AB fault at 50% of Line 12 (a) Zone 1 AB impedance trajectory on R-X plain, (b) trajectory of negative-sequence admittance on a G-B plain

Since the proposed algorithm is also dependent on a phasor calculation, its operating time is comparable with other phasor-based protection functions. However, as can be seen from Figure 4.13 (a, b & f), the proposed algorithm (DIRY2) operated under a cycle (16 ms). Since the proposed directional element asserts before the impedance element, it does not delay (hold back) the operation of the overall protection function. It can also be seen from Figure 4.13 (d & e) how unexpected phase angles of sequence voltages and currents mislead the conventional directional element (DIR_{conv}) while having no effect on the proposed technique.

4.4.5 Impact of Negative-Sequence Current Injection

As mentioned, some grid codes and recent standards mandate injection of a minimum amount of negative-sequence current during faults for IBRs, mainly to avoid system protection related issues. Thus, simulations were performed to evaluate proposed directional algorithm's performance under negative-sequence current injection. Figure 4.15 presents the admittance trajectories with the IBR injecting asymmetrical fault currents during asymmetrical faults.

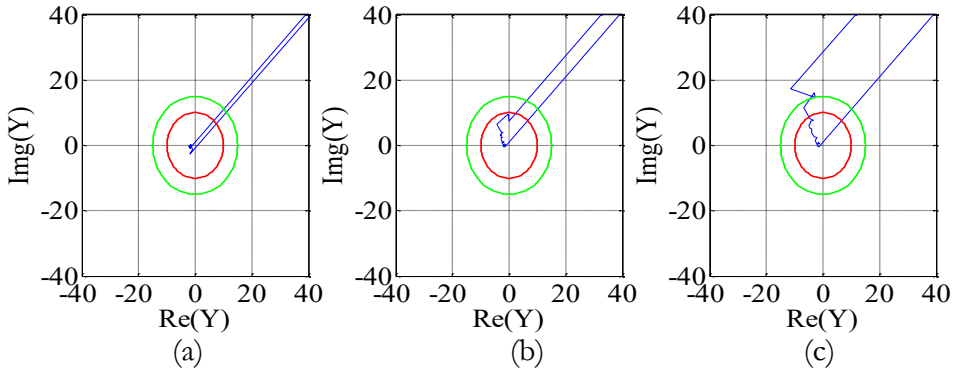

Figure 4.15 Results for a forward bolted AB fault at 50% of Line 12 with negative sequence current injection (a) K = 0, (b) K = 1 and (c) K = 2

Three scenarios with different levels of negative-sequence current injections are compared in Figure 4.15. Here, the *constant K* represents the ratio between per-unitized negative-sequence current and voltage. In these plots, forward zones with two different settings are drawn in the G-B plain. Zones shown in *red* and *green* are set to 25% (10×10^{-3} S) and 37.5% (15×10^{-3} S) of the remote AC network's admittance, respectively. Results indicate the proposed technique operates appreciably (especially with forward zone extended) even when the IBR produces a considerable amount of asymmetrical fault currents. Understandably, however, it was observed that the effectiveness of the proposed technique decreases when K is increased above a certain limit (K is rarely set above 1.0 in practice).

4.4.6 Impact of Conventional Synchronous Generation at IBR Bus

Plotted in Figure 4.16 are the negative-sequence admittance (Y2) trajectories for a forward AB fault at 50% of *Line 12* with different levels of additional synchronous generation connected to *Bus 1* (10 MVA, 20 MVA and 50 MVA). Figure 4.17 presents corresponding results for a reverse fault at *Bus 1* (only the 50 MVA case is shown, other cases also produced similar results). As in Figure 4.15, forward zones with two different settings are drawn on the G-B plain. These results indicate the proposed technique is effective with a considerable presence of conventional generation on the IBR end of the tie-line (representing a hybrid or a co-located plant).

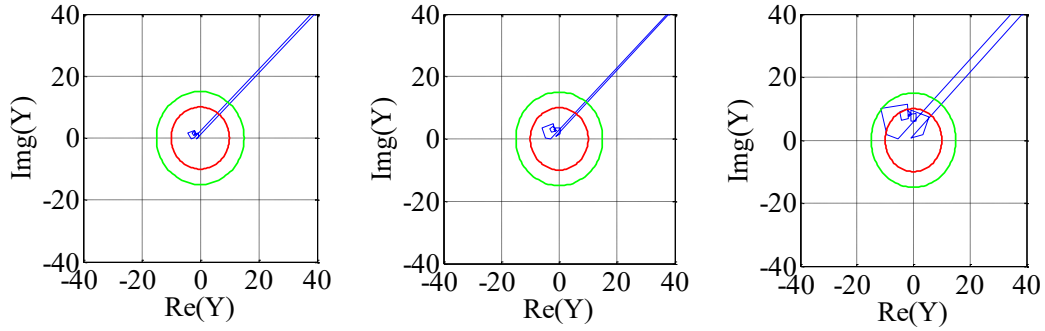

Figure 4.16 Results for a forward AB fault at 50% of Line 12 with additional synchronous generation connected to Bus 1 (a) 10 MVA, (b) 20 MVA and (c) 50 MVA

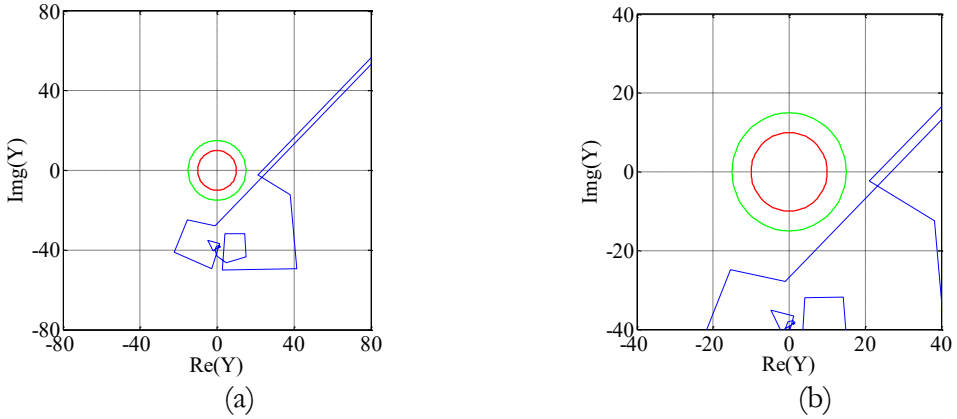

Figure 4.17 Results for a reverse fault (a) with additional 50 MVA synchronous generation connected to Bus 1 (b) magnified view

Figure 4.18 and Figure 4.19, respectively, show behavior of the impedance trajectories for a forward AB fault at 50% of *Line 12* and reverse short circuit AB fault (at *Bus 1*) with only synchronous generation connected to *Bus 1* (no IBR in the system). Here, only the forward zone with a setting of 15×10^{-3} S is drawn. Again, the proposed technique yielded acceptable results even though it operated transiently for reverse faults immediately following fault inception. It can be observed that the negative-sequence admittance trajectories transiently enter (only one sample) the forward zone, but converge well outside of it eventually. This, however, is inconsequential to protection operation as this transient pickup will reset well-before the impedance element sees the fault (refer the plots in Figure 4.13 (c) and (d)).

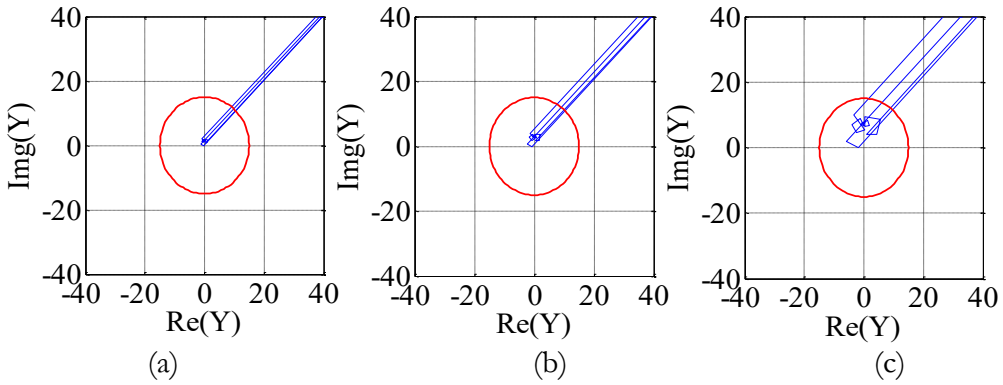

Figure 4.18 Results for a forward bolted AB fault at 50% of the Line 12 with only synchronous generation connected to Bus 1 (a) 10 MVA, (b) 20 MVA and (c) 50 MVA

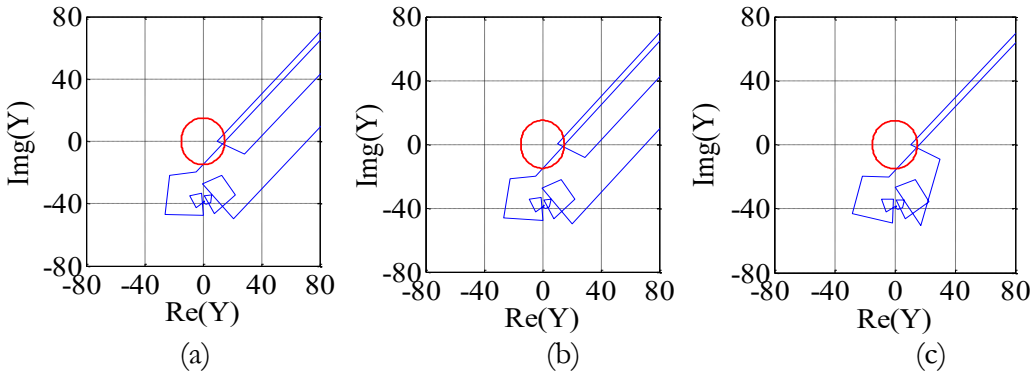

Figure 4.19 Results for a reverse bolted AB fault with only synchronous generation connected to Bus 1 (a) 10 MVA, (b) 20 MVA and (c) 50 MVA

Furthermore, a network configuration where there are parallel transmission lines between *Bus 1* and *Bus 2* would have a similar effect of having co-located conventional SG at the IBR plant (the relay will be fed by both IBR and SG generated currents, and the negative-sequence impedance seen by the relay shall be a combination of the two types of sources). It would obviously lower the effectiveness of the proposed technique for forward faults on a single circuit. However, with proper settings, this technique would still be applicable. The exact behavior of the directional element would be system specific, nevertheless.

4.4.7 Impact of a Weak Remote Grid

This subsection examines the effect of a weaker remote grid on the proposed directional identification technique. The relatively strong remote system in Figure 4.7 (short circuit ratio, SCR ≈ 7) was replaced by a simple voltage source (at *Bus 2*) behind an impedance, the value of which was selected to produce a remote grid with a lower SCR (weaker grid). Figure 4.20 shows result for reverse and forward AB faults with SCR of the remote system set to 1.6 and 2.0. A slightly smaller forward zone with a setting of 4×10^{-3} S is chosen for this scenario for better discrimination. As can be seen in Figure 4.20 -(b), the SCR of the remote grid does

not affect the admittance trajectory for forward faults as expected. However, discriminating between forward and reverse faults becomes harder with a weaker remote grid, as the difference between local and remote negative-sequence impedances becomes smaller.

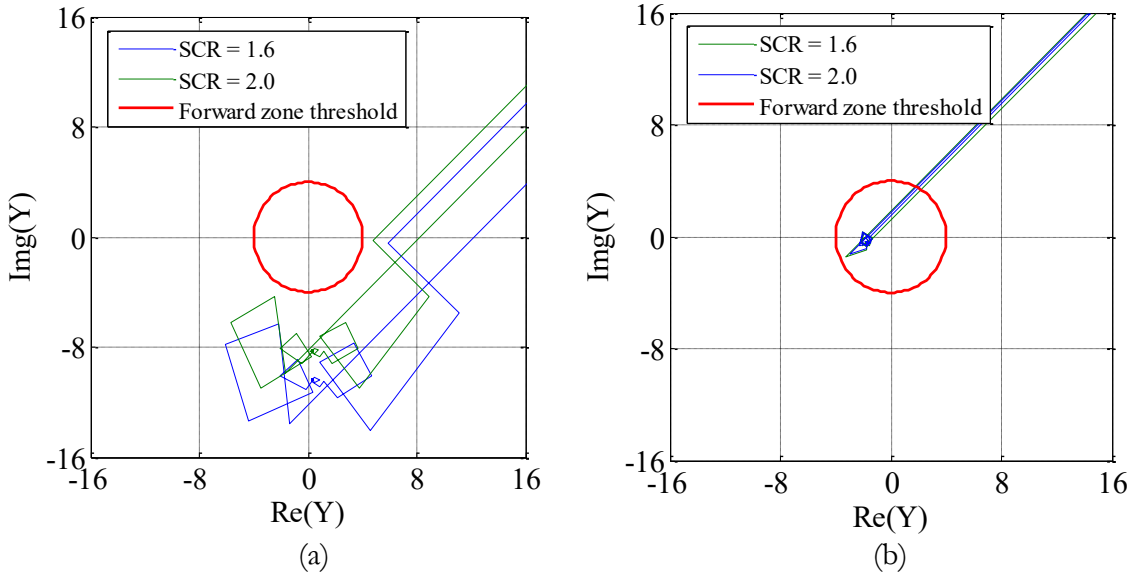

Figure 4.20 Results for a weaker remote grid (a) reverse fault AB fault on Bus 1 and (b) forward AB fault at 50% of the Line 12

In Figure 4.20-(a), one can observe how the point of convergence for reverse faults moves closer to the forward zone as the SCR of the remote grid reduces. This indicates that discrimination between forward and reverse faults becomes infeasible for very low SCR values using this technique. However, above results show that, with properly determined settings, the proposed technique is effective even for relatively weak remote systems.

4.4.8 Impact of Series Compensation

In order to further scrutinize the applicability of the proposed method, it was applied and tested with a transmission system with series compensation as depicted in Figure 4.21-(a).

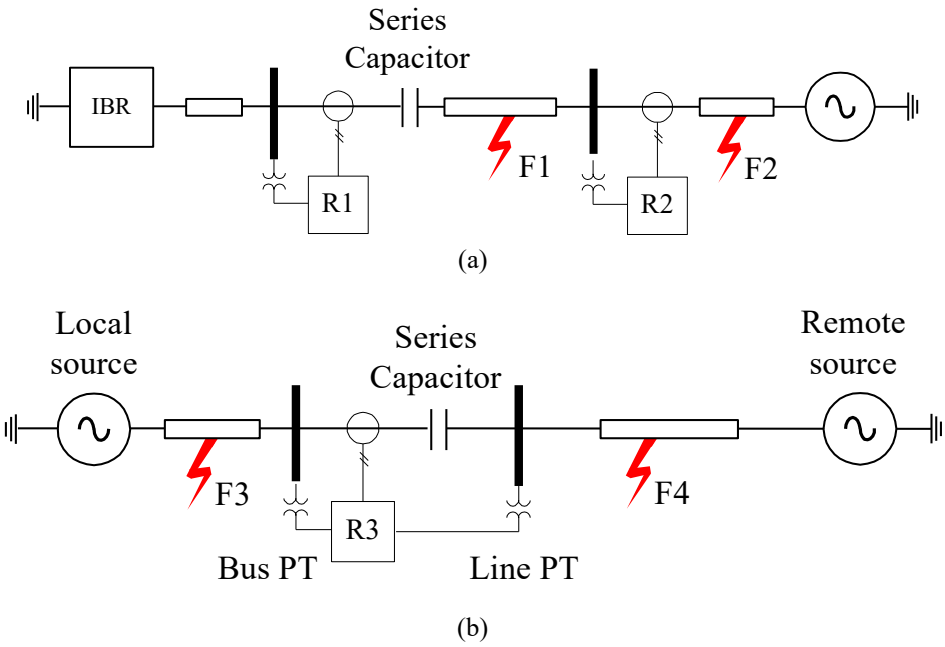

Figure 4.21 Application of the proposed method in a system with series compensation (a) with an IBR, (b) conventional sources

The simulation results of this exercise revealed that the presence of a series capacitor has no significant effect on the proposed method. When the capacitor is in the forward direction (on the line-side with respect to the relay), it only affects the negative-sequence impedance seen by the relay for reverse faults. In this scenario, presence of the series capacitor, in fact, improves the effectiveness of the method as the capacitive impedance of the series capacitor decreases the equivalent negative-sequence impedance (i.e. increases admittance) of the remote system. This, in turn, makes selectivity between the two system systems more straight forward. On the other hand, when the capacitor is located behind the relay (on IBR station

side with respect to the relay), it's capacitive impedance theoretically acts to decrease the equivalent or apparent impedance (i.e. increases admittance) for the local (IBR) system. However, this has little to no effect as on the proposed method as the equivalent negative-sequence impedance of the local system is dominated by that of the IBR, which is significantly larger than the impedances of regular power system elements.

On the other hand, when applied on a system with conventional sources (note that this is not the intended application), the presence of the series capacitor can a have substantial impact on the effectiveness of the proposed technique depending on the relative location of relay and the series capacitor (as shown in Figure 4.21-(b)). It was also observed that the fluctuations in impedance (and admittance) calculations caused by the presence of sub-synchronous components in the series compensated system can cause complications, particularly when determining the forward zone reach threshold (note that the sub-synchronous components mentioned here are those caused by natural oscillations in a RLC circuit; and NOT due to sub-synchronous oscillations phenomena such as sub-synchronous resonance or sub-synchronous control interactions). However, it is important to understand that all impedance/admittance-based protection techniques have a certain amount of vulnerability to sub-synchronous oscillations in system with series compensation.

4.5 Hardware Implementation

In order to further validate the applicability of the proposed directional identification algorithm, it was implemented in an existing generic, computer-based relay model and tested using EMT type hardware-in-the-loop simulations (with the DRTS). A schematic of the laboratory test setup including the computer-based relay is shown in Figure 4.22.

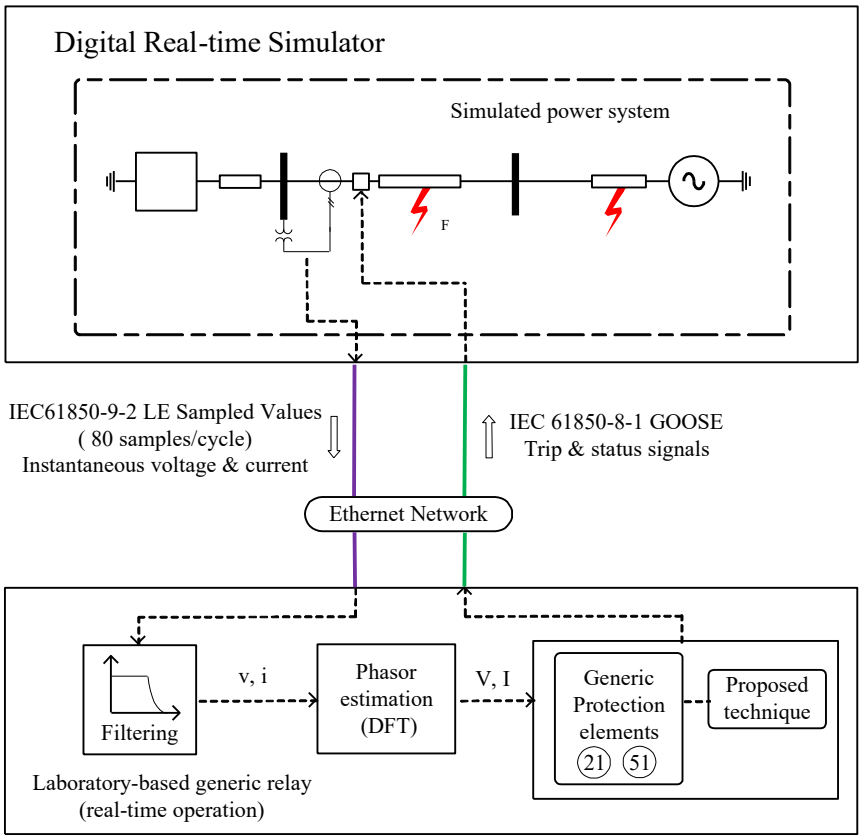

Figure 4.22 Schematic of the hardware-in-the-loop test setup

The above-mentioned relay contains workings of a typical commercial line protection relay. It consists of basic input/output functions, signal processing including front-end filtering, a DFT (Discrete Fourier Transform) based phasor estimation. Furthermore, common protection elements such as distance, directional and over-current are implemented in this

relay. It resides in a dedicated laboratory computer running a real-time operating system and interfaced with the DRTS using contemporary system automation protocols (IEC 61850-9-2 Sampled Values and IEC 61850-8-1 GOOSE). The proposed directional identification algorithm was integrated on top of this existing functionality.

Plotted in Figure 4.23 is a comparison of recorded data from the laboratory-based (hardware) relay and corresponding results obtained from the simulations. As can be seen, the trajectories of the negative-sequence admittance recorded from both platforms follow a similar path for both forward and reverse faults, hence, produce the same output for fault direction.

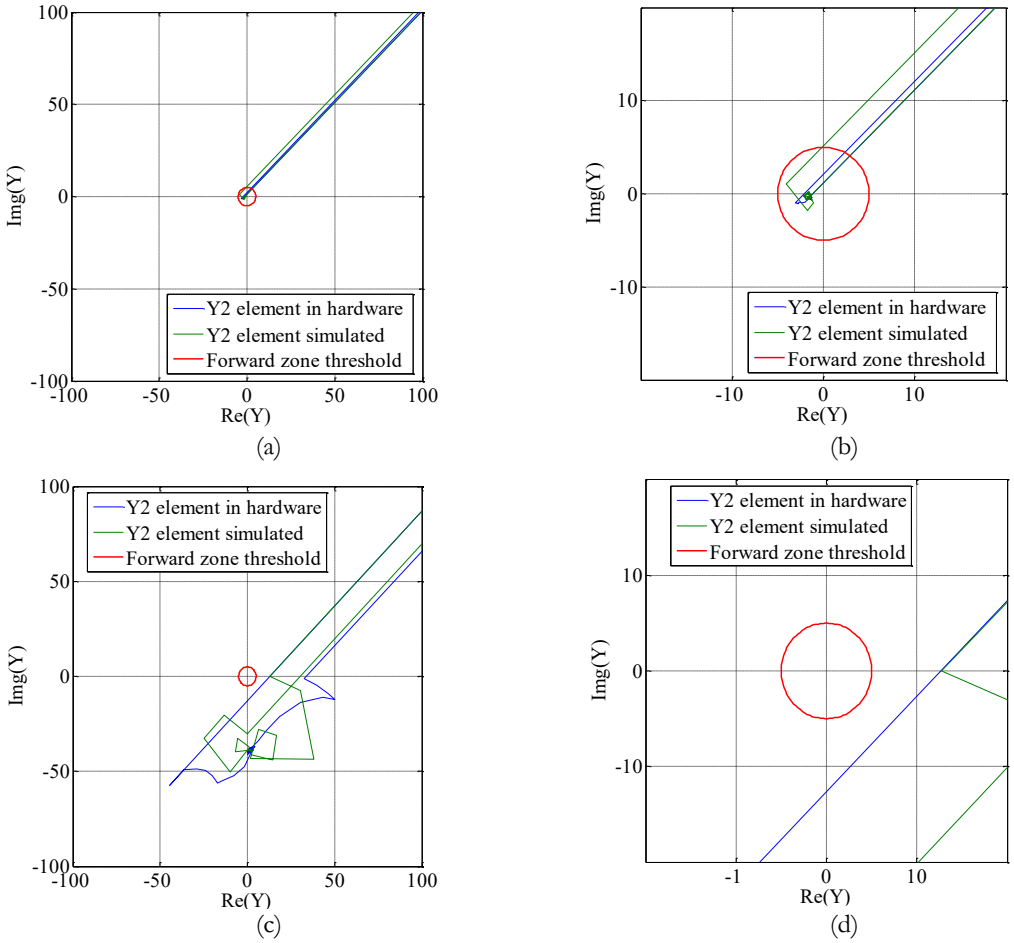

Figure 4.23 Trajectory of negative-sequence admittance on a G-B plain (a) forward AB fault at 50% of Line 12 (b) magnified view (c) reverse bolted AB fault at Bus 1 (d) magnified view

4.6 Discussion

Results presented above subsections indicate that the direction identification method proposed in this work yields superior results in comparison to conventional phase-angle-based directional elements, when protecting a transmission line fed largely by IBRs. IBR-generated currents and voltages are often associated with unexpected and time-varying phase angles, hence, any algorithm that depends on measured phase angles would be prone to mal-operate. One clear approach to overcome this difficulty is to use algorithms based only on magnitudes of currents and voltages, such as the one proposed in this chapter. This key difference of magnitude-only approach makes the proposed method more effective than most of the existing techniques (that depend on measured phase angles in some way, shape or form) in the presence of IBRs. Additionally, the proposed technique offers several further advantages as well. The most significant among them is its imperviousness to conditions of the fault. Attributes of a fault such as location, fault impedance, inception angle and fault type have little to no effect on the operation of the proposed method. Another major benefit of this technique is that it can be very easily implemented in a modern numerical relay with trivial formulae and requires little computational recourses. It is important to note that the two principal elements required for the calculation of the negative-sequence admittance are already available in most line protection relays as they are usually required for other protection functions as well.

It is noteworthy, however, that the proposed method also has a few important limitations that restricts its use to a specific set of applications and demands careful consideration by the user. Firstly, this method is effective only if the (equivalent or apparent) negative-sequence impedances either side of the relay are different in magnitude (at least to a certain

degree). In other words, this algorithm expects that one end of the protected line (by the relay) is connected to an IBR heavy system (or a similar weak source), while the other end is connected to a comparatively stronger system. This is, in fact, a common transmission configuration in which IBRs are connected to existing grids. Most IBR resources are readily available (hence viable) only in remote parts of the land, usually far way from the major transmission facilities (for example, offshore wind). In addition, system contingencies such as lines taken out-of-service (due to faults or maintenance) can also result in similar network topologies.

Moreover, presented results in this work indicates that the effectiveness of the proposed method, to a certain extent, depends on the level of negative-sequence current suppression by IBRs. Irrespective of certain recent requirements (some European grid codes and newly published IEEE std. 2800), many of the real-world IBRs still do not produce significant amounts of unbalanced fault currents (it will take several years for grid operators to enforce and IBR vendors to fully comply to these requirements). As mentioned earlier, even with compliance to such requirements, the related control functions of some IBRs may not response fast enough to be relied upon for primary transmission level system protection functions. Another limitation of this technique is that it is only applicable for unbalanced faults (would not work for balanced three-phase faults, since it is based on negative-sequence quantities). However, this issue is common for the other (conventional) negative-sequence based direction elements as well and for balanced faults, the positive-sequence based directional algorithms are applicable (and generally perform well) as the positive-sequence current is not completely suppressed during faults.

4.7 Concluding Remarks

Fault direction identification is one of the commonly affected protection functions in the presence of IBRs. This chapter presents a novel algorithm to correctly identify fault direction using negative-sequence admittance measurements. Firstly, the theoretical premise of the algorithm was delivered and then it was validated by extensive EMT simulations performed using a DRTS. Results presented in this chapter suggest that the proposed technique operated appreciably well under a variety of conditions and configurations. The proposed technique is robust and reliable and yields better results in comparison to conversional techniques in presence of IBRs. In addition, its operation is simple and can be conveniently incorporated into a modern digital relay.

In this chapter, the authors have provided a detailed discussions on the applicability, settings and limitations of the method and believe that the theoretical premise presented in this work has applications in protecting transmission lines interconnecting IBRs.

Chapter 5

Theoretical Analysis of the Impact of IBRs on Impedance Trajectories during Power Swings

5.1 Introduction

Power swings are triggered by major disturbances to power flow in the system and can be caused by events such as severe faults, loss of large generation or load. Impedance-based protection relays are susceptible to interpret these as faults and trip unnecessarily. Out-of-step (OOS), otherwise known as power swing protection, schemes are designed to mitigate such undesired outcomes during power swings. As explained in previous subsection 1.2.4, two types of OOS protection functions exist; namely, power swing blocking (PSB) and out-of-step tripping (OST) functions [75]-[78]. PSB function is designed to discriminate power swings from system faults, whereas OST separates stable power swings from unstable ones. Traditional OOS protection functions are designed based on electrical and mechanical dynamics of power systems dominated by synchronous machines. In most implementations, OOS protection

functions are based on the speed-of-movement and trajectory of apparent impedance seen by a relay. However, reviewing the design and operation of OOS protection function in system with IBRs is necessary as IBRs can potentially alter both the speed-of-movement and trajectory of apparent impedance seen by a relay.

Main objective of this chapter is to study the effects of IBRs on power swing impedance trajectories. Here, the focus is entirely on electrical trajectories and not on their speed-of-movement (i.e. this analysis does not intend to address the effect of IBR on the swing speed due to reduced inertia, which has been sufficiently scrutinised in literature). This evaluation will be carried out by means of a generic circuit equivalents and basic phase-domain circuit equations, without the use of to complex dynamic models. The work presented in this paper attempts to incorporate IBRs into a similar type of simplified study used in analysis of traditional power swing protection. The impact of potential changes to swing trajectories on traditional power swing protection are also examined in this chapter.

The rest of this chapter is organized as follows. Section 5.2 provides a theoretical model to predict of power swing impedance trajectories in the presence of an IBR, which is validated by EMT simulation in section 5.3. Using the theoretical model presented, results for different operational and system conditions are given in Section 5.4. Sections 5.5 follows with a general discussion on the findings of this work.

5.2 Theoretical Analysis

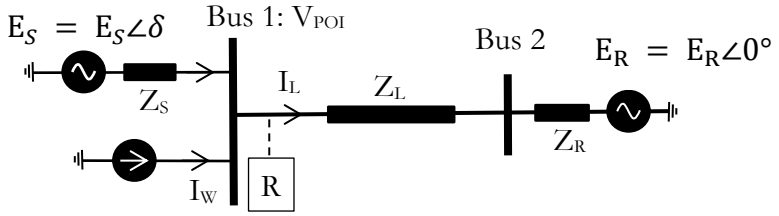

E_S: Sending end voltage (phasor)

E_R: Receiving end voltage (phasor)

I_W: IBR's constant current injection (phasor)

Z_S: Sending end source impedance

Z_R: Receiving end source impedance

Z_L: Line impedance

Figure 5.1 Simplified single line diagram of the power system during a power swing following a disturbance

Given in Figure 5.1 is the simplified single-line diagram of the power system under investigation. It comprises of two conventional synchronous generator based systems (local system represented by a voltage source behind an impedance, E_S/Z_S, and the remote system by E_R/ Z_R), which are connected via a transmission line. Note that Z_S and Z_R are transient impedances of the local and remote sources/systems, respectively [8]. In addition, an IBR is connected to *Bus 1* (of the local system), which is its Point of Interconnection (POI). As depicted in Figure 5.1, the IBR is represented by a current source, that injects current I_W into the POI. All terms in subsequence equations are in phasor-domain unless otherwise stated.

The positive-sequence impedance seen by a relay, R, at the local system bus looking into the transmission line is given by (Z_{Relay}):

$$Z_{Relay} = \frac{V_{POI}}{I_L} = \frac{E_s - Z_S . I_s}{I_L} \tag{5-1}$$

Basic circuit equations are written to determine V_{POI} and I_L in terms of known quantities.

$$\frac{E_s - V_{POI}}{Z_s} = I_s \tag{5-2}$$

$$I_L = I_S + I_W \tag{5-3}$$

Using (5-2) and (5-3),

$$V_{POI} = E_s - Z_S.(I_L - I_W) \tag{5-4}$$

Applying the Ohm's law for Z_L and Z_R and using (5-4), I_L can be written as,

$$I_L = \frac{V_{POI} - E_R}{Z_L + Z_R} = \frac{E_s - Z_S.(I_L - I_W) - E_R}{Z_L + Z_R} \quad \rightarrow \quad I_L = \frac{E_s - E_R + I_W.Z_S}{(Z_L + Z_R + Z_S)} \tag{5-5}$$

Next, by substituting for V_{POI} and I_L in (5-1) from (5-4) and (5-5) respectively, Z_{Relay} can be expressed as,

$$Z_{Relay} = \frac{V_{POI}}{I_L} = \frac{E_s - Z_S.(I_L - I_W)}{I_L} = \frac{E_s}{I_L} - Z_S + \frac{Z_S.I_W}{I_L}$$

$$Z_{Relay} = \frac{(E_s).(Z_L + Z_R + Z_S)}{E_s - E_R + I_W.Z_S} - Z_S + \frac{(Z_S.I_W).(Z_L + Z_R + Z_S)}{E_s - E_R + I_W.Z_S} \tag{5-6}$$

Let the remote source be the angle reference of the system, δ the phase angle of the local voltage source, θ the phase angle of the POI voltage, and 'k' the ratio of per-unit voltage magnitudes of the two voltage sources $(k = |E_S|/|E_R|)$. Then, the phasors of the two voltage sources and that of the POI can be expressed as:

$$E_S = k.|E_R|\angle\delta, \quad E_R = |E_R|\angle 0, \quad V_{POI} = |V_{POI}|\angle\theta \tag{5-7}$$

Substituting in (5-5) and (5-6),

$$I_L = \frac{k.|E_R|.[cos(\delta) + j.sin(\delta)] - |E_R| + I_W.Z_S}{(Z_L + Z_R + Z_S)} \tag{5-5a}$$

$$Z_{Relay} = \frac{k.|E_R|.[cos(\delta) + j.sin(\delta)].(Z_L + Z_R + Z_S)}{k.|E_R|.[cos(\delta) + j.sin(\delta)] - |E_R| + I_W.Z_S} - Z_S + \frac{Z_S.I_W.(Z_L + Z_R + Z_S)}{k.|E_R|.[cos(\delta) + j.sin(\delta)] - |E_R| + I_W.Z_S} \quad (5\text{-}6a)$$

Considering that values of $|E_S|$, $|E_R|$ (or k), Z_S, Z_R, Z_L and $|I_W|$ are known for the system under study, Z_{Relay} becomes a function of δ, which is the phase angle of the local source with respect to the angle reference.

The magnitude of the IBR's current injection, $|I_W|$, can assumed to be known as well. However, phase angle of this current injection is generally known relative to the of the voltage at the POI, V_{POI}. Since V_{POI} is also a function of δ, finding an elegant solution to V_{POI} is not trivial. As a result, an iterative approach is proposed to solve for V_{POI} (= $|V_{POI}|\angle\theta$). The phase angle of V_{POI} can be found following the steps given below.

Using (5-4), V_{POI} can be expressed as,

$$V_{POI} = E_R + I_L.(Z_L + Z_R) = E_R + \frac{[(E_S - E_R) + I_W.Z_S].(Z_L + Z_R)}{(Z_S + Z_R + Z_L)} \quad (5\text{-}8)$$

Here, all resistances are neglected, i.e. $Z_S = j|Z_S|$, $Z_R = j|Z_R|$, $Z_L = j|Z_L|$ and the phase angle of I_W with respect to the angle reference is taken as α° (= θ + β),

$$|V_{POI}|.[cos(\theta) + jsin(\theta)] = |E_R| + \begin{Bmatrix} k.[cos(\delta) + jsin(\delta)].|E_R| - |E_R| \\ +j.|I_W|.[cos(\alpha) + jsin(\alpha)].|Z_S| \end{Bmatrix}.M_Z \quad (5\text{-}9)$$

where,

$$M_Z = \frac{j.(|Z_L| + |Z_R|)}{j.(|Z_S| + |Z_R| + |Z_L|)}.$$

When all resistances are neglected, M_Z becomes a scaler. The value of β, which is the phase angle of I_W with respect to V_{POI}, is assumed to be known (based on the control strategy). However, the value of θ is unknown, and can be found considering the operating conditions of the system. By substituting $I_W = |I_W|.[cos(\alpha) + jsin(\alpha)]$ and rearranging (5-9):

$$|\mathrm{V_{POI}}|.[cos(\theta)+jsin(\theta)]-j.M_Z.|\mathrm{I_W}|.|\mathrm{Z_S}|[cos(\alpha)+jsin(\alpha)] = |\mathrm{E_R}|+\{k.[cos(\delta)+jsin(\delta)]-1\}.|\mathrm{E_R}|.M_Z \quad (5\text{-}10)$$

$$|\mathrm{V_{POI}}|.[cos(\theta)+jsin(\theta)]+M_Z.|\mathrm{I_W}|.|\mathrm{Z_S}|.[sin(\alpha)-j.cos(\alpha)] = |\mathrm{E_R}|.\{1+M_Z.[k.cos(\delta)-1]+j.k.|\mathrm{E_R}|.M_Z.sin(\delta)\} \quad (5\text{-}11)$$

Equating real and imaginary parts of (5-11),

$$|\mathrm{V_{POI}}|.cos(\theta)+M_Z.|\mathrm{I_W}|.|\mathrm{Z_S}|.sin(\alpha) = |\mathrm{E_R}|.\{1+M_Z.[k.cos(\delta)-1]\} \quad (5\text{-}12)$$

$$|\mathrm{V_{POI}}|.sin(\theta)-M_Z.|\mathrm{I_W}|.|\mathrm{Z_S}|.cos(\alpha) = k.|\mathrm{E_R}|.M_Z.sin(\delta) \quad (5\text{-}13)$$

$(5-12)\times sin(\theta)$:

$$|\mathrm{V_{POI}}|.cos(\theta).sin(\theta)+M_Z.|\mathrm{I_W}|.|\mathrm{Z_S}|.sin(\alpha).sin(\theta) = |\mathrm{E_R}|.\{1+M_Z.[k.cos(\delta)-1]\}.sin(\theta)) \quad (5\text{-}14)$$

$(5-13)\times cos(\theta)$:

$$|\mathrm{V_{POI}}|.sin(\theta).cos(\theta)-M_Z.|\mathrm{I_W}|.|\mathrm{Z_S}|.cos(\alpha).cos(\theta) = k.|\mathrm{E_R}|.M_Z.sin(\delta).cos(\theta) \quad (5\text{-}15)$$

$|\mathrm{V_{POI}}|$ can be eliminated to obtain (5-17), by subtracting (5-15) from (5-14) and applying trigonometric identities:

$$M_Z.|\mathrm{I_W}|.|\mathrm{Z_S}|.\cos(\theta-\alpha) = |\mathrm{E_R}|.\{1+M_Z.[k.cos(\delta)-1]\}.sin(\theta)-k.|\mathrm{E_R}|.M_Z.sin(\delta).cos(\theta) \quad (5\text{-}16)$$

$$\mathrm{P_3}.cos(\beta) = \mathrm{P_1}.sin(\theta)-\mathrm{P_2}.cos(\theta) \quad (5\text{-}17)$$

where,

$$P_1 = |\mathrm{E_R}|.\{1+M_Z.[k.cos(\delta)-1]\}, \qquad P_2 = k.|\mathrm{E_R}|.M_Z.sin(\delta),$$

$$P_3 = M_Z.|\mathrm{I_W}|.|\mathrm{Z_S}|, \quad \beta = \alpha-\theta$$

Pre-disturbance generator internal voltages are assumed to remain unchanged during the first swing. With the system impedances known, the values of P_1, P_2 and P_3 in (5-17) can be computed for a known set of values for k, δ, $|\mathrm{I_W}|$, and β. Then, (5-17) can be solved to determine θ. This enables calculation of the magnitude of $\mathrm{V_{POI}}$ using (5-8). Finally, the positive-

sequence impedance seen by the relay at the source bus (R in Figure 5.1) looking into the transmission line can be expressed as:

$$Z_{Relay} = \frac{V_{POI}}{I_L} = \frac{|V_{POI}|\angle\theta.\{j|Z_L| + j|Z_R| + j|Z_S|\}}{|E_s|\angle\delta - |E_R|\angle 0 + |I_W|\angle(\theta+\beta).j|Z_S|} \quad (5\text{-}18)$$

5.2.1 Representing the IBR

Representing gird-following IBRs using (voltage controlled) current sources is a common practice in protection studies [16]. Recognizing that active and reactive power requirements of an IBR are defined at the POM (which is usually the HV side of the main IBR transformer) [12], lumping the entire IBR plant into a current source is a reasonable approximation for a study of this nature. In addition, the simplified current source representation of the IBR used in this study ignores the effects of an interconnection system, which often is a short tie-line between the POM and POI of the IBR (thus, can be left out without significant error). The magnitude and relative phase angle (or power-factor) of the IBR's current injection can be assumed to be a known constant for a given steady-state operating point.

In this study, unity power-factor operation ($\beta=0^o$) at rated power (1.0 pu current injection) is assumed during the regular operation by default. In this scenario, it is worth noting that the maximum magnitude of the current injection does not change drastically, even during a disturbance, due to the current limits imposed by power electronic converters of the IBR. It can be assumed to remain constant (at 1.0 pu) during a slow-moving, balanced phenomena such as a power swing. The phase angle of the injected current, however, may change considerably during such a disturbance, depending on the severity of the excursion and applicable performance requirements. The main dynamic characteristic of an IBR that can have a

significant impact on its behaviour during power swings is current injection during the voltage ride-through (VRT) mode. This is largely due to the fact that VRT performance requirements mandated for IBRs are fast enough to affect power swings (step response < 2.5 cycles and setting time < 4 cycles [12]), hence must be taken into consideration. Conversely, other slower controls and electrical system dynamics are ignored in this analysis. Figure 5.2 provides an example of positive-sequence current injection requirements during VRT operation [6]. The parameter K_{VRT} is the ratio between the per-unitized reactive current and per-unitized voltage deviation (both positive-sequence) at the POI (K_{VRT} defines the boundary of minimum requirement).

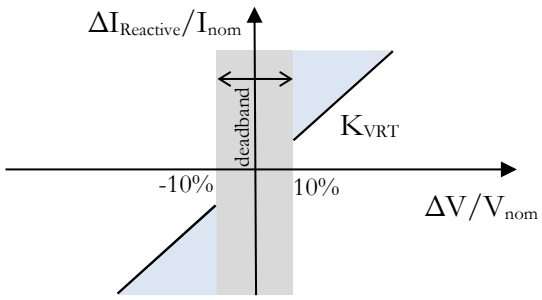

Figure 5.2 Example positive-sequence current injection requirements during voltage ride-through

It is assumed that the IBR under consideration is grid-following and can ride-through at least the first power swing. During regular operation, priority is given to active current injection. Priority switches to reactive current injection during VRT operation, and any residual current injection capacity shall be used for active current (β is set accordingly). VRT operation is triggered when the voltage deviation is greater than a set threshold (for example $\mp 10\%$). Moreover, note that only positive-sequence reactive current injection is applicable for this investigation for power swings are inherently balanced phenomena.

5.3 Validation Using EMT Simulations

The validity of the theoretical derivations presented in above Section 5.2 was verified using EMT simulations of the simplified power system shown in Figure 5.1. The following parameters were used to represent the ***base-case*** power system: local source impedance, Z_s = j0.1 pu, remote source impedance, Z_r = j0.15 pu, the line impedance, Z_l = j0.1 pu, and the ratio between local and remote source voltage magnitudes, k = 1.02. The current injection from the IBR, I_W, was chosen to be a value corresponding to a system SCR (Short Circuit Ratio) of 10. All per-unit values provided are in 230 kV and 100 MVA base. Location of the relay was at the local end of the transmission line as shown in Figure 5.1.

Figure 5.3 compares the theoretically calculated results (dotted line) against those attained from EMT simulations. Simulation results are given for two slip frequencies (which determines the swing speed), set to 0.5 Hz (solid line) and 0.03 Hz (dashed line). The impedances Z_s, Z_r, and Z_l are also shown in the same figure, taking relaying point as the origin.

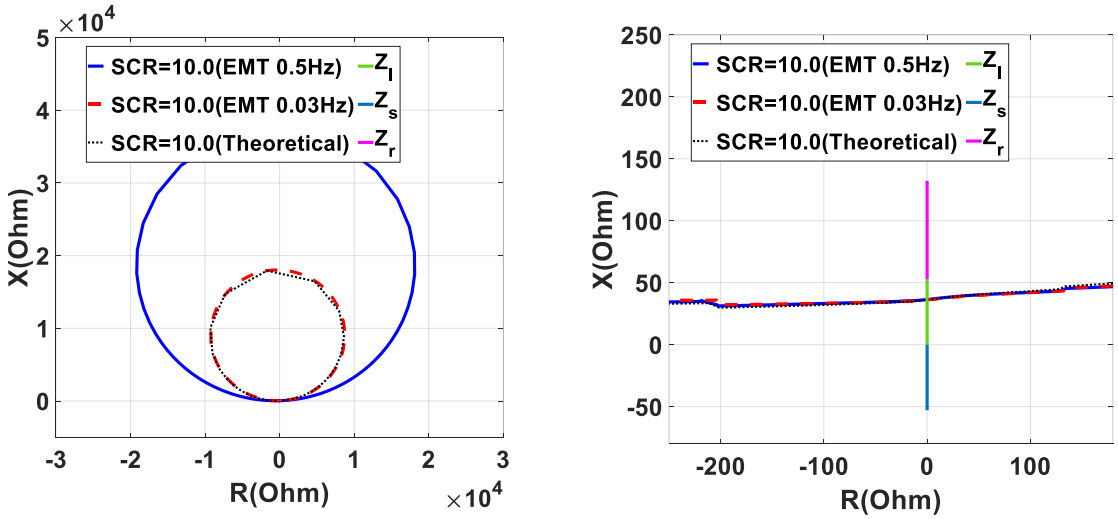

Figure 5.3 Comparison of theoretical and EMT results, (b) Magnified plot with impedances Z_s, Z_l and Z_r

As evident from Figure 5.3-(a), there is substantial mismatch between the impedance trajectories attained theoretically (dotted line) and from EMT simulations for 0.5 Hz slip speed. However, this is primarily due to the effect of signal processing (phasor extraction using a DFT function) in the EMT simulation, which is necessary to determine the impedance seen by the relay. In this context, it is important to note that the theoretical calculations presented in above Section 5.2 are in phasor-domain and as such, have no notion of time (or slip frequency). In contrast, EMT simulations are carried out in time-domain and must be transformed into phasor-domain using appropriate signal processing for a meaningful comparison. This conversion from time-domain to phasor-domain, using signal processing techniques such as DFT based phasor extraction, is inherently associated with delays. System voltages and currents (and the apparent frequency measured by the relay) are in continuous change during a power swing. As a result, there is a persistent lag/error between the theoretically calculated values in phase-domain and the respective phasors extracted using time-domain measurements at any given point in time. This can be inferred by the observation that the mismatches are much larger at fast-moving section of the trajectory ($\delta \approx 0^0$), and are perceptibly smaller at slow-moving parts of the trajectory ($\delta \approx 180^0$, Figure 5.3-(b)), which is explained by the performance of the DFT algorithm during system dynamics.

A further confirmation of the above-mentioned effect is the fact that the mismatches between phasor domain (theoretical) calculations and time-domain simulation results diminished as the slip-frequency was reduced in the EMT simulation. As shown Figure 5.3-(a), the two trajectories are very closely in agreement with each other at a slip-frequency of 0.03 Hz. It should be noted that a power swing at 0.03 Hz is not realistic in real-world; nevertheless,

this exercise was performed to demonstrate the impact of delays and errors caused by phasor extraction (i.e. DFT) operating under continuously varying off-nominal frequencies. Notwithstanding the mismatches at other regions, the two trajectories displayed a close match in the range where the pole-slipping occurs ($\delta \approx 180^0$), which is also the region of interest for power system protection. Therefore, the focus of this analysis shall be on this region of the trajectory in subsequent section of this chapter.

Figure 5.4 offers a comparison between theoretical and EMT results for different system SCR values. Results presented are for SCR values 3, 5, 10 and no-IBR, and all of them are in close agreement with their counterparts. Figure 5.6 provides a comparison of results between a theoretically calculated trajectory and that obtained from a more detailed EMT simulation (performed in DRTS). In this analysis, the IBR was represented using an averaged model with standard d-q domain controls. In addition, the local voltage source was also replaced by a conventional synchronous generator (SG), which was represented using a detailed dynamic model (with both rotor and stator dynamics) from the master component library. Power system parameters used for detailed EMT simulations are provided in Figure 5.5 (per-unit values are in 400 kV and 222 MVA base). The effective impedance of the local source, Z_S, was j0.45 pu and consists of the transient impedance of the synchronous generator (X_d') and the leakage impedance of the generator step-up (GSU) transformer. The pre-disturbance active power flow from the IBR and synchronous generator were approximately set to 200 MW each. The order of events that led to the power swing was triggered by inception of a fault on one of the transmission lines between the generation plant and the remote system and its subsequent tripping (disconnection). The general agreement of the results from the two domains (given

in Figure 5.6) further implies the validity of the theoretical derivations, specifically in the region around $\delta \approx 180^0$. The loop-like segment of trajectory of EMT simulation results (given in red) is due to the fault clearing transient. The deviations of the two trajectories in the other regions can be attributed mainly to the signal processing related issues explained earlier. One can also notice a general similarity in the two sets of EMT simulation results presented in Figure 5.3 and Figure 5.6 (the observed slip frequency in the detailed EMT simulation was approximately 1.8 Hz).

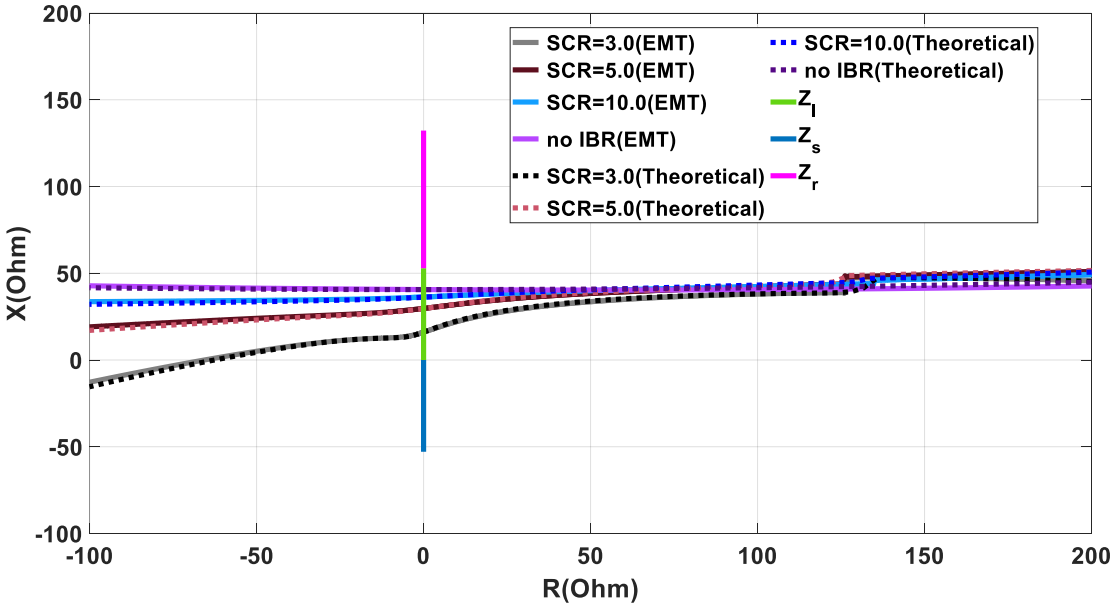

Figure 5.4 Comparison of theoretical and EMT results for different system SCR

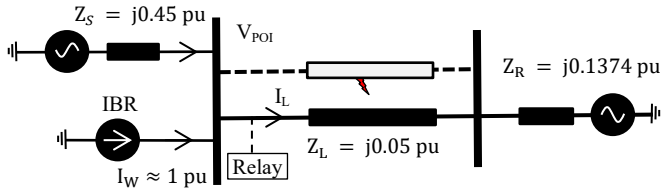

Figure 5.5 Simplified single line diagram of the power system during a power swing following a disturbance

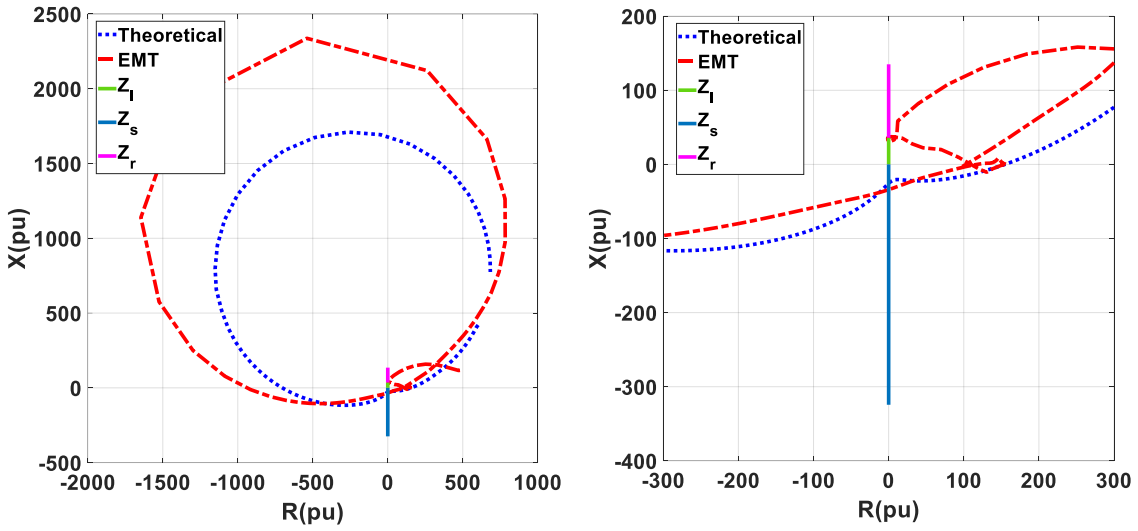

(a) (b)

Figure 5.6 Comparison of theoretical and detailed EMT simulation results

In EMT simulations, three-phase, instantaneous currents and voltages were measured at the relaying location (as in previous simulation). Master library relaying components in the DRTS simulation tool were utilized for signal processing, which provided both voltage and current phasors and the positive-sequence impedance seen at the relaying location.

EMT simulations were performed in this work specifically to validate the theoretical equations derived in above Section 5.2 (results given in Figure 5.3, Figure 5.4 and Figure 5.6 to so evidently). Consistent with the objective of this work, the analysis presented in subsequent sections of this Chapter was carried out using only the derived phasor-domain theoretical equations.

5.4 Results

The following subsections present the results obtained by analyzing the effect of different system parameters on the swing impedance trajectories as revealed by the theoretical equations derived in above Section 5.2. Note that the impedances Z_S, Z_r, and Z_l are also shown in figures as line segments, as a frame of reference when applicable.

5.4.1 Base Case

Presented in Figure 5.7 is a comparison between the swing impedance trajectories of the system described in section 5.3 for no IBR and base-case IBR scenarios. Voltage source impedances, Z_S and Z_r, were chosen to be j0.1 pu and j0.15 pu, respectively. The line impedance, Z_l, was set at j0.1 pu. In addition, the ratio between local and remote source voltage magnitudes was 1.02 pu and the system SCR was taken as 10.

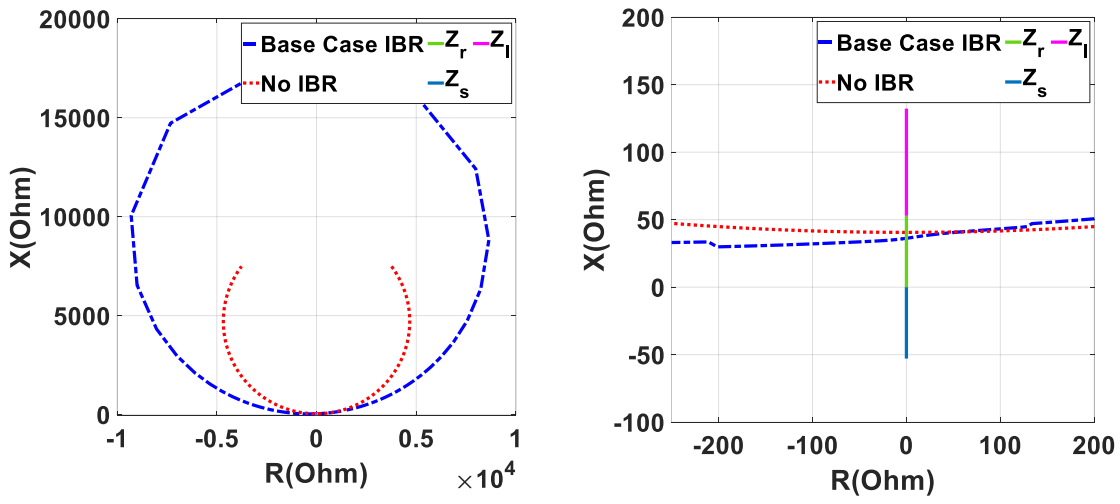

(a) (b)

Figure 5.7 (a) Swing impedance trajectories for no-IBR and base-case IBR scenarios, (b) magnified plot with impedances for Z_s, Z_l and Z_r

5.4.2 Impact of Short Circuit Ratio

Short Circuit Ratio (SCR) of an IBR plant is defined as the ratio between of the short circuit level (SCL) of the AC system at the POI and the power rating of the IBR Plant. A higher SCR value indicates a stronger AC system and vice-versa. In general, SCR values below 2.5 are considered interconnections to weak AC systems. Note that SCR can change with time depending on the system operating conditions, topology and various other system contingencies. Results given in Figure 5.8 are swing impedance trajectories of the system for different AC system SCRs (2.5, 3.0, 5.0, 10.0,12.0) and no-IBR. All other system parameters (including system impedances, voltages etc.) were kept the same as the base-case (as defined in Section 5.3).

Investigating the results, the impact of system SCR on swing impedance trajectories can be separated into two aspects. Firstly, as the SCR decreased (i.e. increase of IBR current injection), the impedance trajectory inverted on the R-axis from being largely on positive X-plain to negative X plain (this is considering the overall trajectories given in Figure 5.8-(a)). In a system with no-IBRs, this is analogous to changing the ratio of local to remote source voltage magnitudes from a value greater than 1.0 to smaller than 1.0. From Figure 5.8-(b), it can be seen that current injection altered the path of the impedance trajectory when $\delta \approx 180^0$.

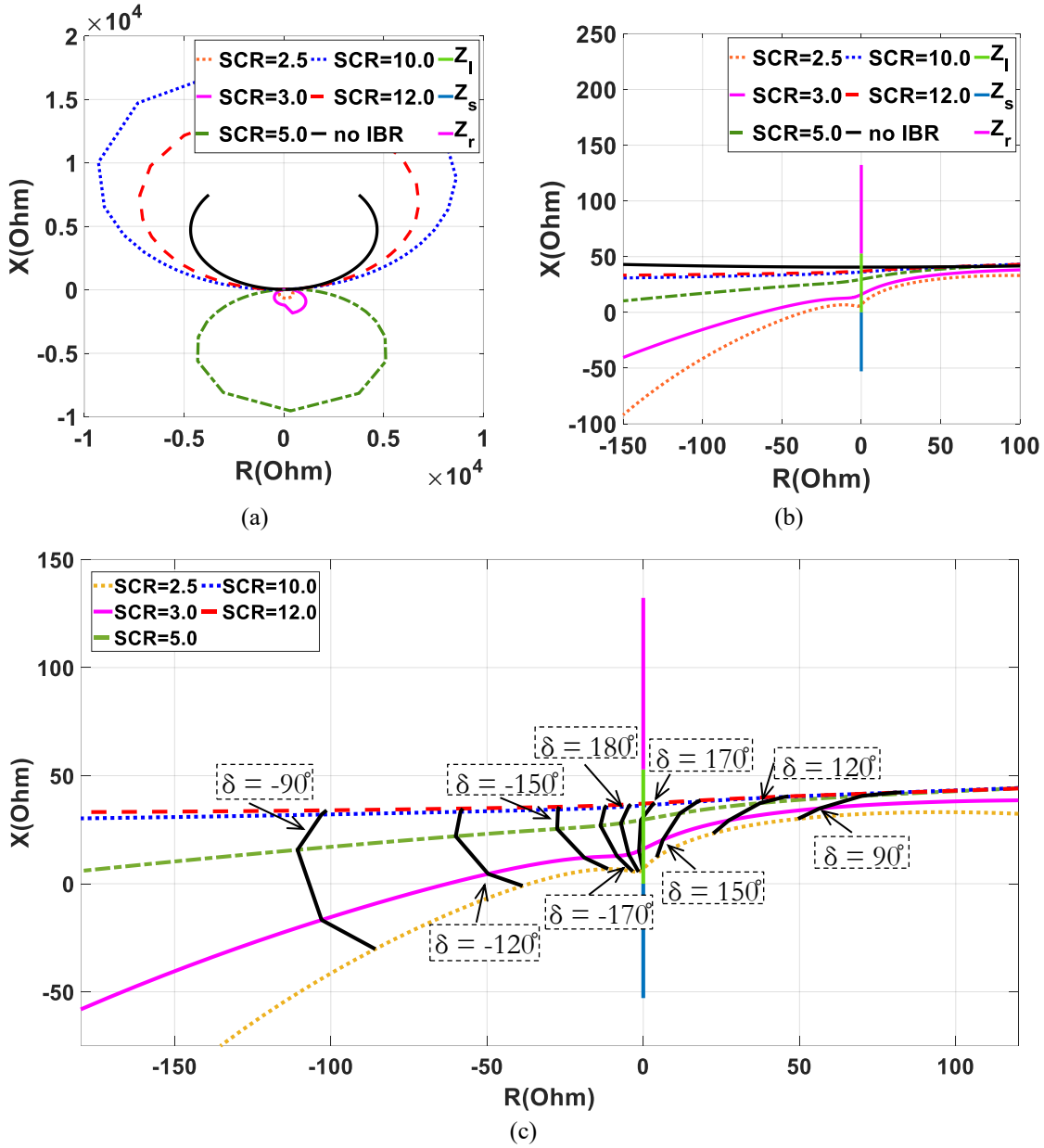

Figure 5.8 (a) Swing impedance trajectories for different SCR values, (b) magnified plot with respective line impedance for Z_s, Z_l and Z_r, (c) variation of δ

Figure 5.9 presents 3-dimensional plots (on a R, X, δ space) of swing impedance trajectories plotted with δ for different SCR values. Here, δ is wrapped between [-180^0, 180^0]. It can be seen from data points correspond to δ (z) ≈ 180^0 that there is a non-zero real part (i.e. a resistive part) in the apparent impedance when there is a non-zero current injection

(theoretically, apparent impedance is purely inductive when $\delta = 180^0$ in no-IBR case). Furthermore, the lower the SCR, the higher the deviation of the trajectories from the no-IBR case.

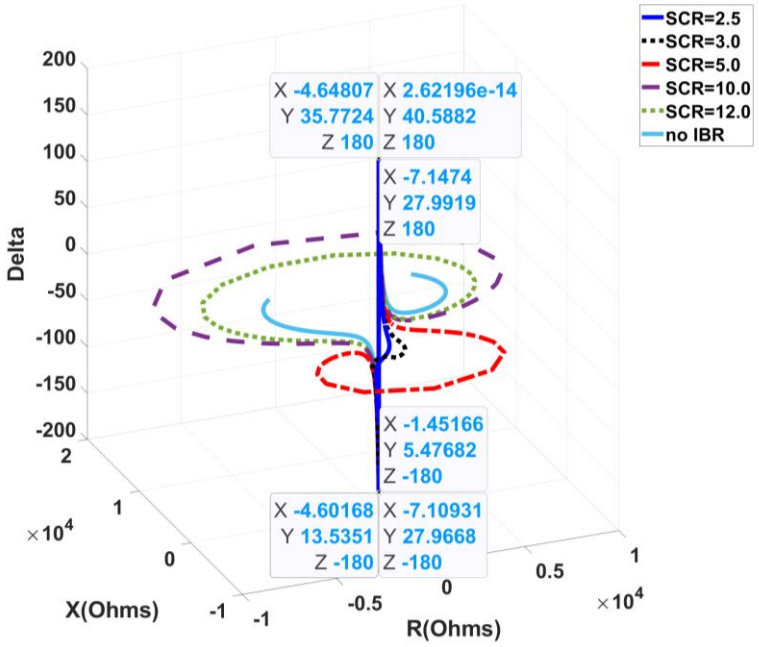

Figure 5.9 (a) Swing impedance trajectories plotted with δ for different SCR values; data points correspond to δ=180⁰

5.4.3 Impact of IBR Active Power Output

Swing impedance trajectories of the system for different active power injections to simulate the intermittency of a typical IBR are given in Figure 5.10. All other system parameters except IBR current injection were kept unchanged from the base-case. Results presented are for 10%, 30% 50% and 100% active power injection and 100% corresponds to the current injection in the base-case. It was observed that while the change of active power injection altered the trajectory of the apparent impedance for lower values of δ ($\delta \approx 0^0$), its effect on the trajectory was relatively small in the $\delta \approx 180^0$ region.

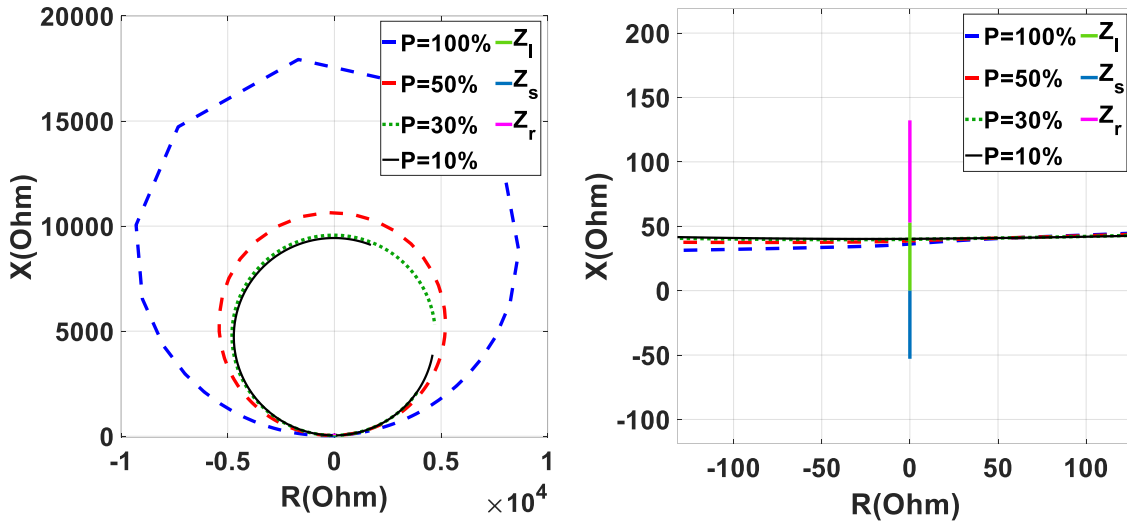

(a) (b)

Figure 5.10 (a) Swing impedance trajectories for different active power injection, (b) magnified plot with respective line impedances for Z_s, Z_l and Z_r

5.4.4 Impact of Source Voltage Magnitudes

Plotted in Figure 5.11 are swing impedance trajectories of the system for different magnitudes of source voltages. The parameter ***k*** is the magnitude ratio of the local and remote voltage sources (each of these equivalents represent two conventional power systems). It was observed that, for cases where $k \geq 1.01$, the trajectories were in the positive X-plain and those where $k < 1.01$ were inverted (in the negative X-plain). It is understood that $k = 1.0$ is the boundary case for conventional systems (without an IBR). Observing these results, it can be stated that current injection from the IBR in this system has an effect similar to decreasing the value of k in a conventional system without IBRs.

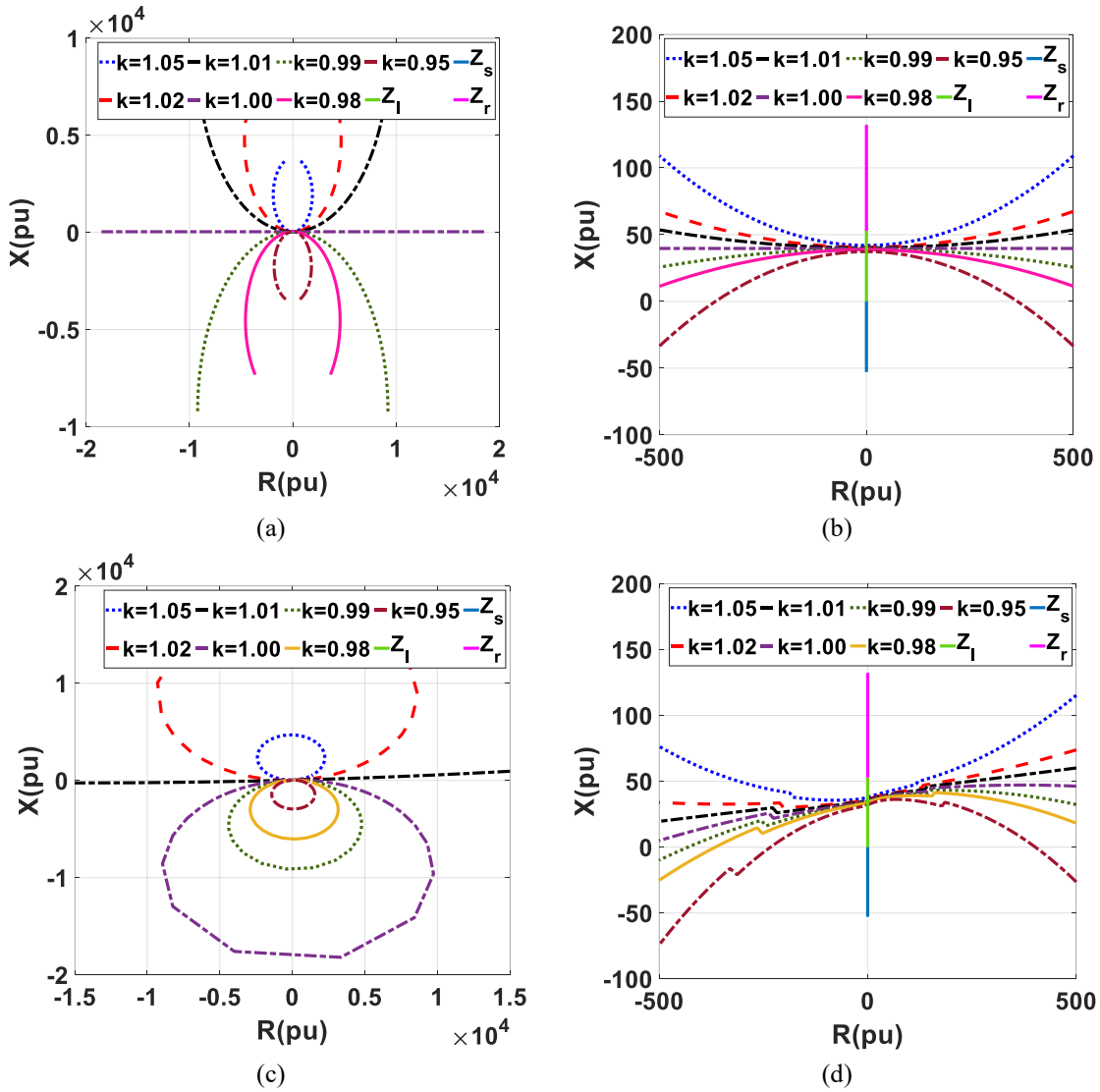

Figure 5.11 Swing impedance trajectories for different source voltage magnitudes (a) no IBR, (b) magnified plot of (a), (c) base-case IBR, and (d) magnified plot of (c)

5.4.5 Impact of Current Injection during Voltage Ride-Through

Most modern IBRs are required to inject reactive current during voltage excursions (i.e. VRT operation) as a performance requirement. Swing impedance trajectories of the system for different levels of (positive-sequence) reactive current injections during VRT operation are plotted in Figure 5.12. The settable parameter K_{VRT} is the ratio between the per-

unitized (positive-sequence) reactive current and per-unitized (positive-sequence) voltage deviation at the POI (represents the current injection characteristic). Here, VRT operation is triggered when the voltage deviation is greater than a set threshold (∓10%). One can seen from Figure 5.12-(a) that all three characteristics are identical except for the period where the VRT operation is being activated. Here, the three trajectories deviate from one another marginally due to differences of the phase angle of the injected current during VRT operation (magnitude remains at 1.0 pu). As expected, this occurs in the valley of the voltage envelop when its magnitude drops below the VRT threshold, which occurs as δ approaches 180^0.

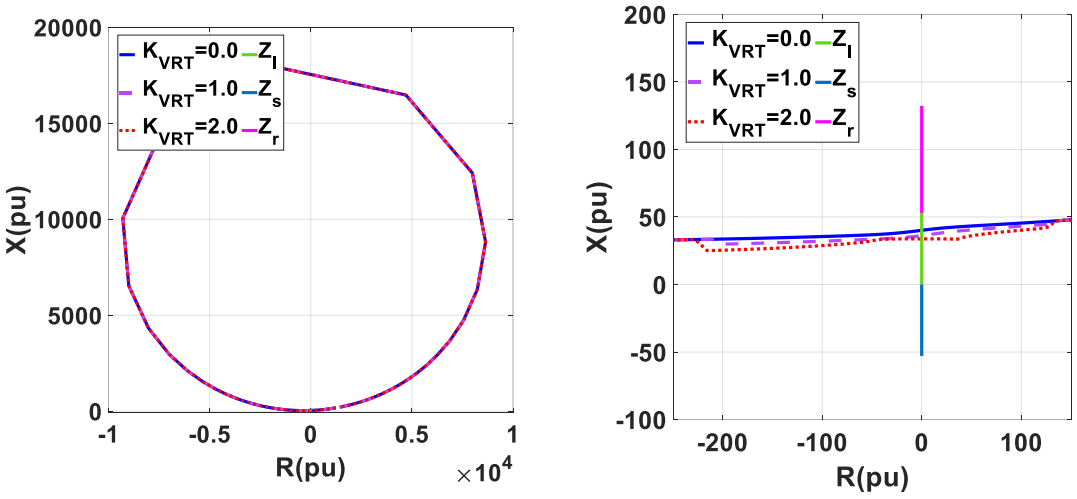

(a) (b)

Figure 5.12 (a) Swing impedance trajectories for different levels of reactive current injection during VRT, (b) magnified plot with respective line impedances for Z_s, Z_l and Z_r

5.4.6 Impact of IBR Type

Figure 5.13 compares swing impedance trajectories of the system for different types of IBR. Results presented are for a renewable energy based IBR (where injection of active power is prioritized), a BESS in charging mode (where absorption of active power is

prioritized) and a STATCOM (where injection of leading reactive power is prioritized). In this exercise, all IBRs were set to have the same current injection capacity.

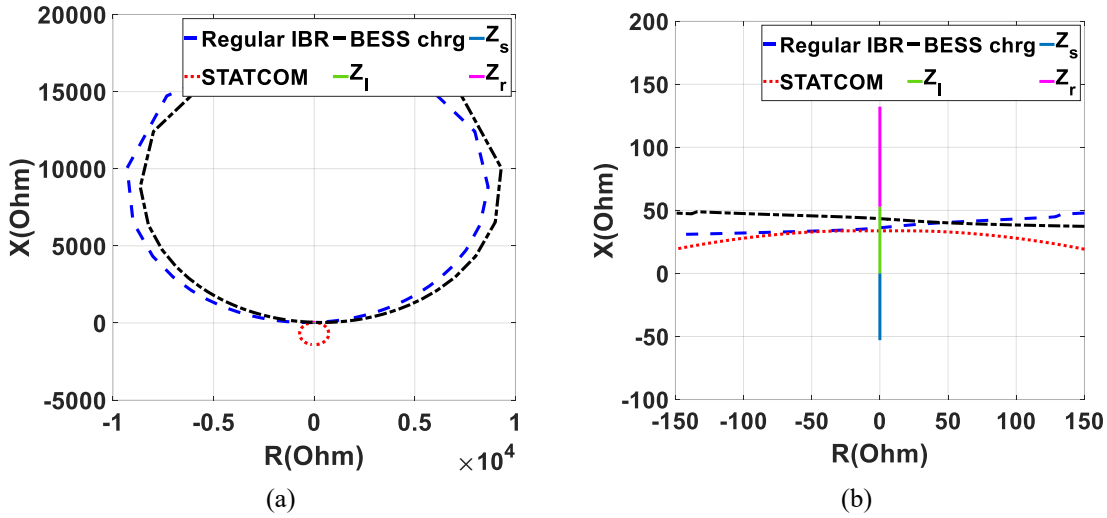

Figure 5.13 (a) Swing impedance trajectories for different IBR types, (b) magnified plot with respective line impedances for Z_s, Z_l and Z_r

It should be mentioned that the regular IBR and BESS cases had the base-case scenario VRT current injection. On the other hand, the STATCOM only had reactive current injection (no VRT mode operation). As seen from Figure 5.13, while the three trajectories did not differ substantially in the region near $\delta \approx 180^0$, the overall swing impedance trajectory for the STATCOM was markedly different (smaller and inverted on the x-axis) from other IRB types.

5.4.7 Impact of System Impedances

In tests carried out in this subsection, the swing impedance trajectories for a different combination system impedance were analyzed. The line impedance, Z_l and remote source impedance, Z_r were selected to be j0.075 pu and j0.05 pu, respectively. The local source impedance, Z_S was changed in each test and set to a different value varying between j0.05 pu and

j0.25 pu (all per-unit values are in 230 kV and 100 MVA base). The current injection from the IBR was set to a value equivalent to a system SCR of 5.0 in all test cases. Figure 5.14 presents the swing impedance trajectories for a different combination system impedance.

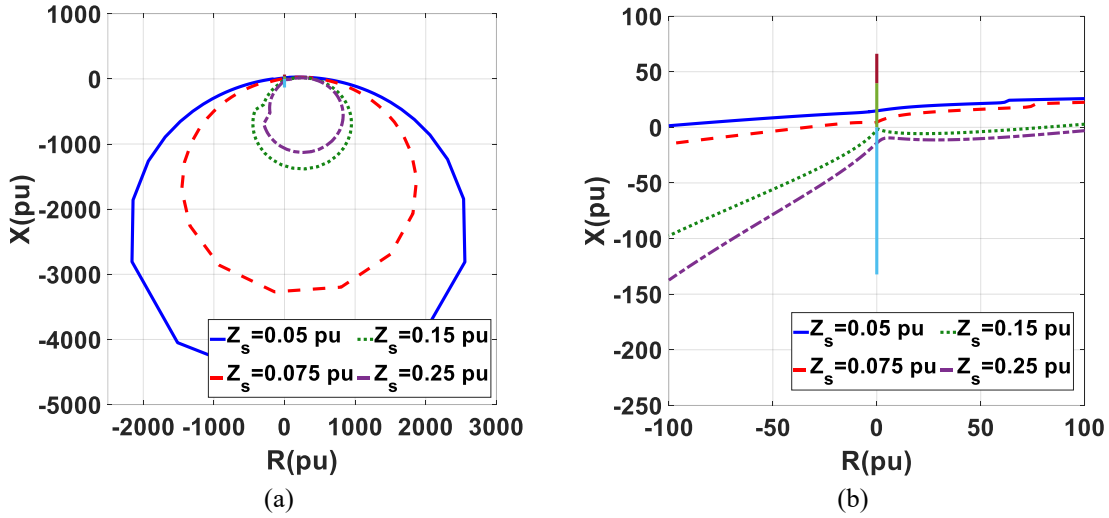

(a) (b)

Figure 5.14 (a) Swing impedance trajectories for different source impedances, (b) magnified plot with respective line impedances for Z_s, Z_l and Z_r

This test was carried out to examine the effects of the AC system parameters on the swing impedance trajectories. It is important to note that the source impedances are directly correlated to respective system strengths and the line impedance to its length. Moreover, varying Z_S with respect to Z_l can also be regarded as changing the Source-to-Impedance-Ratio (SIR, i.e. the ratio of the source impedance to the line impedance) of the AC system. Accordingly, these changes correspond to different system initial conditions (such as power flow) before initiation of the power swing. In Figure 5.14-(b), it can be seen that the point at which the impedance trajectory intersects the Y(reactance)-axis (also the swing-center in these cases) shifts downwards with increment of Z_S. This, however, can be inferred from the corresponding behaviour of a conventional system (without an IBR), in which increment of Z_S pulls to swing center $[(Z_S+Z_L+Z_R)/2]$ towards the negative Y direction.

5.5 Discussion

This section provides an overall discussion on the theoretical derivations and results obtained using them presents in earlier in this work, focusing on the insights gathered, their applicability and limitations.

5.5.1 Interpretation of Results

Observing the expression given in (5-20) for the apparent impedance, which is a rearranged form of (5-6a), one can notice that the current injection from the IBR appears in only one of the terms in the equation.

$$Z_{Relay} = \frac{(E_s + Z_S.I_W)}{I_L} - Z_S = \frac{(E_s + Z_S.I_W).(Z_L + Z_R + Z_S)}{(E_s - E_R) + I_W.Z_S} - Z_S$$
$$Z_{Relay} = \frac{\{|E_s|\angle\delta + |I_W|\angle(\theta+\beta).j|Z_S|\}.\{j|Z_L| + j|Z_R| + j|Z_S|\}}{(|E_s|\angle\delta - |E_R|\angle 0) + |I_W|\angle(\theta+\beta).j|Z_S|} \quad (5\text{-}19)$$

$$Z_{Relay} = \frac{(Z_L + Z_R + Z_S)}{[1 - E_R/(E_s + Z_S.I_W)]} - Z_S$$
$$Z_{Relay} = \frac{(j|Z_L| + j|Z_R| + j|Z_S|)}{[1 - |E_R|\angle 0/\{|E_s|\angle\delta + |I_W|\angle(\theta+\beta).j|Z_S|\}]} - j|Z_S| \quad (5\text{-}20)$$

When the base-case IBR current injection (at SCR 10.0) scenario is considered, it can be noticed that the term $I_w.Z_s$ is considerably smaller than E_s (i.e. $I_w.Z_s << E_s$) around $\delta \approx 180^0$. To illustrate this point, if we consider the $\delta = 180^0$ case, the value of the term $I_w.Z_s$ is $0.14\angle -79.75°$, whereas $E_s = -1.02\ pu$ ($|I_W| = 1.4\ pu,\ Z_S = 0.1j\ pu,\ E_s\angle 180° \approx -|E_s| = -1.02\ pu$). Consequently, it can be reasoned that the impact of the IBR current injection, I_w, is less significant in the region near $\delta \approx 180^0$. Conversely, examination of (5-19) indicates that when δ is small (in the region near $\delta \approx 0^0$), the value of the term $I_w.Z_s$ becomes comparable with the value of

the term ($E_S - E_R$) as the two voltage phasors E_S and E_R are now essentially in-phase (and roughly similar in magnitude), cancelling out each other.

A strong example of this eventuality can be seen in Figure 5.7 where two swing impedance trajectories for no-IBR and with-IBR cases are compared. As observed, deviation between the two trajectories is far greater in the region near $\delta \approx 0^{\circ}$ (when δ is small), as opposed to higher values of δ, where the two trajectories are much more aligned. This phenomenon is plainly evident in most of the other results presented in above Section 5.4 as well.

5.5.2 Implications to Power System Protection

It can be reasoned based on the discussion presented in above subsection 5.5.1 that the impact of an IBR on impedance-based power swing protection is insignificant as it does not considerably alter swing impedance trajectories seen by a relay at higher values of δ (poles slip), where power swing protection is applicable. However, closer inspection of results for lower SCR scenarios (or higher relative current injections) indicates that the presence of IBRs may alter the swing impedance trajectories considerably even at higher values of δ. For systems with low SCR IBR integration, this effect may be required to be taken into consideration when setting blinders for power swing blocking (PSB) and out-of-step tripping (OST).

In Figure 5.15, swing impedance trajectories for SCR=2.5 are plotted with respective impedances Z_s, Z_l, Z_r, and a set of prospective inner and outer OOS protection blinders. For example, due to the asymmetry of the trajectory on Y-axis (reactance axis), it may be required to set right and left blinders at different distances as opposed to setting them at the same distance on either side in a conventional manner.

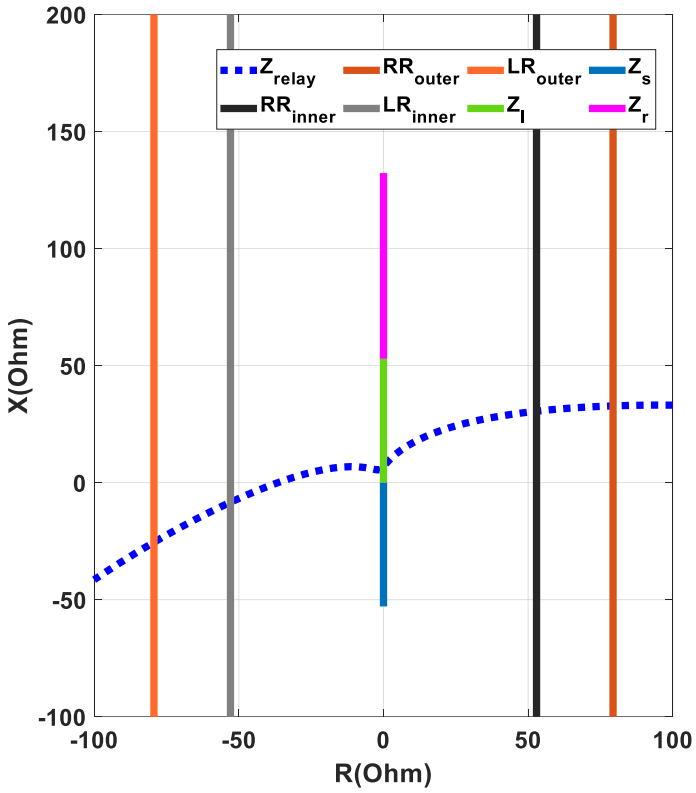

Figure 5.15 Swing impedance trajectories for SCR=2.5 plotted with respective line impedance for Z_s, Z_l, Z_r, and inner and outer PSB and OST blinders

Moreover, real-world relays that estimate the impedance using a signal processing algorithm such as DFT, will see the trajectory similar to those obtained with EMT simulations. Therefore, the impact of delay and errors due to phasor extraction under continuously varying off-nominal frequency (for systems with and without IBRs) must be taken into consideration. However, such errors and delays may be more consequential for systems with IBRs as swing impedances in such systems move faster (due to reduced system inertia), affording less margin for error.

5.5.3 Benefits and Limitations of the Proposed Theoretical Model

The work presented in this chapter amends the well-known analysis of power swing protection (established for synchronous-machine based systems [6], [75]) to incorporate IBRs. Using the presented theoretical derivations, the behavior of power swing impedance trajectories in a system with IBRs can be estimated with a limited effort (and in a way comparable to that of a conventional power system). Usually, real-world power swing protection schemes are configured by performing detailed dynamic simulations considering a variety of system conditions, configurations and contingencies [75]. For understandable reasons, detailed dynamic simulations, such as those performed in an EMT tool, produce more accurate results than a simplified theoretical model similar to the one presented in this work. However, conducting such simulation studies is resource intensive and can produce results that are convoluted and difficult to interpret on their own. The theoretical model proposed in this work offers a generic, easy-to-execute tool that can be used to initialize the settings of a power swing protection scheme (for example, blinder settings) without the need for complicated modelling of the power system (including the IBR). Results produced by this model can then be verified by conducting more complex and detailed dynamic simulations, as necessary. This model is also beneficial for preliminary studies, where only a general idea of the behavior of swing trajectories is needed, and can also be used to interpret (or troubleshoot) results from more detailed dynamic simulations.

This method, therefore, offers a convenient and familiar means to integrate IBRs into out-of-step protection and relaying, which improves design and performance of power system protection consequently. The proposed method also provided a vital point of reference against

which results from more detailed simulation can be compared (which was largely absent at the time of this research). It is based on few fundamental and well-established assumptions and developed in a generic manner. Its adaptation is straightforward and can be implemented using any modern computer coding platform with basic mathematical capabilities.

Finally, it is imperative to reaffirm that this work is primarily carried out in phasor-domain hence, it has no notion of time (for instance, the speed at which the trajectories move on the R-X plain). The entire purpose if this work is to explore the effects of IBRs on electrical (swing impedance) trajectories on the R-X plain. It is intended to be used to examine the behavior swing impedance trajectories with variation of δ (the phase angle separation between the two equivalent systems during the swing). It is vitally important to note that this model is not designed to be used to study any time-varying behavior in its current form. Furthermore, as established in this work, the effects of measurement errors, signal processing can potentially cause discrepancies between the behavior estimated by this model and that of the real power system. Minor inconsistencies between theoretically predicted behaviour and the real-world power system may also be observed due to various system dynamics not considered in the development of this model.

5.6 Concluding Remarks

This chapter presented a theoretical method for investigating impedance trajectories during power swings in the presence of IBRs based on a similar approach as the well-established analysis of power swing protection of conventional systems. Different operational and system conditions were investigated during the work and a selected set of results were presented. In addition, the premise of proposed theoretical analysis was also validated by EMT simulations. A general assessment on the findings of this work including their implications to power system protection was presented, and benefits and limitations of the proposed model were discussed.

Based on the finding of the work, it can be reasoned that (grid-following) IBRs do not alter the swing impedance trajectories significantly enough to impact the OOS protection (blinder setting etc.) in most cases. However, in low SCR system conditions, the effects of IBRs on swing trajectories may need to be taken into consideration for protection applications. The proposed method of analysis has merit in determining the effect of IBRs on swing impedance trajectories and can be easily incorporated into investigations of phasor-based relay setting for application of power swing protection.

Chapter 6

Conclusions and Contributions

This chapter presents high-level conclusions of the research work presented in this Thesis, summarizes its main contributions, and proposes directions for potential future research in relevant areas of work.

6.1 Conclusions

This Thesis presented an investigation of power system protection issues caused by integration of IBRs into modern power systems. Among several potential research gaps identified, three were explored in detail, which are (i) analyzing the impact of IBRs on conventional faulted phase identification algorithms and developing improved solutions, (ii) investigating the effect of IBRs on conventional fault direction identification and developing an enhanced method and, (iii) studying the effects of IBRs on power swing impedance trajectories using theoretical analysis and investigating potential impacts on power swing protection.

Chapter 2 presented a detailed review of exiting literature on the three topics selected as main research themes for this Thesis. This review underlined real-world challenges, explored relevant work existing in literature and identified potential research gaps. In addition, a review of the overall system protection of a system with IBRs was also provided for context.

6.1 Conclusions

The research gaps identified under the three main research topics discussed in Chapter 2 were individually investigated and improved solutions were proposed when applicable, in Chapters 3, 4 and 5, respectively.

Using both theoretical analysis and simulation results, Chapter 3 examined the expected performance of conventional phasor-based faulted phase identification methods implemented in contemporary commercial protection relays in systems with high penetration of IBRs. Furthermore, results obtained in simulations were further validated by testing commercial line protection relays using a hardware-in-the-loop setup. The test results of commercial relays showed that conventional phasor-based faulted phase identification methods fared poorly when fed entirely by IBR-generated fault currents, which also agreed with simulation studies. This work also carried out a basic evaluation of the recently proposed transient quantities-based faulted phase identification techniques, which produced more accurate results in the presence of IBRs.

As part of an attempt to design an improved phase identification technique, effectiveness of using incremental voltages for faulted phase identification was evaluated using theoretical analysis of circuit equations. Based on the theoretical analysis, Chapter 3 also proposed a faulted phase identification method based on the integrals of the incremental voltages. Performance of the proposed method was evaluated for different operational and system conditions using extensive EMT simulations. The results presented indicated that the proposed method of faulted phase identification performed well in systems with IBRs as well as conventional sources under variety of system conditions.

6.1 Conclusions

Listed below are the most significant and specific research deductions drawn from the work covered in Chapter 3.

- Conventional phasor-based faulted phase identification methods are adversely affected when operating entirely on IBR-generated fault currents. Performance improves and becomes reliable with approximately 20% of the fault current from synchronous machines.
- Theoretical analysis of incremental voltages revealed that incremental voltages waveforms seen at the relaying location for LLG faults are out-of-phase, and their relative phase angles are also dependent on system impedances, whereas those for LG and LL faults have predictable and district phase angle relationships.
- Sensitivity of LLG faults to fault inception angle and system impedances make their discrimination significantly more difficult than other fault types in comparison. This also renders single-point measurements (such as a peak) ineffective and demands the use of a time-averaged measurement (such as an integral) to capture the relative strength of incremental voltages.
- Integrals of incremental voltages display a unique pattern for each type of faults, which can be converted into a lookup table of set of indices defined as ratios of these integrals. These indices can then be used for faulted phase identification.
- The precisely set half-cycle integration period is vital to reduce the sensitivity (fluctuation of the indices) to fault inception angle and a critical component of the entire algorithm.

6.1 Conclusions

Chapter 4 studied the challenges relevant to fault direction identification in systems with IBRs. Firstly, it evaluated the effects of IBRs on conventional direction identification methods using simulation studies. Having recognized that fault direction identification is one of the commonly affected protection functions in the presence of IBRs, Chapter 4 proposed a novel algorithm to correctly identify fault direction using negative-sequence admittance measurements. Firstly, theoretical premise of the algorithm was established, which was validated by extensive EMT simulations. Results presented in this chapter suggested that the proposed technique operated appreciably well under a variety of conditions and configurations. The salient feature of the proposed method is that it is based only on the magnitude of measurements, as opposed to both magnitude and phase angle as most of the existing techniques do. The analysis recommended a forward reach setting of 10-25% of the magnitude of the equivalent negative-sequence admittance of the remote end AC system to achieve effective discrimination. The proposed technique was validated to be robust and reliable, and yielded better results in comparison to conversional techniques in the presence of IBRs. Attributes of a fault such as location, fault impedance, inception angle and fault type have had little to no effect on the operation of the proposed method. In addition, its operation is simple and can be conveniently incorporated into a modern digital relay.

A few important limitations of the proposed method were also highlighted in Chapter 4. Firstly, this method is effective only if the (equivalent or apparent) negative-sequence impedances either side of the line relay (i.e. line and source side) are different in magnitude, at least to a certain degree. This is, however, a common configuration in which IBRs are connected to existing grids, making the proposed methods applicable in most cases. Additionally,

the effectiveness of the proposed method, to a certain extent, also depends on the level of negative-sequence current suppression by IBRs. As established earlier in the Thesis, most existing IBRs in real-world do suppress negative-sequence currents and, even the ones that do not may not response fast enough or reliably enough to be relied upon for primary transmission level system protection functions.

What follows is a list of the most significant and specific research conclusions drawn from the work presented in Chapter 4.

- Conventional direction identification methods relying on the phase angle relationship of negative-sequence quantities (in some way, shape or form) are prone to yield inaccurate and unreliable results in systems with heavy IBR penetration.
- In most practical scenarios, the apparent magnitude of the negative-sequence admittance observed by a line relay during forward and reverse faults are significantly different and can be exploited to determine fault direction.

In Chapter 5, a theoretical method of investigating impedance trajectories during power swings in the presence of IBRs was presented. The work presented in this chapter incorporated IBRs into the well-known analysis of power swing protection established for synchronous-machine based systems. Using the proposed theoretical derivations, the behavior of power swing impedance trajectories in a system with IBRs can be approximated with a little effort, and in a manner comparable to that of a conventional power system. As shown in Chapter 5, the theoretical model proposed offers a generic, easy-to-execute tool that can be used to set initial settings of a power swing protection scheme (for example, blinder settings) without the need for complicated modelling of the power system (including the IBR).

Depending on the application, results produced by this model can then be verified by conducting more accurate dynamic simulations. This model is helpful for simplified studies, where only an overall idea of the behavior of swing trajectories is required. In addition, it may also be useful to interpret (or troubleshoot) results from more detailed dynamic simulations. Different operational and system conditions were investigated during the work and a selected set of results were presented. Furthermore, the premise of proposed theoretical analysis was also validated by EMT simulations.

Findings of this work suggested that (grid-following) IBRs do not alter the swing impedance (electrical) trajectories significantly enough to impact OOS protection (blinder setting etc.) in most cases. However, in low SCR system conditions, the effects of IBRs on swing trajectories may need to be taken into consideration for protection applications. The proposed method of analysis has merit in determining the effect of IBRs on swing impedance trajectories and can be easily incorporated into investigations of phasor-based relay setting for application of power swing protection. However, it is imperative to state that this model, in its current form, is not designed to be used to study any time-varying behavior. As demonstrated in Chapter 5, the effects of measurement errors, signal processing and various system dynamics not considered in the development can potentially cause disagreements between the behavior predicted by this model and that of the real power system.

6.1 Conclusions

The most significant deductions drawn from the research covered in Chapter 5 are given below.

- The classical theoretical analysis of power swing protection established for synchronous-machine based systems can be extended to incorporate IBRs to evaluate the effects of IBRs on the power swing impedance trajectories.
- Grid-following IBRs do not alter the swing impedance trajectories meaningfully to influence OOS protection in most cases, except for certain low-SCR system conditions. In low SCR systems, the effects of IBRs on swing trajectories may need to be taken into consideration for protection applications.

6.2 Contributions

Given below is a list of main contributions of the research work presented in this Thesis:

- Validation of theoretical explanations and demonstration of deficiencies of conventional faulted phase identification algorithms in the presence of IBRs through simulations. At the time of this research, the extent of the issues caused by IBRs on faulted phase identification was not fully understood, although there was a theoretical understanding of the reasons behind the aforementioned problems.
- Testing and documenting the performance of commercial relays in a hardware-in-the-loop simulation setup using an EMT type digital real-time simulator to further validate the premise mentioned above.
- Providing a direct comparison of real-time performance of commercial relays and transient quantities-based protection algorithms in the presence of IBRs, leading to clear conclusions.
- Using theoretical analysis, evaluating the effectiveness of using incremental voltages for faulted phase identification. Such theoretical analysis is vital for understanding critical sensitivities and designing protection systems with wider applicability.
- Development of an effective faulted phase identification method based on integrated incremental voltages for systems with high IBR penetration based on the aforementioned theoretical analysis. Results presented indicated that the proposed method of faulted phase identification performed well in systems with IBRs as well as conventional sources under variety of system conditions.

- Development of a novel negative-sequence admittance-based fault direction identification algorithm that is designed to provide reliable results in systems with high IBR penetration. The proposed method is easy to configure and works well for transmission lines fed by an IBR(s), or in a system with weak synchronous infeed. In addition, it can be conveniently implemented on a modern digital relaying platform.
- Development of a theoretical model to investigate the effects of IBRs on power swing impedance trajectories using a generic circuit equivalent, without resorting to complex dynamic modeling. Consistent with analysis of traditional power swing protection, which is generally carried out using simplified system equivalents represented in phasor-domain, the presented theoretical model has incorporated IBRs into this type of simple analysis. The proposed method also provided a vital point of reference against which results from more detailed simulations can be compared.
- Examining and documenting the impact of potential changes to swing impedance trajectories in system with IBRs under variety of conditions (using the theoretical model above), and its effect on traditional power swing protection.
- Development of a fault detection method, where instantaneous power measurements are decomposed and analysed, especially suited for systems with high IBR penetration (as presented in Appendix A).

6.3 Future Work

This Thesis recognizes the following as suggestions for future research in this area.

Faulted phase identification

- Investigate the possibility of distinguishing ground faults from ungrounded faults using the phase angle relationship between incremental voltages. Theriacal derivations presented in Chapter 3 provided clear insights of this possibility, therefore, further investigation of this using simulation is warranted.

Faulted direction identification

- The proposed algorithm has a limitation in that it requires the negative-sequence impedances on either side of the line relay (i.e. line and source side) to be different in magnitude. This may be restricting its applicability in weak AC grids and in protecting AC islands, where both ends of a transmission line may be connected to IBRs. Therefore, it is worthwhile to investigate potential solutions for this shortcoming. In addition, future power systems may contain a significantly higher concentration of IBRs, most of which will likely be in grid-forming operation. Investigating applicability of the proposed method in such inverter-dominated transmission systems and finding possible improvements is an interesting and important future task.

Swing impedance trajectories

- Further investigate the effects of signal processing in relays (phasor extraction, filtering etc.) on the observed swing impedance trajectories, and possibility of adding a correction for these mismatches.

- The work on swing impedance trajectories has assumed that the IBR under investigation is in grid-following mode. It may be interesting to investigate if grid-forming operation of IBRs warrant additional modifications to the analysis.

Overall system protection

- The work presented in this Thesis primarily investigated individual power system protection functions such as faulted phase identification, directionality and fault detection. However, evaluating the performance of overall system protection by developing a comprehensive case-study and implementing a complete protection scheme in a holistic manner may produce important results and new insights.
- Evaluate existing backup protection options and investigate potential for improvements. Evaluate the applicability of the improved protection techniques suggested in above chapters for local backup protection.
- Some AC transmission systems contain AC islands, in which a radial transmission system is usually connected to IBRs (or/and HVDC links) at both of its ends. Offshore wind farm systems often contain such transmission configurations, where the only sources connected are power electronic converters and IBRs. This type of complex systems also contains IBRs in grid-following as well in as grid-forming operation. Protecting such transmission lines is uniquely challenging, even more so than conventional integration of IBRs, hence a thorough investigation is warranted.

Bibliography

[1] H. Ritchie and P. Rosado (2024) - "*Electricity Mix*" Published online at OurWorldInData.org. Retrieved from: 'https://ourworldindata.org/electricity-mix' [Online Resource]

[2] "*Renewables 2025*", International Energy Agency, Paris, France, 2025 [Online]. Available: 'https://www.iea.org/reports/renewables-2025'.

[3] *IEEE Standard for Interconnection and Interoperability of Inverter-Based Resources (IBRs) Interconnecting with Associated Transmission Electric Power Systems*, IEEE Standard 2800-2022.

[4] IEEE Power System Relaying and Control Committee Report of Working Group C32 of the System Protection Subcommittee, "*Protection Challenges and Practices for Interconnecting Inverter Based Resources to Utility Transmission Systems*" Sep. 2020.

[5] IEEE Power System Relaying and Control Committee Report of Working Group C24 of the System Protection Subcommittee, "*Modification of commercial fault calculation programs for wind turbine generators*" July. 2020.

[6] S. H. Horowitz and A. G. Phadke, *Power System Relaying*, 4th edition, Wiley, January 2014.

[7] J. Lewis Blackburn and Thomas J. Domin, *Protective Relaying: Principles and Applications*, 4th Edition, CRC Press, Feb. 2014.

[8] P. S. Kundur and O. P. Malik, *Power System Stability and Control,* 2nd Edition, McGraw Hill, 2022.

[9] NERC, "*1,200 MW Fault Induced Solar Photovoltaic Resource Interruption Disturbance Report*," June 2017.

[10] NERC, "*900 MW Fault Induced Solar Photovoltaic Resource Interruption Disturbance Report*," February 2018.

[11] NERC, "*April and May 2018 Fault Induced Solar Photovoltaic Resource Interruption Disturbances Report*," January 2019.

[12] V. Telukunta, J. Pradhan, A. Agrawal, M. Singh and S. G. Srivani, "*Protection challenges under bulk penetration of renewable energy resources in power systems: A review,*" in CSEE Journal of Power and Energy Systems, vol. 3, no. 4, pp. 365-379, Dec. 2017.

[13] M. Nagpal and C. Henville, "Impact of Power-Electronic Sources on Transmission Line Ground Fault Protection," in *IEEE Transactions on Power Delivery*, vol. 33, no. 1, pp. 62-70, Feb. 2018.

[14] J.C. Quispe and E. Orduña, "Transmission line protection challenges influenced by inverter-based resources: a review," in Prot. Control Mod Power Syst 7, 28 (2022).

[15] EPRI White Paper "*Impact of Inverter-Based Resources on Protection Schemes Based on Negative Sequence Components*", July 2019.

[16] R. Chowdhury and N. Fischer, "Transmission Line Protection for Systems With Inverter-Based Resources – Part I: Problems," in *IEEE Transactions on Power Delivery*, vol. 36, no. 4, pp. 2416-2425, Aug. 2021.

[17] R. Chowdhury and N. Fischer, "Transmission Line Protection for Systems With Inverter-Based Resources – Part II: Solutions," in *IEEE Transactions on Power Delivery*, vol. 36, no. 4, pp. 2426-2433, Aug. 2021.

[18] A. Haddadi, E Farantatos, I Kocar and U Karaagac, "Impact of inverter-based resources on system protection," *Energies*, vol. 14, no. 4, 2021.

[19] F. Lopes, M. Davi, M. Oleskovicz, A. Hooshyar, X. Dong and A. Neto, "Maturity Analysis of Protection Solutions for Power Systems Near Inverter-Based Resources," in *IEEE Transactions on Power Delivery*, vol. 39, no. 5, pp. 2630-2643, Oct. 2024.

[20] M. Nagpal and C. Henville, "BC hydro protection interconnection practices for sources with inverter or converter interface," in *Proceedings of the 45th Annu. Western Protective Relay Conference*, Oct. 2018.

[21] A. Hooshyar, M. Azzouz and E. El-Saadany, "Distance Protection of Lines Connected to Induction Generator-Based Wind Farms During Balanced Faults," in *IEEE Transactions on Sustainable Energy*, vol. 5, no. 4, pp. 1193-1203, Oct. 2014.

[22] Y. Fang, K. Jia, Z. Yang, Y. Li and T. Bi, "Impact of Inverter-Interfaced Renewable Energy Generators on Distance Protection and an Improved Scheme," in *IEEE Transactions on Industrial Electronics*, Sept. 2019.

[23] NERC Reliability Standard PRC-024-3, "*Frequency and Voltage Protection Settings for Generating Resources*".

[24] NERC Reliability Standard PRC-029-1, "*Frequency and Voltage Ride-through Requirements for Inverter-based Resources*".

[25] R. Teodorescu, M. Liserre and P. Rodriguez, *Grid Converters for Photovoltaic and Wind Power Systems*, Wiley-IEEE Press, 2007.

[26] A. Yazdani and R. Iravani, *Voltage-Sourced Converters in Power Systems*, Wiley-IEEE Press, 2010.

[27] E.M. Carrasco, M.P.C. Moreno, M.T.V. Martínez and S.B. Vicente, "Improved Faulted Phase Selection Algorithm for Distance Protection under High Penetration of Renewable Energies," *Energies* 2020, 13, 558.

[28] J. Keller and B. Kroposki, "*Understanding fault characteristics of inverter-based distributed energy resources*", Technical Report NREL/TP-550-46698, January 2010.

[29] A. Haddadi, M. Zhao, I. Kocar, U. Karaagac, K. W. Chan and E. Farantatos, "Impact of Inverter-Based Resources on Negative Sequence Quantities-Based Protection Elements," *IEEE Transactions on Power Delivery*, Volume 36, Issue 1, Pages 289-298, February 2021.

[30] A. Hooshyar, M. A. Azzouz and E. F. El-Saadany, "Distance Protection of Lines Emanating from Full-Scale Converter-Interfaced Renewable Energy Power Plants—Part I: Problem Statement," in *IEEE Transactions on Power Delivery*, vol. 30, no. 4, pp. 1770-1780, Aug. 2015.

[31] A. Hooshyar, M. A. Azzouz and E. F. El-Saadany, "Distance Protection of Lines Emanating from Full-Scale Converter-Interfaced Renewable Energy Power Plants—Part II: Solution Description and Evaluation," in *IEEE Transactions on Power Delivery*, vol. 30, no. 4, pp. 1781-1791, Aug. 2015.
[32] B. Chen, A. Shrestha, F. A. Ituzaro and N. Fischer, "Addressing protection challenges associated with Type 3 and Type 4 wind turbine generators," in *Proceeding of 68th Annual Conference for Protective Relay Engineers*, College Station, TX, USA, 2015.
[33] A. Alves Júnior, M. Davi, D. Jorge, D. Barbosa, M. Oleskovicz and D. Coury, "Challenges and recommendations for enhancing protection of onshore wind farm collector systems," in *Electric Power Systems Research*, Volume 250, 2026.
[34] VDE-AR-N 4130, "Technical Requirements for the Connection and Operation of Customer Installations to the Extra High Voltage Network (TCR Extra High Voltage), Nov. 2018.
[35] I. Erlich and U. Bachmann, "Grid code requirements concerning connection and operation of wind turbines in Germany," in *Proceedings of the IEEE Power Engineering Society General Meeting*, 2005, San Francisco, CA, USA, 2005.
[36] R. H. Lasseter, "Smart Distribution: Coupled Microgrids," in *Proceedings of the IEEE*, vol. 99, no. 6, pp. 1074-1082, June 2011.
[37] A. Hooshyar and R. Iravani, "Microgrid Protection," in *Proceedings of the IEEE*, vol. 105, no. 7, pp. 1332-1353, July 2017.
[38] A. A. Memon and K. Kauhaniemi, "A critical review of AC microgrid protection issues and available solutions," in *Electric Power System Research*, vol. 129, pp. 23–31, Dec. 2015.
[39] S. A. Hosseini, H. A. Abyaneh, S. H. H. Sadeghi, F. Razavi, and A. Nasiri, "An overview of microgrid protection methods and the factors involved," in *Renewable and Sustainable Energy Reviews*, vol. 64, pp. 174–186, Oct. 2016.
[40] S. Teimourzadeh, F. Aminifar, M. Davarpanah and M. Shahidehpour, "Adaptive Protection for Preserving Microgrid Security," in *IEEE Transactions on Smart Grid*, vol. 10, no. 1, pp. 592-600, Jan. 2019.
[41] P. Mahat, Z. Chen, B. Bak-Jensen and C. L. Bak, "A Simple Adaptive Overcurrent Protection of Distribution Systems With Distributed Generation," in *IEEE Transactions on Smart Grid*, vol. 2, no. 3, pp. 428-437, Sept. 2011.
[42] E. Price and B. Warren, "The Performance of Faulted Phase Selectors used in Transmission Line Distance Applications," in *Proceedings of the 61st Annual Conference for Protective Relay Engineers*, College Station, TX, USA, 1–3 April 2008; pp. 484–490.
[43] L-PRO 4000 Transmission Line Protection Relay, Manual, ERLPhase Power Technologies Ltd. Available online: https://www.erlphase.com/downloads/manuals/L_PRO_4000_manual.pdf (accessed on).
[44] D. Costello and K. Zimmerman, "Determining the Faulted Phase," *In Proceedings of the 36th Annual Western Protective Relay Conference*, Spokane, WA, USA, 20–22 October 2009.
[45] J. Wijekoon and A. D. Rajapakse, "Instantaneous Incremental Current-Based Faulted Phase Selection Algorithm" in *Proceedings of the International Conference on Power Systems*, Thessaloniki, Greece, Jun., 2023.
[46] "Single phase tripping and auto reclosing of transmission lines-IEEE Committee Report," in *IEEE Transactions on Power Delivery*, Jan. 1992,
[47] B. Kasztenny, B. Campbell and J. Mazereeuw, "Phase Selection for Single-Pole Tripping—Weak Infeed Conditions and Cross-Country Faults," in *Proceedings of the 27th Annual Western Protective Relay Conference*, Spokane, WA, USA, 24–26 October 2000.
[48] J. B. Roberts and E. O. Schweitzer, III, "Fault identification system for use in protective relays for power transmission lines," U.S. Patent 5 515227, May 1996.
[49] S. Kariyawasam, J. Wijekoon, and A.D. Rajapakse, "Assessment of the Performance of Phasor-Based and Transients-Based Faulted Phase Identification Techniques in the Presence of Inverter Interfaced Resources" *Energies* 16, no. 2: 640, 2023.
[50] J. Wijekoon, A. Rajapakse, N.M. Haleem, "Fast and Reliable Method for Identifying Fault Type and Faulted Phases Using Band Limited Transient Currents," in *IEEE Transactions on Power Delivery*, vol. 36, no. 5, Oct. 2021.
[51] X. Dong, W. Kong, T. Cui, "Fault Classification and Faulted-Phase Selection Based on the Initial Current Traveling Wave," in IEEE *Transactions on Power Delivery,* 2008, 24, 552–559.
[52] F. Namdari, M. Salehi, "High-Speed Protection Scheme Based on Initial Current Traveling Wave for Transmission Lines Employing Mathematical Morphology," in *IEEE Transactions on Power Delivery*, 2017, 32, 246–253.
[53] K. M. Silva, B. A. Souza and N. S. D. Brito, "Fault detection and classification in transmission lines based on wavelet transform and ANN," in *IEEE Transactions on Power Delivery*, vol. 21, no. 4, pp. 2058-2063, Oct. 2006
[54] A. Abdullah, "Ultrafast Transmission Line Fault Detection Using a DWT-Based ANN," in *IEEE Transactions on Industrial Applications*, 2017, 54, 1182–119.
[55] Z. He, L. Fu, S. Lin and Z. Bo, "Fault Detection and Classification in EHV Transmission Line Based on Wavelet Singular Entropy'" in *IEEE Transactions on Power Delivery,* 2010, 25, 2156–2163.
[56] Y. Liu, D. Xie, W. Xiao, W. Wang, Y. Zheng, "Research of fault phase selection on UHV transmission lines based on wavelet analysis," in *Proceedings of the 2016 International Conference on Smart Grid and Clean Energy Technologies*, ICSGCE 2016, Chengdu, China, 19–22 October 2016; pp. 284–289.

[57] M. Mobashsher, S. Hosseini, A. Abdoos, S. Hashemi, M. Sanaye-Pasand and M. Azzouz, "Fault Type Classification in the Presence of Inverter-Based Resources: Review, Challenges, and Future Works," in *IEEE Access*, 2025.
[58] S. Paladhi and A. Pradhan, "Adaptive Fault Type Classification for Transmission Network Connecting Converter-Interfaced Renewable Plants," in *IEEE Systems Journal*, 2020, 15, 4025–4036.
[59] G. Benmouyal and J. Mahseredjian, "A combined directional and faulted phase selector element based on incremental quantities," in *IEEE Transactions on Power Delivery*, vol. 16, no. 4, pp. 478-484, Oct. 2001.
[60] S. Huang, L. Luo and K. Cao, "A Novel Method of Ground Fault Phase Selection in Weak-Infeed Side," in *IEEE Transactions on Power Delivery*, Oct. 2014.
[61] M. T. Villen et al., "A computer-assisted Faulted Phase Selection Algorithm for dealing with the effects of Renewable Resources in Smart grids," in *Proceedings of the NEIS 2023; Conference on Sustainable Energy Supply and Energy Storage Systems*, Hamburg, Germany, 2023, pp. 192-197.
[62] M. T. Villen et al., "Faulted phase selection multicriteria algorithm implemented in generic hardware for centralized P&C in smart grids," in *International Journal of Electrical Power & Energy Systems*, Volume 155, Part A, 2024.
[63] M. J. B. B. Davi, M. Oleskovicz and F. V. Lopes, "A Novel High Sensitivity Time-Domain Fault Classifier Applied to Inverter-Based Resource Interconnection Lines," in *IEEE Access*, vol. 13, 2025.
[64] H. Samkari and B. Johnson, "Impact of Distributed Inverter-Based Resources on Incremental Quantities-Based Protection," in *Proceedings of the IEEE Power & Energy Society General Meeting (PESGM)*, Washington, DC, USA, 2021.
[65] P. G. McLaren, G. W. Swift, Z. Zhang, E. Dirks, R. P. Jayasinghe and I. Fernando, "A new directional element for numerical distance relays," in *IEEE Transactions on Power Delivery*, April 1995.
[66] A. Jalilian, M. T. Hagh and S. M. Hashemi, "An Innovative Directional Relaying Scheme Based on Postfault Current," in *IEEE Transactions on Power Delivery*, Dec. 2014.
[67] J. Tang, G. Song, and C. Wang, "Adaptability analysis of directional relays in power systems with wind farms," in *Proceedings of the 13th Int.Conf. Develop.Power Syst. Protection* 2016, Edinburgh, 2016.
[68] H. Jafarabadi Ashtiani, H. Samet, and T. Ghanbari, "Evaluation of directional relay algorithms in the presence of FCL," in *IET Science, Measurement & Technology*, vol. 11, no. 6, pp. 713–722, Sep. 2017.
[69] Q. Lai, Z. Zhang, K. Xu and X. Yin, "A New Method of Fault Direction Identification for Different Types of Renewable Energy Source Integrations," in *IEEE Transactions on Power Delivery*, Oct. 2021.
[70] S. Liangzhi, J. Kaili, J. Pi, J. Lixiao and C. Zijian, "Sequence component direction element based on power frequency variation," in *Proceedings of the E3S Web of Conferences 252*, 02083 (2021), [Online]. Available: https://www.e3s-conferences.org/articles/e3sconf/pdf/2021/28/e3sco nf _pgsge2021_0 2083.pdf
[71] K. Jia, Z. Yang, Y. Fang, T. Bi, M. Sumner, "Influence of Inverter-Interfaced Renewable Energy Generators on Directional Relay and an Improved Scheme," in *IEEE Transactions on Power Electronics*, Dec. 2019.
[72] C. Wang, G. Song, and J. Zhang, "A novel principle of directional relay for wind power integration based on model recognition in time-domain," in *Proceedings of the 2016 IEEE PES Asia-Pacific Power Energy Engineering Conference*, Xi'an, 2016.
[73] P. Adhikari and S. Brahma, "Source-Agnostic Time-Domain Directional Relay," in *IEEE Transactions on Power Delivery*, vol. 39, no. 2, pp. 1247-1258, April 2024.
[74] A. Hooshyar and R. Iravani, "A New Directional Element for Microgrid Protection," *in IEEE Transactions on Smart Grid*, Nov. 2018.
[75] "Power swing and out-of-step considerations on transmission lines," IEEE Power System Relaying and Control Committee (PSRC) Working Group WG-D6, Jul. 2005.
[76] "Protection System Response to Power Swings," NERC System Protection and Control Subcommittee, August 2013.
[77] N. Fischer, G. Benmouyal, D. Hou, D. Tziouvaras, J. Byrne-Finley, and B. Smyth, "Tutorial on Power Swing Blocking and Out-of-Step Tripping," in *Proceedings of the 39th Annual Western Protective Relay Conference*, Spokane, Washington, Oct. 2012.
[78] J. Mooney and N. Fischer, "Application Guidelines for Power Swing Detection on Transmission Systems," in *Proceedings of the 42nd Annual Minnesota Power Systems Conference*, Saint Paul, Minnesota, Nov. 2006.
[79] A. Haddadi, I. Kocar, U. Karaagac, H. Gras and E. Farantatos, "Impact of Wind Generation on Power Swing Protection," in *IEEE Transactions on Power Delivery*, vol. 34, no. 3, pp. 1118-1128, June 2019, doi: 10.1109/TPWRD.2019.2896135.
[80] A. Jalilian and D. Robinson. "Impact of Inverter-Based Resources on Transmission Line Relaying-Part II: Power Swing Protection." In *Frontiers in Electronics* 4: 1144383
[81] M. Jayamohan, S. Das and S. Brahma, "Impedance Trajectories during Stable and Unstable Power Swings in Presence of PQ Control based PV Generations," in *Proceedings of the 2023 IEEE Power & Energy Society General Meeting (PESGM)*, Orlando, FL, USA, 2023, pp. 1-5.
[82] M. Nasr and A. Hooshyar, "Power Swing in Systems with Inverter-Based Resources—Part I: Dynamic Model Development," in *IEEE Transactions on Power Delivery*, vol. 39, no. 3, pp. 1889-1902, June 2024.
[83] M. Nasr and A. Hooshyar, "Power Swing in Systems with Inverter-Based Resources—Part II: Impact on Protection Systems," in *IEEE Transactions on Power Delivery*, vol. 39, no. 3, pp. 1903-1917, June 2024.
[84] M. Jayamohan, H. Pandit, S. Das and S. Brahma, "Analysis of the impact of PLLs on stable power swings in presence of Grid Following PV," in *Electric Power Systems Research*, Volume 245, 2025.

[85] Y. Xiong, H.Wu, X. Wang, and Y. Li. "Efficacy Analysis of Power Swing Blocking and Out-of-Step Tripping Functions in Grid-Following VSC Systems," arXiv preprint arXiv:2311.05247 (2023).
[86] "IEEE Guide for Application of Digital Line Current Differential Relays Using Digital Communication," in *IEEE Std C37.243-2015*, vol., no., pp.1-72, 7 Aug. 2015.
[87] N. Perera, K. Narendra, D. Fedirchuk, R. Midence, and V. Sood, "Performance evaluation of a sub-harmonic protection relay using practical waveforms," *Proceedings of the 2012 IEEE Electrical Power and Energy Conference*, pp. 51-56.
[88] "Reader's guide to sub-synchronous resonance," in *IEEE Transactions on Power Systems*, vol. 7, no. 1, pp. 150-157, Feb. 1992.
[89] D. R. Gurusinghe, S. Kariyawasam, and D. S. Ouellette, "Protection against sub-synchronous oscillations, a relay model," in *Electric Power Systems Research*, Vol. 223, 2023.
[90] L. C. Gross, "Sub-synchronous Grid Conditions: New Event, New Problem, and New Solutions", in *Proceedings of the 37th Annual Western Protective Relay Conference*, Spokane, Washington, October 19th – 21st, 2010.
[91] Bill Fleming, "Negative-Sequence Impedance Directional Element," in *Proceedings of the 10th Annual ProTest User Group Meeting,* California, Feb. 1998.
[92] Y. Gong, Y. Xue, and B. Mehraban, "A new sub-synchronous oscillation relay for renewable generation and series compensated transmission systems," in *Proceedings of the 2015 Grid of the Future Symp*., pp. 1–10.
[93] G.D. Irwin, A.K Jindal, A.L. Isaacs. "Sub-synchronous control interactions between type 3 wind turbines and series compensated AC transmission systems", in *Proceedings of the IEEE Power and Energy Society General Meeting*, July 2011.
[94] S. Kariyawasam, J. Wijekoon, and A. Rajapakse, "Assessment of the Performance of Phasor-Based and Transients-Based Faulted Phase Identification Techniques in the Presence of Inverter Interfaced Resources," in *Energies* 16, no. 2: 640, 2023.
[95] J. Wijekoon (2024), "Improving Speed of Transmission Line Protection: Exploring the Use of Dynamic Phasors, Transients, and Incremental Components [Doctoral dissertation, University of Manitoba]", MSpace University of Manitoba Institutional Repository, Retrieved from: 'https://mspace.lib.umanitoba.ca/items/12727b90-2005-4f07-93d1-f439808f6af4' [Online Resource].
[96] IEC 61400-27-1; Wind Energy Generation—Part 27-1: Electrical Simulation Models—Generic Models. IEC: Geneva, Switzerland, 2020.
[97] Negative sequence directional element for a relay useful in protecting power transmission lines by Jeffrey B. Roberts and Edmund O. Schweitzer, III (2000, April 11) Patent CA2108443C, [Online]. Available: https://patents.google.com/patent/CA2108443C
[98] Controls Library Manual: Multi-Function Relay Elements, RSCAD help Manual, RSCAD FX version 2.1.1, 2023.

Appendix A

Fault Detection in Systems with High IBR Penetration Using Instantaneous Power Measurements

A.1 Introduction

This Appendix proposes a technique, where instantaneous power measurements are decomposed and used to detect occurrences of faults, suited for systems with high IBR penetration. The proposed method has no dependence on fault current magnitude (as is the case with many conventional fault detection algorithms), making it especially beneficial for systems with high IBR penetration. The rest of this appendix presents the formulation of the proposed algorithm, its implementation and validation through simulations and an overall discussion.

A.2 Proposed Method of Fault Detection

The proposed method of fault detection is based on the calculation of instantaneous power, determined using voltages and currents of a 3-phase power system. When instantaneous voltages and currents of a 3-phase power system are generally defined as,

$$\begin{aligned} v_a &= \sqrt{2}.V_a \sin(\omega t - \theta_a) & i_a &= \sqrt{2}.I_a \sin(\omega t - \phi_a) \\ v_b &= \sqrt{2}.V_b \sin(\omega t - \theta_b) & i_b &= \sqrt{2}.I_b \sin(\omega t - \phi_b) \\ v_c &= \sqrt{2}.V_c \sin(\omega t - \theta_c) & i_c &= \sqrt{2}.I_c \sin(\omega t - \phi_c) \end{aligned} \quad \text{(A-1)}$$

Where ω is the nominal angular frequency of the system in rad/s. The instantaneous power, p_i, of such a system can be calculated as,

$$p_i = v_a i_a + v_b i_b + v_c i_c \quad \text{(A-2)}$$

$$p_i = P_{dc} - P_2 \cos(2\omega t - \alpha) \quad \text{(A-3)}$$

where,

$$P_{dc} = V_a I_a \cos(\theta_a - \phi_a) + V_b I_b \cos(\theta_b - \phi_b) + V_c I_c \cos(\theta_c - \phi_c)$$

$$P_2 = \sqrt{P_m{}^2 + P_n{}^2}, \quad \alpha = \tan^{-1}(P_n/P_m)$$

$$P_m = [V_a I_a \cos(\theta_a + \phi_a) + V_b I_b \cos(\theta_b + \phi_b) + V_c I_c \cos(\theta_c + \phi_c)]$$

$$P_n = [V_a I_a \sin(\theta_a + \phi_a) + V_b I_b \sin(\theta_b + \phi_b) + V_c I_c \sin(\theta_c + \phi_c)]$$

As can be seen from (A-3), the instantaneous power of a 3-phase system consists of a constant component (P_{dc}) and an oscillatory component (P_2). Voltage and currents are largely balanced and symmetrical under normal operation of a power system. Therefore, it can be shown that the oscillatory components of the three phases cancel out, resulting in a constant, DC power ($p_i = P_{dc}$, $P_2 = 0$). However, when there is an imbalance in the system such as an asymmetrical fault, there is a significant presence of an oscillatory component in instantaneous power. It was observed that the frequency of this oscillatory component is twice the power system fundamental. This can be exploited to detect system faults.

This method proposes the use of a single parameter defined in (A-4) for fault detection. The proposed parameter, P_r, is defined as the ratio between the magnitude of the oscillatory component and the DC component of instantaneous power.

$$P_r = \left|\frac{P_2}{P_{dc}}\right|, \quad \text{if } \left(P_r > P_{trshld} \rightarrow \text{fault}, P_{r_dtc} = 1\right) \tag{A-4}$$

As (A-4) indicates, the ratio P_r is zero (or very small) during normal, balanced system operation since the oscillatory component, P_2, is absent in system measurements. On the other hand, there is a clear change in the value of P_r when the system experiences an asymmetry such an asymmetrical fault. Fault identification is based on a simple limit-check and, the faults can be declared when the ratio P_r is greater than a pre-set threshold value, P_{trshld}.

Overall Fault Declaration

As shown in Figure A.1, the overall fault declaration is based on two decisions; fault detection based on instantaneous power and a direction identification. Here, any suitable conventional or unconventional direction identification element can be used such as the method proposed in Chapter 4 in this Theis. Time delays can also be incorporated to these elements to enhance security.

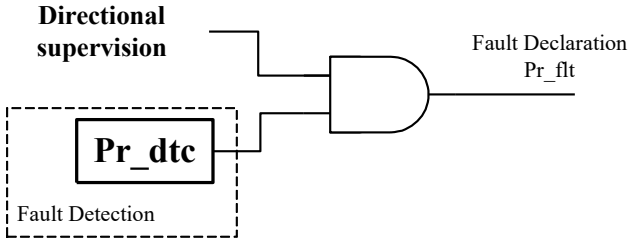

P_{r_dtc}: Fault detection from the proposed instantaneous power element

Figure A.1 Overall logic diagram

Protection Scheme with Communication

Although the proposed method works as a single-ended protection scheme, it can also be combined with a communication aided protection scheme such as a weak in-feed or directional comparison blocking scheme (for a more robust protection scheme). An example is shown in Figure A.2.

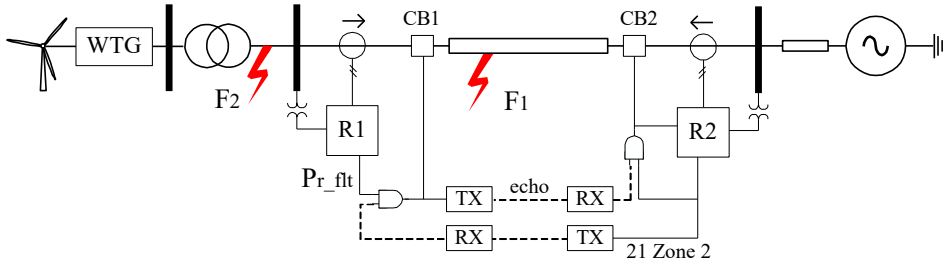

Figure A.2 An IBR connected to a remote grid via a transmission line, with communication scheme

A.3 Implementation

To test its validity, the fault detection method explained above was implemented in an EMT type DRTS. The instantaneous power element determines the ratio between the magnitude of the oscillatory component and the DC component of instantaneous power (P_i) calculated as per (A-4). As shown in Figure A.3, the DC component, P_{dc}, is extracted simply by low-pass filtering of the instantaneous power signal, P_i. The filter used is a 4^{th} order Butterworth filter with a cut-off frequency of 20 Hz. On the other hand, the same P_i signal is sent through a high-pass filter to isolate the oscillatory component. Extraction of the magnitude of the oscillatory component (P_2) is done by a Discrete Fourier Transform (DFT) calculation (at 120 Hz). In turn, the ratio of the two components can be calculated and, the 'P_r Element' declares a fault ($P_{r_dtc} \rightarrow 1$) when the magnitude of the ratio P_r exceeds a pre-set threshold.

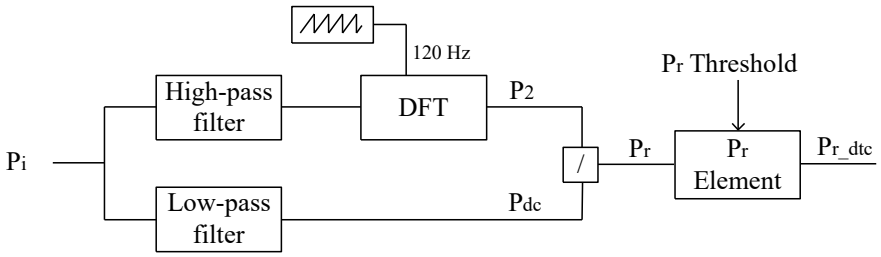

Figure A.3 Implementation of the instantaneous power element

A.4 Results

The above-presented method was tested validated by performing detailed EMT simulations using a DRTS. Figure A.4 presents the single line diagram of the test network used for these simulations. An IBR rated at 100 MW and pushes power via a short, 138 kV transmission line. The remote end of this line is connected to a 230 kV/60 Hz grid through a transformer and an adjacent transmission system. The focus this work is the protection of *Line12*, which connects the IBR to the rest of the power system. The proposed protection technique is presumably implemented in the line protection relay (R), deployed at *Bus 1* looking into *Line12*. Results presented are mainly for faults along *Line12* (forward) and on *Bus 1* (reverse).

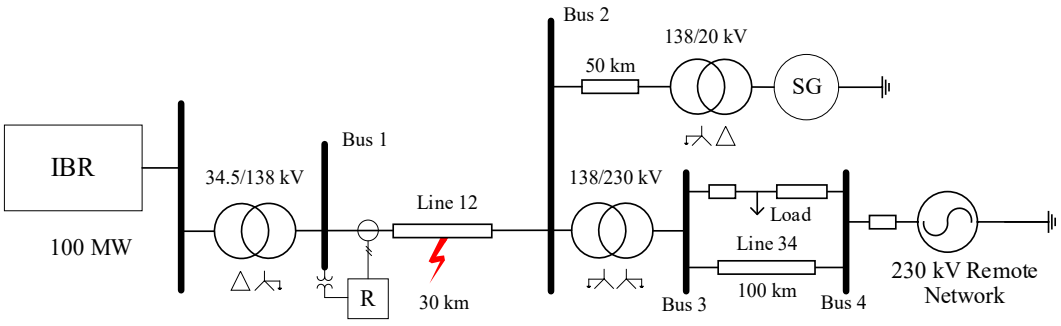

Figure A.4 Single line diagram of the test network simulated in the DRTS

Figure A.5 presents fault detection parameters for a line-line (AB) fault at 50% of *Line 12*. From Figure A.5-d, it can be observed that the ratio P_r is close to *zero* (or very small) prior to the fault, and following the fault inception, rises rapidly to value marginally above 1. Hence,

it can be reasoned that with a suitably set threshold, the value P_r can be effectively used to identify faults in this system. It is imperative to understand that the choosing a value for $P_{r_thrshld}$ represents a compromise between detection speed and protection security. In this work, the above-mentioned threshold is set to 0.3, which yields sub-cycle fault detection in most cases while also providing adequate security. In addition, a trivial directional element based on RMS current seen by the relay is used for this exercise for demonstration purposes (this can be coupled with any suitable directional identification method, however).

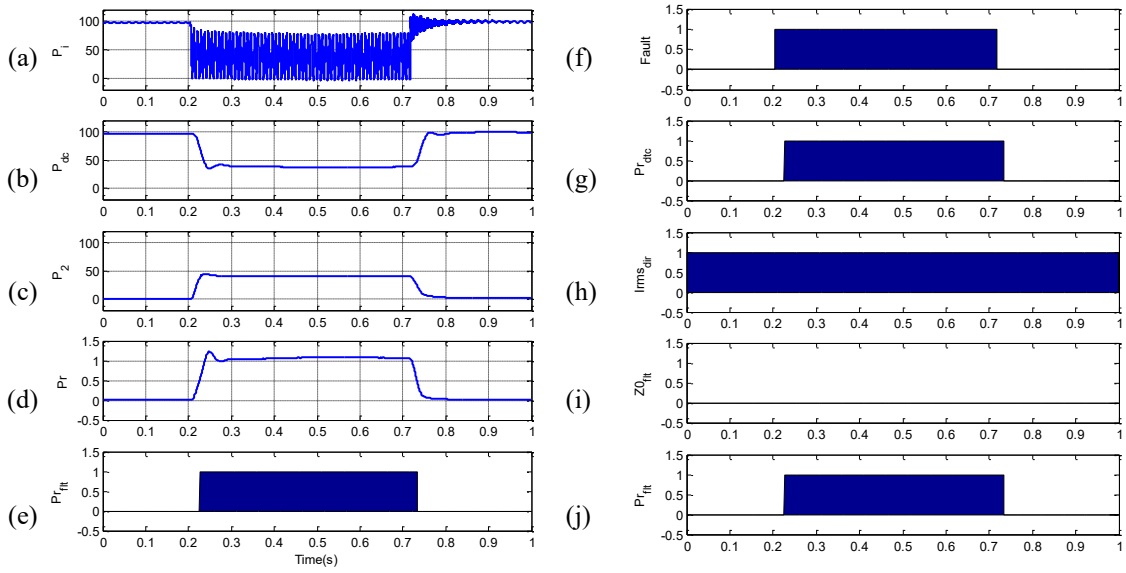

Figure A.5 Fault detection parameters for a forward line-line (AB) fault at 50% of Line 12, (a) P_i, 3-thase instantaneous power (in MW) (b) P_{dc}, DC component of P_i, (c) P_2, magnitude of the (120 Hz) oscillatory component of P_i, (d) P_r, magnitude of the ratio of P_2/P_{dc}, (e) P_{r_flt}, overall fault declaration (f) Fault signal (indicating the duration of the fault), (g) P_{r_dtc}, fault detection based on P_r, (h) I_{rms_dir}, $[I_{rms}]$ based directional element, (i) Z_{0_dir}, conventional ground directional signal and (j) P_{r_flt}, overall fault declaration.

Figure A.6 presents fault detection parameters for forward and reverse faults of different types (AB and AG). Plots given for each scenario are instantaneous current, RMS current, fault detection based on P_r, $[I_{rms}]$ based directional element, conventional ground directional signal (Z_{0_dir}) and Overall fault detection in that order (from top to bottom).

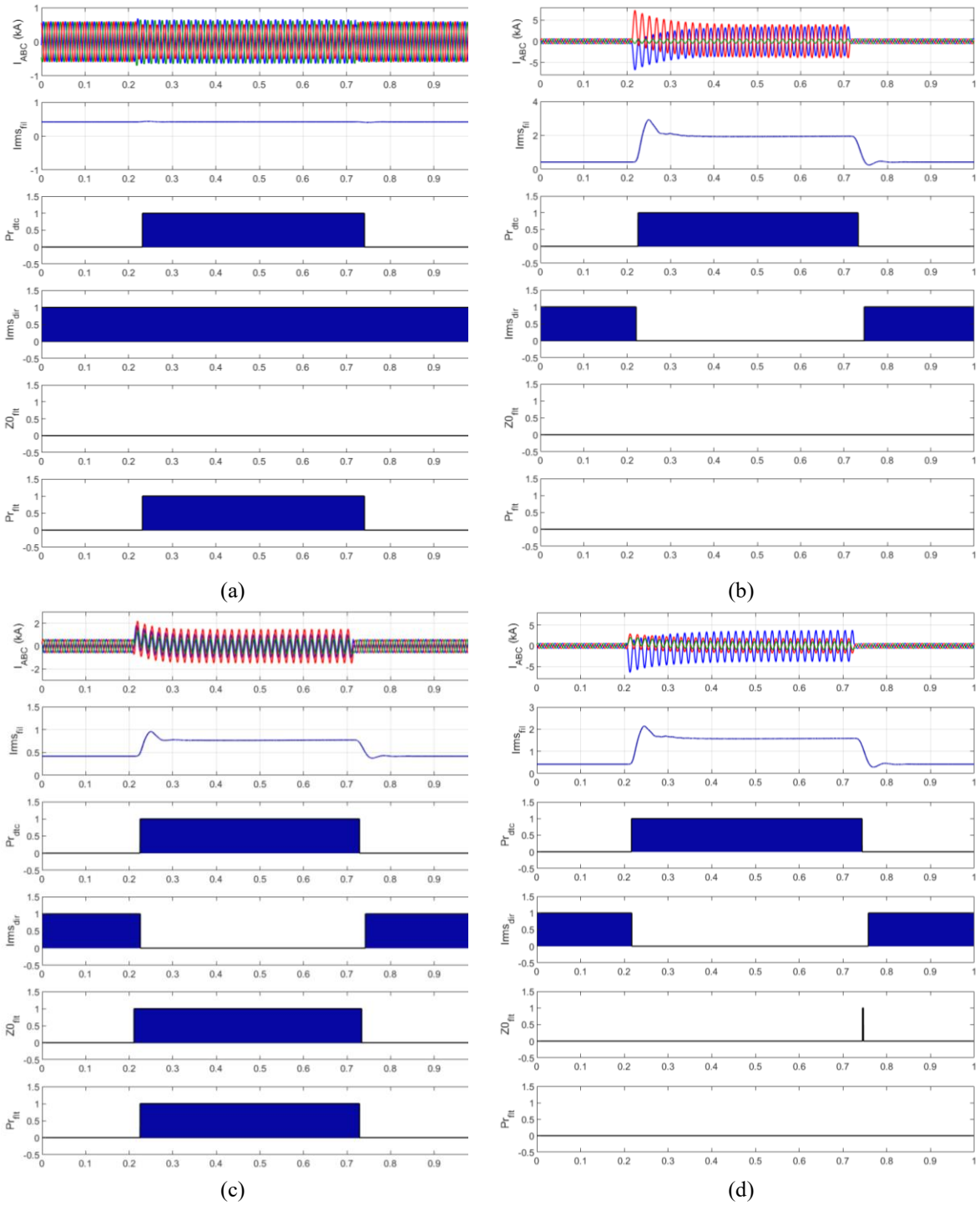

Figure A.6 Fault detection parameters for (a) forward line-line (AB) fault at 50% of Line 12, (b) reverse line-line (AB) fault at Bus 1, (c) forward line-to-ground (AG) fault at 50% of Line 12 and (d) reverse line-to-ground (AG) fault at Bus 1

Results given in Figure A.5 and Figure A.6 indicate that proposed scheme can successfully identify different faults in a system with IBRs. Figure A.7 presents values recorded for parameter P_r for different fault types (at 50% of *Line 12* and at *Bus 1*). All fault scenarios presented produce significantly larger values of P_r (than pre-fault) during different types of faults, both forward and reverse, allowing it to be used for fault detection effectively.

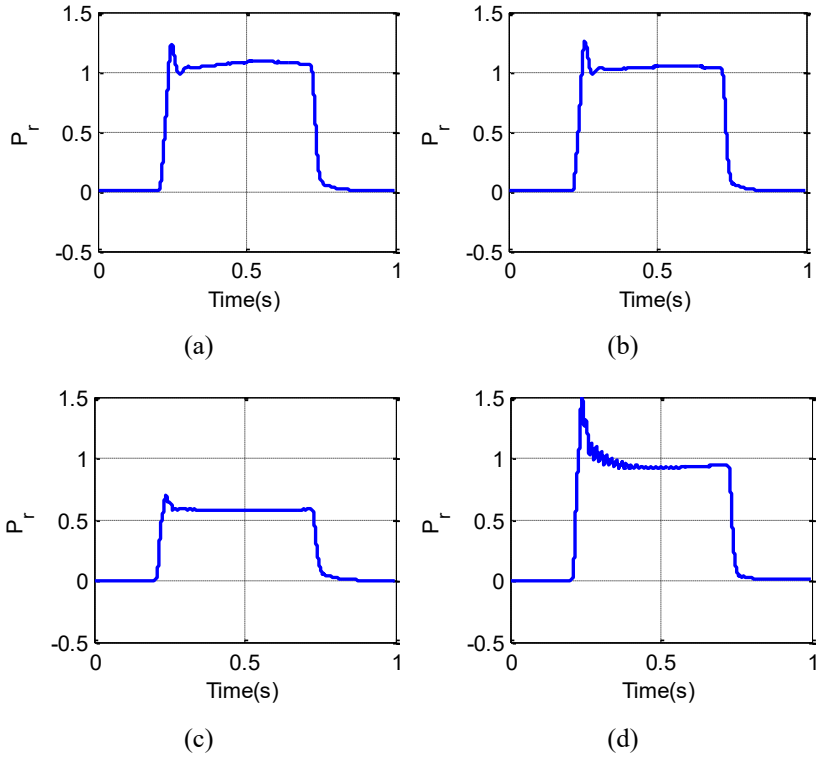

Figure A.7 Parameter P_r for different fault types (a) forward, AB fault 50% of Line 12 (b) reverse, AB fault at Bus 1 (c) forward, AG fault 50% of Line 12 (d) reverse, AG fault at Bus 1.

A.5 Discussion

Results presented above indicate that the proposed fault detection method produces reliable performance in protecting a transmission line fed predominantly by IBRs. Many conventional fault detection principles are either trigger by high fault currents (instantaneous and time over-current elements) or directly supervised by overcurrent elements (distance protection elements). Consequently, IBR generated fault currents pose significant challenges to conventional fault detection as they may not reach levels much higher than load currents (in a significant number of cases depending on the configuration). The core advantage of the proposed fault detection method is the fact that it has little dependence on fault current magnitude and, this feature makes it especially suitable for systems with high IBR penetration. Furthermore, conditions of the fault such as fault location and type have relatively low impact on the performance of this technique. Another benefit of this method is that it can be implemented in a modern relaying hardware using standard functions (most of which already exists in a modern digital relay) and little computational burden.

The proposed technique is applicable to all power systems in general even though it offers special value for systems with low fault current contributions such as those with IBRs. In essence, the proposed method of fault detection is a measure of system unbalance and the results obtained during the study indicated that it is more sensitive to faults than simple a under/over voltage element. Moreover, since this is a method using both voltage and current measurements, it is generally more robust than an element relying on only one of those measurements. Note that the proposed fault detection element can also be coupled with other suitable conventional or unconventional directional identification elements, if necessary.